



UNIVERSIDAD
NACIONAL
DE COLOMBIA

Evaluation of the Volumetric Mass Transfer Coefficient as Scale Up Parameter for CHO cell Cultures for Monoclonal Antibodies Production

Andrés Javier Bello Hernández

Universidad Nacional de Colombia

Facultad de Ingeniería, Departamento de Ingeniería Química y Ambiental

Bogotá D.C., Colombia

2021

Evaluación del Coeficiente Volumétrico de Transferencia de Masa como Parámetro de Escalamiento de Cultivo de una línea celular CHO para la producción de Anticuerpos Monoclonales

Andrés Javier Bello Hernández

Tesis o trabajo de investigación presentada(o) como requisito parcial para optar al título de:
Magister en Ingeniería – Ingeniería Química

Director (a):

Ing. Rubén Darío Godoy Silva PhD.

Línea de Investigación:

Bioprocesos

Grupo de Investigación:

Grupo de Investigación en Procesos Químicos y Bioquímicos

Universidad Nacional de Colombia

Facultad de Ingeniería, Departamento de Ingeniería Química y Ambiental

Bogotá D.C., Colombia

2021

*Was wir wissen, ist ein Tropfen, was wir nicht
wissen, ein Ozean.*

Isaac Newton

Declaración de obra original

Yo declaro lo siguiente:

He leído el Acuerdo 035 de 2003 del Consejo Académico de la Universidad Nacional. «Reglamento sobre propiedad intelectual» y la Normatividad Nacional relacionada al respeto de los derechos de autor. Esta disertación representa mi trabajo original, excepto donde he reconocido las ideas, las palabras, o materiales de otros autores.

Cuando se han presentado ideas o palabras de otros autores en esta disertación, he realizado su respectivo reconocimiento aplicando correctamente los esquemas de citas y referencias bibliográficas en el estilo requerido.

He obtenido el permiso del autor o editor para incluir cualquier material con derechos de autor (por ejemplo, tablas, figuras, instrumentos de encuesta o grandes porciones de texto).

Por último, he sometido esta disertación a la herramienta de integridad académica, definida por la universidad.



Andrés Javier Bello Hernández

Fecha: 09/04/2021

Agradecimientos

A pesar de que este trabajo lleva solamente mi nombre y el del profesor Rubén Darío Godoy en el título, este es el resultado del apoyo de muchas personas, quienes aportaron desde una llamada hasta las instalaciones donde pude realizar los experimentos.

A la Universidad Nacional de Colombia por permitirme ser el profesional que soy hoy en día. El haber sido admitido como estudiante de Ingeniería Química hace ya una década ha sido uno de los factores que definió el rumbo que tomó mi vida. Por ende, mis agradecimientos a los profesores del Departamento de Ingeniería Química y Ambiental, de quienes aún sigo aprendiendo. Especialmente, al profesor Rubén Darío Godoy Silva por la confianza que me otorgó con este proyecto, por permitirme equivocarme para darme cuenta de que esa es la forma de mejorar, por la paciencia, por las clases de fluidos, diseño de procesos bioquímicos, ingeniería bioquímica, electricidad, mecánica, diseño, y por otras tantas enseñanzas de vida. Adicionalmente, muchas gracias a los profesores Álvaro Orjuela Londoño, Marcelo Enrique Riveros Rojas, Óscar Yesid Suárez Palacio, Luis Alejandro Boyacá Mendivelso, Juan Guillermo Cadavid Estrada, Julio César Vargas Sáenz, Néstor Ariel Algecira Enciso y Paulo César Narváez Rincón, quienes me apoyaron en mi proceso formativo, no solo como estudiante, sino también como docente.

Al profesor Carlos Arturo Guerrero Fonseca por brindarme un espacio de trabajo para terminar mi trabajo de grado durante una pandemia. Asimismo, a Carlos Maya y a Miguel Ospino, miembros del grupo de Biología Molecular de Virus de la Facultad de Medicina de la Universidad Nacional, quienes siempre me brindaron su apoyo desinteresado y estuvieron pendientes de lo que necesitaba. Al profesor Fabio A. Aristizábal por brindarnos la línea celular con la que se realizó el proyecto. A los profesores Juan Carlos Serrato Bermúdez y Mario Enrique Velásquez Lozano, del grupo de investigación en Procesos Químicos y Bioquímicos, quienes me colaboraron siempre con los equipos a su cargo que necesitaba y con la capacitación por parte de sus estudiantes, entre ellos, Fabián Rico Rodríguez, Margareth Andrea Patiño Lagos y Yenny Paola Morales Cortés.

A la Dirección Académica de la Universidad Nacional por el programa Beca Asistente Docente, con la cual financié parte de mis estudios de maestría, así como a Janeth Alejandra García Herrera, profesional

de la Vicedecanatura de Investigación y Extensión de la Facultad de Ingeniería, por su ayuda con la corrección de estilo de esta tesis y de los artículos publicados. Mil gracias por toda la paciencia.

A Ana Rosa Salamanca Paternina, por la amistad, las charlas, las risas y los consejos. A todo el personal del Laboratorio de Ingeniería Química (LIQ) de la Universidad Nacional de Colombia, en especial a Ricardo Cortés Segura por su amabilidad constante. A Clarita y a don Julio de Servicios generales y al personal de vigilancia del LIQ por estar pendientes de nosotros cuando las jornadas de trabajo se extendían hasta la madrugada. A don Javier Lamprea, don Hernando Narváez y don Enrique Camargo por haberme enseñado un poco de su labor y tenerme paciencia.

Al Servicio Alemán de Intercambio Académico (DAAD) por la beca para “Viajes de estudio para grupos de estudiantes extranjeros” del año 2017.

To Philip D. Howes and Prof. Andrew De Mello from the ETH Zürich, for allowing me being part of their research group and carry out a project that may contribute to better the life quality of people in Colombia. Thank you for that opportunity. Also, thanks to my research subgroup, Daniel Richards and Monika Colombo for your patience and the knowledge you have contribute to me.

A Brenda Caballero Mendoza por ser un polo a tierra durante varios momentos de mi vida. Gracias por tu amabilidad y afecto. A Johan Andrés Pasos Panqueva (P) por ser prácticamente mi hermano, mi compañero de estudio, trabajo y de fiesta. Gracias por las enseñanzas y la compañía. A Leslie Vanessa Sánchez Castillo (B) por compartir las experiencias que cambiaron muchos paradigmas en las vidas de los dos. Gracias por la paciencia y la fortaleza. A Juliana Vargas Gracia (T) y Fabián Leonardo Rondón González (L) por ser dos faros de luz cuando todo se veía oscuro. Gracias por el apoyo. A Astrid Nausa Galeano (B) por su cariño desde el principio, por haberme brindado las herramientas técnicas para enfrentar este proyecto y una que otra cerveza. A Ana Isabel Ramos Murillo (R) por haber creído siempre en mí, por los consejos y la guía en varios momentos durante este camino.

A las personas que compartieron conmigo en el grupo de investigación en Procesos Químicos y Bioquímicos: María Alejandra García (P), Miguel Ángel Flórez, Juan David Tibocho (S), Diego Alejandro Sánchez (B), Elizabeth Rodríguez (L), Andrés Camilo Forero (F), Mateo Quintero (N), Natalia Cuéllar, Mateo Rodríguez (E), Cindy Carolina Latorre (H), Valeria Colón (B), Lorena Galván y Andrés Arias (K). Aunque no suelo llamar a todos por el nombre que menciono acá, pero los aprecio mucho por su compañía y apoyo cuando lo necesitaba.

A mis amigos del pregrado en Ingeniería Química: Luisa Fernanda López González (P), Elizabeth Andrea Olivares Martínez (L), José Ángel Beleño Alcázar, Ángela Dubois Camacho (B), Diana María García Valencia (P), Johan S. Chaparro Álvarez (C), Alicia Andrea Torres Hernández (T) y Sebastián Camilo Salazar Bautista (P), por haber compartido conmigo tantas experiencias y siempre recordarlas con una sonrisa. Especialmente, le agradezco a la vida por contar dentro de mis personas de confianza a Laura Camila Casas Mateus y Juan David Reyes Fernández, quienes me acompañaron y conocen el detalle de lo que significó para mí este proceso.

A mis amigos del posgrado en Ingeniería Química: Andrea Suaza Fontalvo (C), Cristian Camilo Rodríguez Páez (R), Javier Andrés Arrieta Escobar (P) por su apoyo, compañía y colaboración. Particularmente, agradezco a la Karen Giovanna Bastidas Gómez por su cariño y complicidad, a Andrés Felipe Cabeza Pulido (M) por su infinita amabilidad y a Francisco Javier Quintero Cortés y Pedro Jose Arias Monje por su incondicional ayuda.

A mis compañeros del Departamento de Aseguramiento Técnico de la Vicepresidencia de Activos con Socios de Ecopetrol S.A. por enseñarme una mentalidad totalmente diferente para abordar problemas y sus soluciones. Gracias por su paciencia y permitirme aprender de un área de mi carrera profesional que desconocía. De este equipo quisiera agradecer particularmente al Ing. Nelson Gabriel González Posada por haberme brindado la mano cuando lo necesitaba, a la Ing. Liliana Holguín Vega por tantas lecciones de vida y a Carolina Vásquez Bautista por su confianza y cariño.

A las personas con las que he compartido muchos momentos agradables y que recuerdo con cariño. To the people I have shared amazing moments and I dearly remember: Erika Liliana Malagón, Charlie Paz Idarraga, Jonathan Delgado Espinosa, Lucía Diz Pintos, Astrid Schmidt, Alfred Halverson, Daniela Cuervo Salcedo, Sebastián Castaño Duque, Laura Carolina Barón, Nicolás Sebastián Yascual, María Augusta de Carvalho Silvelo, Paula Cristina Sáenz Castañeada, Nicholas Adrian Burk (B), Miguel Ángel Munévar, Irfan Custovic (B), Matthieu Rimlinger (M) y Martina Cerisoli (F). Muchas gracias, Dankeschön, moitas grazas, tack så mycket, muito obrigado, hvala ti puno, merci beaucoup, grazie mille.

Desde el fondo de mi corazón le quiero agradecer y dedicar este trabajo a mi familia. Infinitas gracias por la paciencia, la exigencia y la fe que tuvieron en mí. A mi mamá, Rosa, por sus oraciones, su buena energía en todo lo que emprendo, por su trabajo incansable, humildad, fortaleza y ser la columna vertebral de nuestra familia. Gracias por haber pagado mi examen de admisión a la Universidad Nacional y creer en el potencial que tenía. A mi papá, Andrés, gracias por su dedicación, su esfuerzo y por ser el ejemplo vivo de que no hay desfallecer cuando todo parece perdido. A mis hermanas por su compañía durante toda mi vida.

A Claudia Mireya por su tenacidad porque ser madre e ingeniera no es fácil, y a Janeth Marcela por su apoyo, su tolerancia e integridad como ser humano. A mis padrinos, Orlando y Nidia, y a mis tíos porque sin ellos no hubiese podido acceder a un colegio que me ha dado las bases de lo que soy hoy en día. A Sara Daniela y Andrés Felipe por ser simplemente quienes son, porque con su dulzura e inocencia me hacen los días más felices.

A mi abuela Omaira (Q.E.P.D.) por ser la raíz de nuestra familia. Gracias por responder siempre a mis llamadas por teléfono cuando era el único número que me sabía y por tu prudencia. Es extraño pasar Navidad, Año Nuevo o cumpleaños sin ti, pero sé que algún día nos volveremos a encontrar. A Laura Alejandra, Paula Lorena y Daisy Tatiana por haberme acompañado en mi infancia y confiar en mí en cuanto idea se me cruzaba por la mente. Estoy seguro de que ustedes serán grandes profesionales y espero que la vida no nos tenga mucho tiempo lejos uno del otro.

Finalmente, le agradezco a Dios la oportunidad de haber logrado este hito en mi vida que me transformó en muchas dimensiones que desconocía y me permitió compartir con todas las personas que mencioné y muchas que se escapan de mi memoria al escribir esto.

A veces es solo cuestión de tiempo.

Resumen

Evaluación del coeficiente volumétrico de transferencia de masa como parámetro de escalamiento de cultivo de una línea celular CHO para la producción de anticuerpos monoclonales

Actualmente, los anticuerpos monoclonales (mAbs) corresponden al segmento más importante en el mercado de productos biotecnológicos con efecto terapéutico. La síntesis a escala industrial de este tipo de proteínas recombinantes se lleva a cabo en biorreactores empleando líneas celulares provenientes de un mamífero, las cuales son modificadas genéticamente para incluir dentro de su metabolismo la síntesis del mAb. Para comprender mejor la manera en la que estas células deben ser cultivadas, se realizan ensayos a escala laboratorio, en las cuales se determinan las condiciones más apropiadas para la producción en el biorreactor a escala industrial.

Dentro de los retos más desafiantes en términos técnicos a replicar en reactores a escalas mayores a las del laboratorio se encuentra la velocidad de transferencia de masa de oxígeno. Este gas es vital para el cultivo de las células de mamífero dado su rol en la respiración, por lo tanto, en la obtención de energía para la vida celular. No obstante, dada la baja solubilidad del oxígeno en el agua, es necesario agitar y/o burbujear el medio de cultivo, y así, el gas se solubilizará más rápido en el líquido. La presente tesis de maestría evaluó la cinética del crecimiento, consumo de sustratos y síntesis de coproductos por una línea parental celular de Ovario de Hámster Chino en dos geometrías de cultivo, Erlenmeyer y Spinner. Con el fin de comparar los resultados en las dos configuraciones de biorreactores, se definieron las condiciones de operación (agitación y burbujeo) de manera tal que la velocidad de transferencia de oxígeno fuera igual en las dos geometrías.

Palabras clave: Cultivos de células animales, coeficiente volumétrico de transferencia de masa, biorreactor.

Abstract

Evaluation of the volumetric mass transfer coefficient as Scale-up parameter for cultures of a CHO cell line for Monoclonal Antibody production.

Nowadays, monoclonal antibodies (mAbs) correspond to the most important segment in the market for biotechnological products with therapeutic effect. The synthesis of this type of recombinant proteins in industrial scale is carried out in bioreactors using mammalian cell lines, which are genetically modified to include mAb synthesis within their metabolism. To better understand the way in which these cells should be cultured, tests are carried out on a laboratory scale, in which the conditions for production in the bioreactor on an industrial scale are determined rather.

Assuring an adequate oxygen mass transfer rate is one the most demanding challenges in technical terms to be replicated in reactors on larger scales than laboratory vessels. This gas is vital for the cultivation of mammalian cells given its role in respiration, and thus, in obtaining energy for cellular life. Nonetheless, since oxygen is sparingly soluble in water, it is necessary to stir and/or bubble the culture medium, for increasing the solubilization rate of the gas in the liquid. In this master's thesis, the kinetics of growth, consumption of substrates and synthesis of co-products by a parental cell line of Chinese Hamster Ovary were evaluated in two culture geometries, Erlenmeyer and Spinner. In order to compare the results in the two bioreactor configurations, the operating conditions (stirring and bubbling) were defined in such a way that the oxygen transfer rate was the same in the two geometries.

Keywords: Mammalian cell cultures, volumetric mass transfer coefficient, bioreactor.

Content

1. Introduction.....	5
1.1 Biopharmaceuticals.....	6
1.2 Monoclonal antibodies (mAb).....	9
1.3 Chinese Hamster Ovary (CHO) cells	11
1.4 Industrial cultures of mammalian cells	14
1.5. Bioreactor scale-up for Mammalian Cells.....	15
1.4.1 Scale-up limitations for suspended Mammalian Cells	19
1.4.2 Role of Oxygen in Mammalian Cells.....	24
1.4.3 Oxygen-Water Phase equilibrium thermodynamics.....	28
1.5 Gas-liquid mass transfer in bioreactors	30
1.6 Gas-liquid mass transfer in bioreactors	35
1.6.1 Dynamic gassing methods.....	37
1.7 $k_{L,a}$ as scale-up parameter	41
2. Improved experimental determination of the Volumetric Mass Transfer Coefficient for two bioreactor configurations and the specific oxygen consumption rate for a CHO cell line.	45
2.1 Introduction	46
2.1.1 Bioreactor Scale-up.....	46
2.1.2 Oxygen mass transfer.....	47
2.1.3 Dynamic Gassing in/out methods for $k_{L,a}$ and q_{O_2} determination.....	48
2.2 Materials and Methods.....	51
2.2.1 Bioreactor description.....	51
2.2.2 Determination of the Volumetric Mass Transfer Coefficient ($k_{L,a}$)	55
2.2.3 Determination of the specific oxygen consumption (q_{O_2}) for a CHO cell line.....	60
2.3 Results and discussion.....	64
2.3.1 Characteristic and dead time	64
2.3.2 Relevance of headspace change time and delay due to DO probe response for the $k_{L,a}$ measurement.....	65
2.3.3 $k_{L,a}$ values for two bioreactor configurations.....	71
2.4 Conclusions	80
3. CHO cells cultures at determined $k_{L,a}$ values in two bioreactor geometries.	82
3.1 Introduction	82
3.2 Materials and Methods.....	83
3.2.1 Cells and culture medium	83
3.2.2 Bioreactor configuration and operation conditions	84

3.2.3	Culture monitoring.....	86
3.3	Results and discussion	86
3.3.1	Cell growth and Viability	86
3.3.2	Monitoring of Dissolved oxygen concentration.....	88
3.3.3	Monitoring of metabolites.....	90
3.4	Conclusions	95
4.	<i>Conclusions and suggestions</i>	97
4.1	Conclusions	97
4.2	Suggestions	98

List of Figures

	Pág.
<i>Figure 1-1. Sales (billions of USD) of the top ten selling biopharmaceuticals in 2017. [11], [19]</i>	9
<i>Figure 1-2. IgG structure (Hansel et al. 2010)</i>	10
<i>Figure 1-3 Aerobic and anaerobic (lactic acid) respiration pathways of a mammalian cell [96]. ...</i>	25
<i>Figure 1-4: Oxygen solubility in NaCl aqueous solutions exposed to air at 1bar with different temperatures [113].</i>	30
<i>Figure 1-5: Scheme of the path of an oxygen molecule from the headspace to the mitochondria.</i>	31
<i>Figure 1-6: Two-films theory scheme.</i>	31
<i>Figure 1-7: Expected measured data for A: dynamic gassing out and B: dynamic gassing in. Data analysis for k_La determination by C: dynamic gassing out and D: dynamic gassing out methods. .</i>	39
<i>Figure 2-1: Expected measured data for A: dynamic Gassing out and B: dynamic Gassing-in. Data analysis for k_La determination by C: dynamic Gassing out and D: dynamic Gassing out methods.</i>	50
<i>Figure 2-2: Description of Erlenmeyer flask bioreactor configuration: (A) 3D isometric view, (B) front view, (C) cross-section, and (D) 3-baffled bottom.</i>	52
<i>Figure 2-3: Description of Spinner flasks and impeller geometry: (A) 3D isometric view, (B) bottom geometrical disposition, (C) impeller, and (D) cylinder and magnetic stirrer bar.</i>	53
<i>Figure 2-4: Diagram of the equipment for dynamic gassing k_La determination. V: Valve, PI: Pressure indicator, FI: Flow indicator, F: 0.22μm filter, DOI: Dissolved oxygen indicator.....</i>	56
<i>Figure 2-5: k_La measurement cycle: (I) Stabilization of Headspace and liquid oxygen concentration, (II) reduction of headspace oxygen concentration with Nitrogen, (III) dynamic gassing out k_La measurement, (IV) stabilization of Headspace and liquid oxygen concentration, (V) increase of the headspace oxygen concentration with air and (VI) dynamic gassing-in k_La measurement.....</i>	57
<i>Figure 2-6: Considerations for oxygen mass balance for determining Headspace change time.</i>	58
<i>Figure 2-7: k_La measurement cycle: (I) Stabilization of Headspace and liquid oxygen concentration, (II) reduction of headspace oxygen concentration with Nitrogen, (III) dynamic gassing out k_La measurement, (IV) stabilization of Headspace and liquid oxygen concentration, (V) increase of the headspace oxygen concentration with air and (VI) dynamic gassing-in k_La measurement.....</i>	60
<i>Figure 2-8: q_{O_2} measurement cycle: (I) Stabilization of headspace oxygen concentration, (II) reduction of headspace oxygen concentration with Nitrogen, (III) dynamic gassing out k_La measurement, (IV) change of headspace oxygen concentration, (V) increase of the headspace oxygen concentration with air and (VI) dynamic gassing-in k_La measurement.....</i>	62

Figure 2-9: Measurement of the probe response to a step change. The darkest continuous line is the first-order transfer function with an average of the parameters obtained from Experiments 1 to 5. 65

Figure 2-10: Real (C_L and C_g) and expected (C_m) DO concentration for Scenario A: the change of oxygen solubility is considered, and Scenario B: the gas oxygen concentration is regarded as zero. 68

Figure 2-11: Actual and measured linearized values of DO concentration for Scenario A. 69

Figure 2-12: Relative error in k_{La} determination during the first 200s of the measurement stage with a sensor characteristic time of 33s. 70

Figure 2-13: k_{La} values for the Erlenmeyer bioreactor configuration with A: Distilled water / B: Dynamis® cell culture. N=3. Error bars: σ 72

Figure 2-14: k_{La} values for the Spinner bioreactor configuration with A: Distilled water / B: Dynamis® cell culture. N=4. Error bars: σ . The thicker error bar corresponds to the bubble flow of 0.33ml s^{-1} 73

Figure 2-15: Potential model and its comparison with experimental data for calculating k_{La} in the Spinner flask for A: Water and B: Dynamis® Culture Medium. Stirring speed (SS in rpm) and bubble flow (FB in ml s^{-1}). 74

Figure 2-16: Bubble layer in Spinner flask Bioreactor with 100ml Dynamis® culture medium at 37°C , 100rpm, and 0.44ml s^{-1} 75

Figure 2-17: Polynomial model and its comparison with experimental data for the calculation of k_{La} in the Spinner flask for A: Water and B: Dynamis® Culture Medium. Stirring speed (SS in rpm) and bubble flow (FB in ml s^{-1}). 77

Figure 2-18: Relative error of two k_{La} measurements employing the gassing-in method. 78

Figure 2-19: CHO cell growth kinetic during exponential stage in 100ml Spinner-type bioreactors with 40ml of Dynamis® medium 8mM l-glutamine supplemented, and cultured at 37°C , 5% CO_2 and 115rpm. N=3. Error bars= σ 78

Figure 2-20: OUR as a function of cell concentration for the stirred experiments. N=8. Error bars: σ 79

Figure 2-21: OUR as a function of cell concentration for the stirred experiments. N=3. Error bars: σ . The darkest error bars correspond to gassing out experiments. 80

Figure 2-22: DO concentration in terms of air saturation at operation conditions during the culture of the CHO cell line. 81

Figure 3-1. Picture of the real culture environment for the Erlenmeyer bioreactors. 85

Figure 3-2. Picture of the real culture environment for the Spinner bioreactors. 85

Figure 3-3. Cell concentration (continuous) and viability (dotted) in a 30ml(top)/100ml(bottom) batch culture of CHO cells performed in an Erlenmeyer(top)/Spinner(bottom) bioreactor. n=4 and Error bars= σ 87

Figure 3-4. Monitoring of DO concentration in a 30ml/100ml batch culture of CHO cells performed in an Erlenmeyer(continuous)/Spinner(dotted) bioreactor. n=1. 89

Figure 3-5. Comparison of actual and expected DO concentration for Erlenmeyer bioreactor. 89

<i>Figure 3-6. Glucose (continuous) and lactic acid concentration (dotted) in a 30ml(top)/100ml(bottom) batch culture of CHO cells performed in an Erlenmeyer(top)/Spinner(bottom) bioreactor. n=4 and Error bars=σ.....</i>	<i>92</i>
<i>Figure 3-7. pH (continuous) and osmolality (dotted) in a 30ml(top)/100ml(bottom) batch culture of CHO cells performed in an Erlenmeyer(top)/Spinner(bottom) bioreactor. n=4 and Error bars=σ... </i>	<i>93</i>
<i>Figure 3-8. Free LDH concentration in a 30ml/100ml batch culture of CHO cells performed in an Erlenmeyer/Spinner bioreactor. n=4 and Error bars=σ.</i>	<i>94</i>
<i>Figure 4-1: Calibration curve for the rotameters or Flow Indicators (FI). Air at 20°C and 15.83 psia was employed. N=4 and Error bars = σ.</i>	<i>130</i>
<i>Figure 4-2: Calibration curve of the enzymatic method for glucose concentration determination after shaking the sample in a 96-well plate during 30 min at 37°C. Trendline equation: $y=0.632x$, $R^2 = 0.9989$; x=Glucose concentration, y=Absorbance.</i>	<i>132</i>
<i>Figure 4-3: Calibration curve of the HPLC method for lactic acid concentration determination. N=2, Error bars=σ.</i>	<i>133</i>
<i>Figure 4-4: Calibration curve of the enzymatic method for free LDH concentration determination after shaking the sample in a 96-well plate for 20 min at 22°C. Trendline equation: $y=0.0955$, $R^2 = 0.993$; x=equivalent lysed cell concentration, y=relative fluorescence units.</i>	<i>136</i>

List of tables

<i>Table 1-1. Therapeutic applications of monoclonal antibodies [18].</i>	7
<i>Table 1-2: Cell models used for monoclonal antibody production.</i>	12
<i>Table 1-3: Lethal consequences of subjecting cells to lethal conditions.</i>	17
<i>Table 1-4. Shear stress of some types of agitators [86].</i>	22
<i>Table 1-5. Sensibility of cells to shear stress rates.</i>	23
<i>Table 1-6. Suggestions for CHO cell culture operation conditions</i>	23
<i>Table 1-7. Specific oxygen consumption rate for different microorganisms [120], [121].</i>	33
<i>Table 1-8: Methods of k_{La} and q_{O_2} determination</i>	35
<i>Table 2-1: Valve state during measurement stages in k_{La} determination.</i>	60
<i>Table 2-2: Valve state during measurement stages in q_{O_2} determination.</i>	63
<i>Table 2-3: Summary of parameters for step perturbation for the DO probe.</i>	65
<i>Table 3-1: Operation conditions for cultures at determined k_{La} values.</i>	85

Context

Biopharmaceuticals or biotechnological products are a segment of biopharma for referring to synthesized products due to modifications in the genome of a host organism. Since the approval of Orthoclone OKT3 in 1986, biopharmaceuticals have exponentially gained the interest of scientists and industrials for commercial, research, and therapeutic applications. As a result, Biologics' market sales in 2017 reached USD 106.9 billion, and it is projected that 2024 global sales achieve USD 383 billion. Furthermore, it is forecasted since 112 new products were approved and entered the market between 2015 and 2018, while just 82 were commercialized before 2014. Among the commercial recombinant proteins, monoclonal antibodies (mAb) are highlighted because of their relevance in the biotechnological market, whose sales represent more than 50% of global sales for 2016.

mAbs are primarily produced in mammalian cell cultures since the properties of the proteins synthesized by these cell lines present fewer compatibility problems with patients. The cell line selection depends on several aspects such as specific cell productivity, biomass yield, genetic stability of the cell clone, and antibody quality, defined as the correct amino acid sequence and post-translational modifications. Among the used cell lines for mAbs synthesis on an industrial scale, Chinese Hamster Ovary cells (CHO) are the most widely model. Up to 2018, more than 60% of the therapeutic monoclonal antibodies approved are produced in CHO cell lines because these cell lines are adapted for growth in suspension in chemically defined media. Additionally, regulatory agencies streamline approval processes based on trust, given the extensive knowledge of the genome and metabolism of CHO cell lines.

The industrial production of recombinant proteins requires compliance with stringent quality parameters to ensure product biosafety and process stability. Advances in the cell line, the

culture media, and the bioreactors have been developed for improving the process yield and production costs. Before reaching the industrial production of the antibody, it is necessary to establish medium properties, operation parameters, and culture strategies for profitable production. These studies are typically carried out in lab vessels since these devices are easy to control and cheap in terms of occupied space, time, and resources. Many reported studies could be easily found in the literature, where the effect of several parameters is discussed, such as temperature, osmolality, stirring speed, dissolved oxygen, among others, and high clone-specific dependence. Consequently, every new product development requires an operational parameter study.

After finding the optimal conditions for cultures in laboratory-scale tests, it is necessary to translate that information to industrial-scale bioreactors. Although this process may seem trivial, it is not at all. Specific operating conditions depend on the bioreactor shape since they are related to the transport phenomena within the culture medium; in other words, the ways momentum, energy, and mass are transferred to supply cell needs. For example, since oxygen is poorly soluble in culture media for animal cells, it is necessary to induce movement of the culture medium to increase the rate with which oxygen dissolves in the liquid and thus, satisfy respiratory cell needs. Due to the movement, Oxygen is continuously supplied as long as the oxygen source is an oxygen-containing gas.

The volumetric mass transfer coefficient is a parameter required to quantitatively determine the amount of oxygen that enters the culture medium given certain operating conditions in the bioreactor. This parameter depends on the shape of the bioreactor and the turbulence of the culture medium. It is directly proportional to the amount of oxygen that is dissolved by the liquid. As oxygen transfer is a mass transport phenomenon, the greater the value of the volumetric mass transfer coefficient, the greater are turbulence in the medium and the amount of oxygen that dissolves in the medium.

This work can be divided into two parts. The first part is the experimental determination of two key parameters to predict the behavior of dissolved oxygen throughout a culture. The volumetric mass transfer coefficient is the parameter that correlates the rate at which oxygen dissolves in the medium. In contrast, the specific oxygen consumption is the parameter for

estimating the oxygen demand by cells. The second part consisted of comparing mass oxygen transfer of two bioreactor geometries through the execution of three cultures under three operational conditions with three different volumetric mass transfer coefficient values. Significantly different behavior of the dissolved oxygen concentration would be expected, therefore, of the cell concentration.

Nevertheless, extreme turbulence has adverse effects on the viability of cells. In highly turbulent environments, the shear stresses that cells are subjected to can be lethal. In addition to causing cell death of the affected cell, detritus is liberated to the culture medium and could also affect other viable cells.

In conclusion, oxygen supply is a critical parameter in the culture of a mammalian cell line. As the cell concentration increases, the oxygen demand increases as well. Suppose the oxygen requirements of the cells are estimated. In that case, it is possible to propose the best-operating conditions for a bioreactor, thus having higher titles of the product of interest.

1. Introduction

Mammalian cell culture technology has become a significant field in modern biotechnology since commercial well-established products are synthesized by these “cell factories,” comprising viral vaccines, therapeutic monoclonal antibodies, and other types of recombinant therapeutic proteins [1]. The success of the employment of mammalian cell cultures to produce biopharmaceuticals is attributed to their ability to synthesize complex and high human-compatible proteins that other cell lines are not able to [2]. Although a wide variety of types of cells can be designated with the term “mammalian cell,” just a few cell lines have been developed as suitable hosts for protein manufacturing at the industrial level. These include Chinese Hamster Ovary (CHO), Baby Hamster Kidney (BHK), mouse myeloma (NS0) cells as they are readily modified by genetic engineering and show robust growth in suspension on large scale bioreactors. [3].

Process developers for biopharmaceutical facilities must design bioreactors, which ensure favorable environments for cell proliferation. In the first place, cells maintain themselves by constantly processing nutrient molecules to obtain energy, building blocks for new living material, and synthesizing a product of interest. Hence, the culture medium must contain carbohydrates, fats, amino acids, vitamins, and inorganic components as raw materials metabolic processes. Secondly, as cells grow submerged within the medium, temperature and component concentration are evident operating conditions influencing cell behavior. Furthermore, the characteristics of the bioreactor, such as liquid height, stirring mechanism, or the number of baffles, also have a critical influence on cell behavior.

Regarding mammalian cells, the absence of a cell wall and the dependence of an adequate oxygen supply are vital factors to consider at the facility's design stage for culturing these cell lines. On the one hand, unlike bacteria, fungi, and plant cells, animal cells do not count on a rigid external structure that defines their shape and protects them before sudden changes in their surroundings.

But, on the other hand, mammalian cells rely on oxygen availability for efficient energy uptake; otherwise, their metabolism will rely on pathways with lethal consequences for the integrity of the cell membrane.

In this chapter, the main issues related to mammalian cell culture are presented. Then, since oxygen transfer is a relevant factor to be considered in bioreactor design for these cell lines, an analysis of how oxygen is delivered to mitochondrial and the factors that influence its transfer rate within culture media is introduced. In the end, some reported scale-up strategies are reviewed as a tool for decision-making for the setting of operating conditions for mammalian cell cultures.

1.1 Biopharmaceuticals

In a broad sense, a biopharmaceutical can be defined as a substance extracted or semi-synthesized from biological sources, used for diagnosing, healing, treating, or preventing a disease [4]. However, some regulatory agencies restrict the term biopharmaceutical only to protein or nucleic acid-based substances used for therapeutic or *in vivo* diagnostic purposes, produced by means other than direct extraction from natural (non-engineered) biological sources. According to this definition, hormones, growth factors, cytokines, and monoclonal antibodies (mAb) are biopharmaceuticals. In contrast, blood-derivates, vaccines, and plant-based products directly extracted from a native producer are not [5].

Nowadays, biopharmaceuticals represent an efficient and safe therapeutic alternative for untreatable diseases and pathological conditions. Since the use of conventional drugs involves risks associated with their non-selectivity, intrinsic toxicity, and possible side effects, the complex structure of biopharmaceuticals induces a specific response in the patient, thus, more effective treatment for a variety of patients of illnesses. [6][7]. However, these biomolecules' biosynthesis and subsequent large-scale purification are still very complex, resulting in costly final products [8].

The biopharmaceutical market has shown great potential with further dynamic growth in response to the growing demand for this type of medication. In 2017, biopharmaceuticals outstripped projections [9], contributing globally USD 208 billion in sales, which corresponds to 25% of the worldwide prescription & over-the-counter (OTC) drug sales. If this upward tendency is maintained, current estimations aim to sell around USD 383 billion by 2024 [10]. These figures are mainly

attributed to two factors: the exponential growth of the number of innovative biopharmaceuticals launched during the last decades on the market and the high prices of this group of drugs compared with conventional medications [11]. Therefore, biopharmaceuticals are the fastest growing sector in the pharmaceutical industry in the last decades [12].

The growth of the biopharmaceutical market is also reflected in the rates of approvals for commercial products. Before 1995, only 25 biopharmaceutical products were approved either by the U.S. or European regulatory agencies. However, between 1995 and 2014, an average of 57 products was approved every five years, whereas 112 products were just approved between 2015 and July 2018 [13]. This remarkable increase is attributed to the entry of biosimilars, which are versions of an original biopharmaceutical manufactured after the innovative patent expiration [14], [15].

Among the category of biopharmaceuticals, the more relevant market segment corresponds to recombinant proteins, which are peptide biomolecules synthesized by a host cell line whose genome was modified to include the interest synthesis product in its metabolism [7]. Currently, commercialized products obtained by recombinant technology include clotting factors, thrombolytics, anticoagulants, hormones, growth factors, interferons, interleukins, tumor necrosis factors, and vaccines. Nevertheless, the monoclonal antibodies (mAbs) represent the most significant profits in biopharmaceutical sales due to their employment in treating high-impact diseases, as listed in *Table 1-1*. MAbs products and derivatives, which include antibody fragments, fusion proteins, antibody-drug conjugates, and other conjugated antibody products, are the most produced biopharmaceutical at large scale [16], [17].

Table 1-1. Therapeutic applications of monoclonal antibodies [18]

Disease category	Specific Indication	Example product
Allergy	Asthma, chronic idiopathic urticaria	Xolair®
Bone diseases	Osteoporosis	Prolia®
Cardiovascular	Primary hyperlipidemia	Praluent®
Hematologic	Anti-platelet prevention of blood clots in high-risk percutaneous transluminal angioplasty and	Reopro®

Disease category	Specific Indication	Example product
	refractory angina when percutaneous coronary intervention is planned	
Immune and autoimmune diseases	Rheumatoid arthritis, juvenile idiopathic arthritis, psoriatic arthritis ankylosing, spondylitis, Crohn's disease, ulcerative colitis, plaque psoriasis, hidradenitis suppurativa, and uveitis	Humira®
Infectious diseases	Prevention of respiratory syncytial virus (RSV) infections in children	Synagis®
Macular degeneration	Neovascular (wet) age-related macular degeneration, macular edema following retinal vein occlusion, diabetic macular edema, and diabetic retinopathy	Lucentis®
Oncology	Non-Hodgkin's lymphoma, chronic lymphocytic leukemia	Rituxan®

In 2017, mAbs sales reached USD 106.9 billion, representing nearly 56% of the total combined sales of biopharmaceuticals and no recombinant vaccines, corresponding to a 205% increase since 2008, when the sales of these products were about USD 35 billion [11], [19]. Correspondingly, six of the top ten selling biopharmaceutical products in 2017 are mAbs, as presented and resalted in black in *Figure 1-1*.

Given the importance of these products in the current pharmaceutical market and their potential for the treatment of chronic diseases, part of the research and development budget of pharmaceutical companies is dedicated to the study of the pharmacokinetics of monoclonal antibodies, as well as how to synthesize them efficiently. In this chapter, some general information about monoclonal antibodies and ways to obtain them on an industrial scale are presented to provide a context for the addressed study problem.

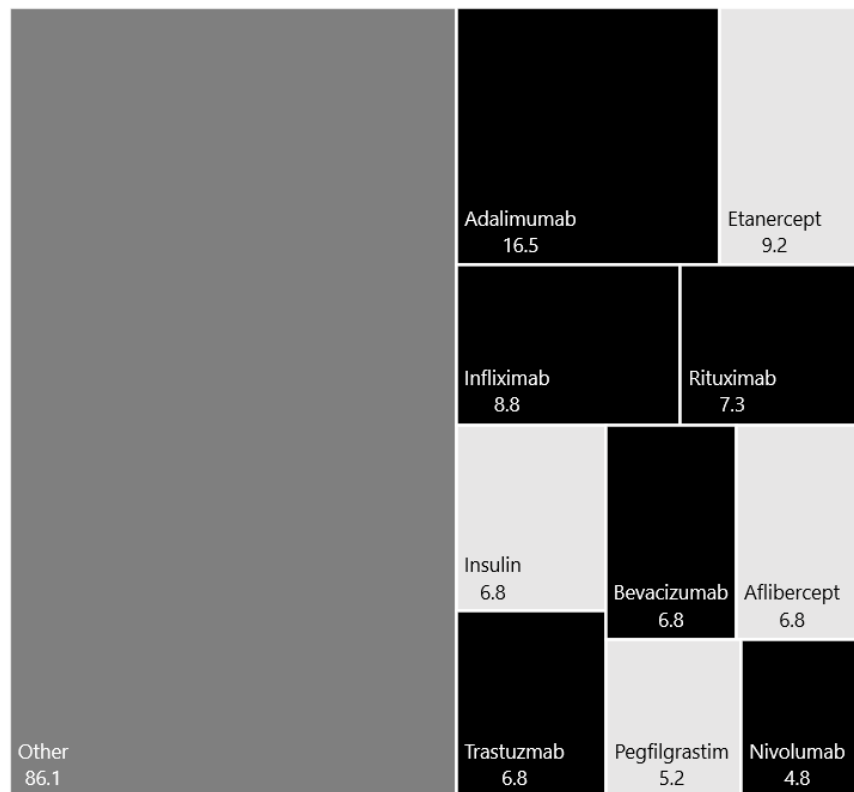


Figure 1-1. Sales (billions of USD) of the top ten selling biopharmaceuticals in 2017. [11], [19]

1.2 Monoclonal antibodies (mAb)

An antibody or immunoglobulin (Ig) is a glycoprotein produced by plasma cells that play an active role in recognizing and defense mechanisms against pathogens. Its action is based on the particular interaction between the antibody and an antigen. In a broad definition, an antigen could be any substance, own or foreign, that activates the adaptive immune system of an animal. For instance, antigens can be proteins expressed on the surface of a pathogen. When the antibody is bound to the antigen, it acts as a marker, facilitating the immune system's recognition and elimination of the pathogen [20]. The basic functional unit of an antibody is the immunoglobulin monomer. Two or more Ig monomers can form a single antibody. Antibodies' weight and size are about 150 kDa and 10nm [21]. They can be classified into isotypes according to their protein structure, biological properties, functional locations, number of Ig monomers, and ability of the antibody to recognize different types of antigens [22]. There are five identified isotypes of antibodies in placental

mammals denominated IgA, IgD, IgE, IgG, and IgM [23]. IgG is the primary class of immunoglobulins in humans, accounting for about 10–20% of the plasma protein in human serum [24].

A characteristic IgG structure is presented in *Figure 1-2*; an Ig monomer consists of two identical heavy chains, each of about 50 kDa, and two identical light chains, each of approximately 25 kDa. Heavy chains are composed of four regions, one variable (V_H), and three constants (C_{H1} , C_{H2} , and C_{H3}). Light chains have two areas: one variable (V_L) and one constant (C_L). C_{H2} and C_{H3} regions conform to the crystallizable fragment (F_c), while C_{H1} , V^H , and the light chains constitute the antigen-binding fragment (F_{ab}), also known as variable fragment (F_v). A specific region located in the F_v is responsible for the interaction between the antigen the antibody. These sites, known as the complementarity-determining regions (CDRs), are specific for each monoclonal antibody. Typically, an Ig monomer has a Y-shaped structure due to a flexible hinge region between F_{ab} and F_c and disulfide bonds that connect the antibody fragments [25], [26].

Antibodies present an attractive option for developing therapies and molecular drug targets due to their ability to recognize an antigen with high specificity and induce a response by the adaptive immune system. Since the publication of the first achievements in hybridoma technology by Köhler and Milstein in 1976 [27], the production of recombinant antibodies has occupied an important place both in the scientific and the industrial field. Additionally, the increasing knowledge of the genome and structure of immunoglobulins and the development of recombinant DNA technology have allowed the genetic design of a great variety of antibody products [28].

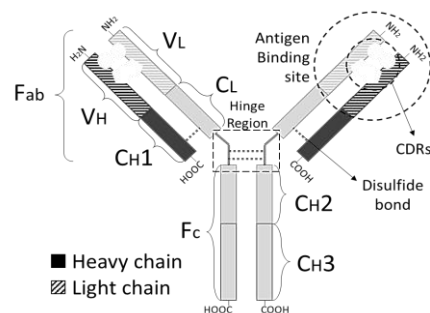


Figure 1-2. IgG structure (Hansel et al. 2010)

Antibodies synthesized by recombinant technology can be classified into mono- or polyclonal, according to the nature of the cells from which they come. Polyclonal antibodies represent a

collection of antibodies from different clones that recognize the same antigen in multiple sites. In contrast, monoclonal antibodies are produced by a single clone and bind the antigen in just one place. Since mAbs are homogeneous and consistent structures, they constitute the ideal solution for biopharmaceutical applications that require large volumes of identical antibody, corresponding to a specific antigen [29].

According to the origin of primary structure, mAbs can be classified into murine (mouse), chimeric, humanized, and human. Chimeric mAbs contain variable regions (V_L and V_H) that stem from a murine source and constant regions from a human source. Humanized mAbs are mainly derived from human sources, except for the CDRs, which come from a murine source. Both murine and human mAbs are derived entirely from mouse and human sources, respectively [30]. The first approved mAb for therapeutic use was Orthoclone OKT3[®] in 1976, an immunosuppressant of murine origin, helpful in reducing acute rejection in patients with organ transplants [31]. In the past four decades, technology has been switched from mouse, via chimeric, and humanized, to fully human mAb to reduce potentially immunogenic undesirable responses. Nonetheless, there are still a few approved murine products.

1.3 Chinese Hamster Ovary (CHO) cells

As glycoproteins, antibodies are proteins with chains of carbohydrate units attached to some of their amino acid residues [32]. Different cell models are employed to produce mAbs at laboratory and industrial scales, such as bacteria, plants, insects, yeast, mammals, and even microalgae [33]. According to the cell model employed, mAb specific production rate can vary, as well as mAb quality in terms of glycosylation patterns and stability of the expression system [34]. A summary of the cell models used for mAb synthesis is presented in

Bacteria and yeast models are easily cultivable and proliferate. Even though they do not have natural glycosylation machinery compatible with humans, they are suitable for producing various antibody fragments (e.g., Ranibizumab and Certolizumab pegol), which do not include the Fc region and do not need to be glycosylated. New improvements in glycoengineering of yeast and glycosylated IgG constitute an opportunity for microbial organisms to produce full-length mAbs [38].

Table 1-2.

Bacteria and yeast models are easily cultivable and proliferate. Even though they do not have natural glycosylation machinery compatible with humans, they are suitable for producing various antibody fragments (e.g., Ranibizumab and Certolizumab pegol), which do not include the Fc region and do not need to be glycosylated. New improvements in glycoengineering of yeast and glycosylated IgG constitute an opportunity for microbial organisms to produce full-length mAbs [38].

Table 1-2: Cell models used for monoclonal antibody production.

Model	Advantages	Disadvantages	Reference
Bacteria	Fast growth (Duplication time: 20 min) Easy genetic manipulation Easy and unexpensive cultivation	Lack of natural glycosylation machinery Proteins are not secreted	[35], [36]
Yeast	Fast growth (Duplication time: 75-120min)	Manose-rich glycosylation systems	[37]–[39]
Plant	Easy and unexpensive cultivation	Glycosylation patterns differ from humans. Low productivity	[40]–[42]
Insect	Cheap cultivation Similar transcription, mRNA processing, and translation to human	Slow growth (Duplication time: 18-30hours) Glycosylation patterns differ from human cells. The high oxygen demand of cells Moderate productivity (0.5g L^{-1})	[43]
Mammal	High productivities (Approx. 10g L^{-1}) Similar transcription. mRNA processing and translation to humans. Similar glycosylation patterns to human	Slow growth (Duplication time: 24 hours) Large and complex genome Complex, more prolonged, and expensive cultivation Expensive culture media Glycan heterogeneity	[44]–[46]

Insect cells are well-known models for the production of vaccines and recombinant proteins [47]. They can be cultured at lower temperatures compared to mammalian cells, significantly reducing infrastructure and production costs. Nevertheless, there are no approved products derived from insect cell lines due to their average reported productivity and the incompatibility of the nature of oligosaccharide chains with humans [43].

Plant cells have been recently evaluated as a candidate model for the industrial production of mAbs. Even though plants glycosylation patterns are not identical to human ones, the lower production cost for plant cultivation has attracted researchers' attention. Once again, glycoengineering has emerged as an alternative for successful mAb production [40]. However, low reported productivities justify that no approved product using this kind of cells has been developed until now.

Since mAbs produced by bacterial, fungi, plant, and insect cells present compatibility problems with humans, mammalian cell lines are currently the most used models used in biomedical research and industrial production. The most used models are derived from rodents or humans, among which stand Chinese Hamster Ovary (CHO), Mouse Myeloma (NS0, Non-Secreting Murine Myeloma), Kidney Baby Hamster (BHK), Human Embryo Kidney (HEK), and Human Retina (PER-C6) (Ho et al. 2014). However, requirements for mammalian cell cultivation are far from trivial since complex and expensive facilities, culture media, and staff training are required [2].

The focus of researchers in the past two decades regarding mammalian cells has been the increase of their productivity, reaching an improvement of more than 20-folds [48]. In addition, antibody titers have increased exponentially, overcoming the theoretical limit of around 10 g L^{-1} imposed by growth limitations at high cell density conditions. These achievements are the result of multidisciplinary efforts in high-inoculum adaptation, high culture densities, chemically defined medium (CDM), and increased feeding rate in advanced culture strategies [49]–[51].

From the 22 mAbs reported in Annex A, 50% are produced by CHO clones, making it the preferred cellular model for obtaining this type of biopharmaceutical. In the second place, there are other murine cell lines (NS0, SP2/0, and hybridomas). Thus, CHO cells are the most used mammalian host

at large-scale commercial production of biopharmaceuticals, attributed to five reasons. First, CHO cells have proven to be a safe host; thus, they are accepted as a GRAS organism (Generally Recognized as Safe). Second, the genome of the CHO-K1 cell line was recently sequenced [52], which is essential for developing new recombinant proteins. Third, high mAb specific productivities were achieved after gene amplification. Fourth, CHO cell lines show efficient post-translational processing of complex proteins, maintaining high similarity between the glycosylation patterns of human and CHO-derived products. Finally, their successful adaptation to serum-free and suspension cultures facilitates their culture in conventional bioreactor configuration, hence expediting up-scaling and improving productivity [49], [52]–[54].

1.4 Industrial cultures of mammalian cells

Industrial production of recombinant proteins requires compliance with stringent quality parameters to ensure product biosafety and process stability [55]. Therefore, before reaching the industrial production of a mAb, it is necessary to establish medium properties, operational parameters, and culture strategies under which a profitable production can be assured. Furthermore, since mammalian cells are susceptible to environmental changes, different values of culture parameters, either in media components or in bioreactor settings, will influence the final product properties and titers.

On the one hand, culture media must supply all the required nutrients for cell growth and the synthesis of the interested product. Essentially, media for mammalian cell cultures contain carbohydrates, amino acids, pH-buffers, proteins, inorganic ions, growth factors, and vitamins, which are present in determining concentrations according to the requirements of the cultured cell line [56]–[60].

On the other hand, cell performance also depends on the operational parameters settled by the bioreactor environment, for example, temperature, gas transfer rates, and shear stress. Extensive knowledge of those parameters' impacts on cell growth and product outcomes is the basis of scale-up processes [61]. In terms of cultivation strategies, advanced approaches have been adding up to the classical batch operation. Fed-batch, continuous, and perfusion include adding a feed stream that replenishes spent nutrients while allowing the accumulation of cells. As a result, more

extended cultures with high cell densities and productivities have been reached at the laboratory, pilot, and industrial scales. Even when additional configurations are needed and contamination risk increases, these approaches are now mostly preferred for industrial-level processes.

Specifically, single-use bioreactors have been developed and successfully adapted to different operation strategies [62]. They can be as simple as wave bioreactors or as complex as perfusion in scales that range from milliliters to 1,000 liters. In this sense, disposable bioreactors constitute a robust, easily standardized, and transferable platform for cells culture [63]–[65].

1.5. Bioreactor scale-up for Mammalian Cells

Generally, the term “Process Development” refers to the exercise of creating a means to achieve production rates of a product of interest based on economic criteria. In the case of bioprocesses, it involves the selection and sequencing of process steps from a repertoire of unit operations, in which physicochemical transformations are performed by microorganisms or parts of them [66]. Thus, cell culture processes can be essentially divided into three parts:

- The substrates conditioning.
- The biochemical transformation of substrates into the product of interest.
- The subsequent recovery and purification of the product of interest.

Although authors differ in setting the biochemical transformation [67] or the downstream processing [68] as the costliest process step in terms of both variable costs (raw materials and utilities) and capital investment, the efforts for obtaining a more significant economic income are primarily focused on synthesizing the sufficient quantities of the product of interest with the minimum cost. [69]

Therefore, knowing the cell behavior under bioreactor operating conditions is essential for understanding the desired chemical transformation. However, a complete description of the phenomenology of bioreactors is unfeasible due to the complexity of biological systems. To identify the optimal conditions, the behavior of the microorganisms under different culture conditions is tested in screening assays. These assays are commonly carried out in laboratory scale vessels since the time of experimentation and resource expenditures are significantly reduced. At that scale,

each experiment requires fewer quantities of raw materials in comparison with large bioreactors. Additionally, multiple experiments can be performed in parallel at very controlled conditions, which allows to carry out thorough studies of the behavior of biochemical transformations [70]. Although the number of studied culture conditions differs according to the novelty of the study case, some commonly evaluated variables are the nutrient composition in the media, stirring intensity, pH, and temperature (Doran, 2013). Nevertheless, the process's economic feasibility will probably claim production volumes that are not easily achieved in laboratory equipment. Thus, it is necessary to replicate the best-found conditions in larger vessels where more significant quantities of the product of interest can be synthesized [67], [71]. Although shifting the size of the equipment seems relatively trivial, the increase in the production capacity leads to variations in the microorganism performance. It may even turn the process into economically unfeasible [72]–[74].

In bioreactors, and in general, for all process units, momentum, heat, and mass transfer phenomena simultaneously interact for transforming material inputs into products that will be treated in a different unit or commercialized. There are neither gradients of temperature, pressure, or velocity nor composition of every component within the medium in the ideal bioreactor configuration. However, this is physically unfeasible. For instance, the stirred tank configuration is commonly used as a bioreactor. These devices rely on an impeller device for moving the liquid within the vessel. According to the momentum transfer principles, liquid molecules on the impeller will essentially move as fast as the impeller itself.

In contrast, the liquid molecules on the vessel wall will have no relative velocity due to the no-slip condition. The simultaneous presence of two different limit conditions implicates the existence of a velocity gradient within the liquid. A similar situation applies to temperature, pressure, and component concentration. Heat transfer will depend on the heating/cooling strategy and the inherent heat losses of the system. Pressure will be defined by the liquid level and the velocity profile. Mass transfer is affected by all the mentioned parameters, the gas-liquid interfacial area, the inlet of nutrients, and the culture time, among others [67].

Critical values of relative velocity, pressure, temperature, component concentration, or severe gradients in the cell surroundings will inevitably influence the culture performance.

Table 1-3 describes a series of lethal consequences after subjecting mammalian cells to critical conditions that could be experienced within a bioreactor. The specific cell line settles the determined high and low critical values and the extreme gradient values. Moreover, the subjection time and the magnitude of the out-of-range variable influence the destructive potential of a critical parameter value in a cell.

Table 1-3: Lethal consequences of subjecting cells to lethal conditions.

Properties	High critical value	Low critical value	Severe gradient around the cell
Relative velocity	Given that all the medium moves at the same velocity, cells will not be theoretically affected by a critical high relative velocity value. Nevertheless, this feature is technically impossible.	As the mammalian cell lines cultured at a large scale grow in suspension, they could grow, forming clusters if they remain under low stirring conditions or precipitate and increase on the vessel's bottom.	Cells are subjected to high shear stress rates, which could infringe membranal integrity, eventually causing necrosis.
Pressure	Cell size is affected.		Although a gradient exists in the bioreactor, the differences are not significant in terms of pressure, temperature, or composition at distances with the same magnitude order
Temperature	If cells contact some points in the bioreactor at either elevated or low temperatures that exceed their resistance, there will be necrosis.	If cells endure the temperature, although it is not within a desirable range, they will have to modify their metabolic activities to survive, probably with affection on the productivity of the interested product. These conditions are	

	referred to as hyper- or hypothermia, correspondingly.		as cell diameter. Therefore, no single cell will experiment with any of those gradients in their immediate surroundings.
Substrate/product concentration	Depending on the substrate or product nature and cell tolerance, they could be inhibited or damaged.	Cells will switch their metabolism according to the new conditions. For example, cells eventually die if the substrate is a crucial metabolite and is not continuously supplied, or the product is highly harmful and not promptly eliminated.	Critical gradients between the intra- and extracellular environment cause loss of membrane integrity.

It is estimated that the number of operating parameters in a single bioreactor easily exceeds one hundred, and their combined effect is highly non-linear [75], which makes it impossible for the detailed description of the influence of every variable on cell performance. Despite this constraint, the augmentation of bioreactor volumes has been successfully carried out by several enterprises during the last decades. For this purpose, process developers have established scale-up processes, which are procedures based on a combination of their prior knowledge and experimental data.

A scale-up process can be defined as the successful startup and operation of a processing unit, whose design and operating procedures are based upon experimentation in smaller devices and acquired work methodologies in industrial production [76], [77]. The main aim of upscaling is to reach a similar product quality and yield as those previously obtained at a small scale. Focused on mammalian cells bioreactors, several key factors are frequently considered: the satisfactory and

predictable mixing, gas-liquid dispersion, suspension of solids, homogenization of components, mass transfer of gases (particularly oxygen and carbon dioxide) and nutrients; the prevention of cell damage and minimization of adverse alterations to cell physiology through control of shear and pressure effects [1].

1.4.1 Scale-up limitations for suspended Mammalian Cells

Inherent constraints for the bioreactor configuration arise since the cell line is selected. Thus, both the cell and the curious product nature essentially establish the type of medium and the bioreactor configuration to use. Specifically, the culture media formulation for mammalian cell cultures has evolved from clots, coagulants, tissue extracts, and other natural biological fluids to chemically defined media, implying a safe and efficient production of recombinant proteins with therapeutic effects [78]. As the basic requirements of the culture media are widely known, the influence of its components on cell productivity has become the focus of the current research [58]. For this reason, the most challenging constraints imposed by mammalian cell nature for large-scale cultures are related to protecting the cell integrity from lethal shear stress rates, removing toxic side products that diminish cell viability, and satisfying the cell oxygen requirements.

Since mammalian cell lines for biopharmaceutics production are adapted to grow in suspension, a crucial parameter for the bioreactor design is maintaining the medium in continuous movement. However, this feature must be carefully regarded. In the absence of movement, cells either precipitate and proliferate on the bottom of the vessel or start to grow in clusters, which negatively affects the culture. Furthermore, the inner cluster cells have a high probability of death because their neighbors block them, impeding their access to nutrients. Once they achieve a lethal condition, proteases are released, increasing the likelihood of necrosis of the remaining living cells and degradation of the product of interest.

Nonetheless, above a specific value, cells are exposed to lethal shear stress rates. Moreover, in contrast to bacteria, fungi, and plant cells, mammalian cells do not possess rigid cell walls, which help maintain a determined shape and guard the membrane integrity. It is believed that this feature constraint the hydrodynamic conditions cells can withstand. Cells with a rigid cell wall are cultured in bioreactors under rougher stirring conditions than mammalian cells.

Likewise, the presence in the medium of certain side products of the culture has inhibitory effects on cells, specifically lactic acid, ammonium, and carbon dioxide. [79]. Lactic acid is produced when cells are forced to use the metabolic pathway of the lactic acid for energy attainment [80]. Ammonium is produced by the degradation of the amino acids in the medium or through the cell metabolism [81], and carbon dioxide is a product of aerobic respiration [82]. The presence of these compounds has relevant implications in pH and osmolality of cell surroundings due to their acid-base character in aqueous solutions [83]. The challenge of the bioreactor design is to obtain a configuration that can remove these side products to assure a better environment for cells. For this purpose, advanced culture strategies like perfusion are already implemented.

Stirred tank is the bioreactor configuration the most used for large-scale cultures. It consists of a vessel that has incorporated an agitation system, which moves the culture medium. Due to the action of a mechanical system, an impeller of the agitation system rotates and moves the liquid. According to the volume size, the mechanical system varies from magnetic stir bars coupled to the impeller geometry, as in laboratory cultures, to motors that shift from the top or bottom of bench-scale and industrial bioreactors.

Some standard bioreactor features are considered for cultures of suspended mammalian cell lines at a large scale [84]. For instance, the classic shape of stirred tanks is cylindrical with a curved bottom and baffled in some cases. This configuration reduces the inhomogeneities on the bottom in comparison with flat designs. Another consideration is the material in- and outlet disposition. Rigorous control systems must be implemented in the bioreactor since mammalian cell behavior is affected by multiple variables, such as temperature, pH, dissolved oxygen, or CO₂ concentration in headspace gas. Therefore, bioreactors cannot be completely sealed. Still, these must count with in- and outlet material devices, such as spargers for direct gas supply to the liquid or probes for temperature, pH, dissolved oxygen, carbon dioxide, or foam measurement. Indeed, according to the culture operation mode, recurrent medium in or outtake is required.

Bioreactor vessels and accessories must be as inert as possible; that is, these must be strictly made of materials that do not react at culture conditions nor liberate substances to the medium that may influence cell growth. The material of bioreactor vessels depends on whether they employ single-use or reusable technologies. In single use stirred bioreactors, the culture medium is in bags made of polymers like polycarbonate, polymethyl methacrylate, or polyethylene. Rigid metallic support holds these bags. Reusable bioreactors are made of either glass or stainless steel. Impellers are

made of PTFE or stainless steel, and bioreactor accessories, such as probes or spargers are made of glass, stainless steel, or silicone.

Stirred tanks are widely used in the industry because of the accumulated knowledge of this bioreactor configuration and its versatility [85]. Nevertheless, the presence of mobile parts that interacts out and inside the bioreactor increases the contamination risks. But also, the shear stress rates that can be achieved due to the impeller rotation can harm lethally the cultured cells, which will harm bioreactor performance.

Furthermore, oxygen mass transfer constraints have been reported as relevant issues in bioreactor scale-up, not only for mammalian cells but also for other cell lines. Therefore, the role of oxygen in cell metabolism and the methods for the bioreactor characterization based on gas mass transfer are presented further. In terms of mass oxygen transfer, oxygen can be supplied to a medium in a bioreactor from either the headspace or bubbles. However, the parameters that make oxygen dissolve rapidly are the turbulence within the liquid and the contact area between the headspace or bubble gas as the oxygen source and the medium. The higher the turbulence and the greater the surface area, the faster the oxygen will enter the liquid.

On the one hand, stirring is essential in cultures of suspended cell lines. Without medium movement, the cells would precipitate or aggregate among themselves, decreasing cell viability by cluster formation. In cell clusters, cells are assembled, creating a structure such that there will be cells whose direct contact with the medium will be limited by the steric hindrance imposed by their neighbors. The cells on the cluster surface can quickly be supplied by nutrients and oxygen, while the interior cells are constrained, which would cause that cell stress, changes in their metabolism, and eventually, cell death. Because internal cells are not programming their metabolism for death, proteases and other undesired cell products may be liberated, occasioning death in cascade reaction in the cell cluster.

One of the decisive factors when selecting an impeller is the sensitivity of the culture to shear stress. All stirrers have high shear stress zones near the stirring blades [45]. Thus, according to what has been reported in the literature for studies of stress generated by different reactors. It is observed that the magnetic stirrer and the marine propeller are the ones that present the lowest value compared to the turbine-type stirrers. On an industrial scale, there are different types of agitators. Their selection and design depend mainly on viscosity, turbulence, shear force, and

power. In bioreactors, turbine or propeller agitators are usually employed, with impeller diameter/vessel diameter ratios close to 1/3, 1/2, and 2/3, leaving significant space between the walls and the agitator. They operate at high speeds to produce efficient mixing. For low stirring rates and viscosities between 1 to 10^4 centipoises, the turbines and propellers adjust well to the dispersion of the liquid [72].

The main agitation systems comprise the Rushton turbine-type paddle agitators or the propeller agitators to which the elephant ear or marine propeller-type agitator belongs. In this case, Rushton turbines can handle high gas flows and efficiently disperse them. For their part, the propellers are not as efficient in distributing the gas flow, but they have a high pumping capacity and are more efficient in dispersing energy.

Table 1-4. Shear stress of some types of agitators [86].

Impeller	Maximum Shear Stress Rate (Pa)
Magnetic stirrer	0,268
Marine propeller	1,33
Rushton Turbine	193,7
Inclined vane turbine	15,63

Generally, mammalian cells are considered to have low shear strength, and cell lysis occurs after a specific range, as shown in Table 1-5. Increases of 100-600 rpm have been shown to produce a significant reduction in cell viability and at speeds up to 1500 rpm massive cell destruction [87]. Due to the need for increased oxygen transfer and carbon dioxide removal in animal cell cultures, it has been shown that the use of defoaming agents can significantly improve the resistance of the culture to high agitation speeds.

On the other hand, bubbling enhances the oxygen transfer and helps to remove the generated carbon dioxide, which harms cells. Although bubbling increases the gas-liquid contact, the presence of zones with high shear stress rates at bubble rupture concerns the use of this method for longer and healthier cultures. Gas flow and bubble size are vital because they can generate cell rupture upon reaching the culture surface in the gas-liquid system-generated depending on their size. Tiny

bubble sizes dissolve in the medium before reaching the surface, while if the measure is considerable, there is a loss in the area for mass transfer. This phenomenon is also associated with the mechanical damage associated with the bubble's bursting, which in the case of bubbles with diameters smaller than 2 mm is greater than the damage generated in large bubbles [88]. Therefore, several studies focus on the optimization of the gas flow and the bubble size generated. Studies in CHO cell cultures document cell damage in gas flows higher than 0.054 vvm in 0.15 μm dispersers and 0.025 vvm in 0.5 μm dispersers. Likewise, bubble sizes between 2-3 mm in diameter are recommended [89].

Table 1-5. Sensibility of cells to shear stress rates.

Cell	Average Size (μm)	Sensibility to shear stress rates
Bacteria	1-10	Low
Vegetal	100	Middle – High
Animal	20	High

In Table 1-6, some thumb rule-based recommendations for Chinese hamster ovary cell cultures are presented.

Table 1-6. Suggestions for CHO cell culture operation conditions

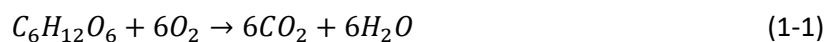
Parameter	Value	Unit	Reference
Bubble diameter	2-3	mm	[90] [91]
Gas Flow	0,025-0,067	vvm	
Volumetric mass transfer coefficient	3,8-10,3	h-1	
Shear stress rate	0,3-0,69	Pa	[92]
Linear stirring speed	<1,65-2	m/s	[93]
Temperature	33-37	$^{\circ}\text{C}$	[94]

1.4.2 Role of Oxygen in Mammalian Cells

Oxygen (O_2) is a crucial substrate in mammalian cell cultures due to its role in cell metabolism, particularly as the final electron acceptor in the aerobic respiration pathway. Respiration processes are metabolic pathways whereby cells retrieve the required energy for completing vital cell activities, such as synthesizing new cellular constituents, maintaining membranal ionic and osmotic equilibrium, and thermogenesis and motility [95]. As chemoorganotroph organisms, mammalian cells rely on nutrients in their surroundings to enlarge their size or breeding. In general terms, substrates are transformed by the cell in two main macro processes, catabolism, and anabolism. In catabolism, large nutrient molecules are incorporated into the cell environment to be broken down into intermediate metabolites or relatively small molecules used as raw material in anabolism to construct large molecules with a specific function for the cell [96].

Nutrients can be roughly classified according to their role in the cell metabolism as carbon, nitrogen, or energy sources. Carbohydrates and lipids are the main carbon sources, while amino acids are carbon and nitrogen sources for mammalian cells. These biomolecules are the raw materials for the synthesis of new cellular constituents [97] and sources of free energy since they are also chemically reduced. The energy stored in reduced molecules can be retrieved by removing electrons through chemical oxidation [98].

Since carbohydrates, lipids, and amino acids can be converted to common intermediate metabolites through several pathways, the following analysis starts from glucose, the most common monosaccharide in culture media formulations for mammalian cells [99]. Considering the net complete oxidation of glucose presented in (1-1), a total of 2,831kJ of energy is released for each oxidized glucose mole. However, all the glucose molecules were oxidized at once; the released energy would even burn the cell up. Instead, the cell relies on enzyme-controlled metabolic pathways that regulate the liberation of energy. These pathways are based on the movement of electrons through electron transport chains and other coupled oxidation-reduction reactions, which transfer the chemical energy stored in nutrient molecules to ATP (Adenine Tri Phosphate) and other carrier molecules. These catabolic pathways are better known as respiration [98].



At the end of the respiration process, a final electron acceptor withdraws the transferred electrons from the energy source. Otherwise, the enzymatic machinery of the respiration pathway would be

stalled, leading to a significant diminution in ATP production rates. An eventual ATP lack has severe consequences to cell integrity since the enzymes for the competition of vital cell activities require ATP. In mammalian cells, ATP-dependent enzymes are directly involved in protein and DNA synthesis and the maintenance of osmotic equilibria [95]. Yet, the disruption of the synthesis of new cell constituents stops cell growth and protein synthesis processes, the breakdown of osmotic balances has lethal consequences for the cell. The failure of ATP-dependent ionic pumps in cell membrane precedes massive potassium (K^+) outflux from and (Na^+) influx. When the potassium concentration in the cell surroundings drops to specific values, e.g., about 12 to 13 mM for neurons, changes in the chemical potential of the membrane surroundings become large enough to open voltage dependent Ca^{2+} channels and induce a largely uncontrollable influx of Ca^{2+} . The increase of Ca^{2+} concentration interferes in several intracellular reactions, particularly in the activation of phospholipases or enzymes that may collapse the membrane through the hydrolysis of phospholipids [100].

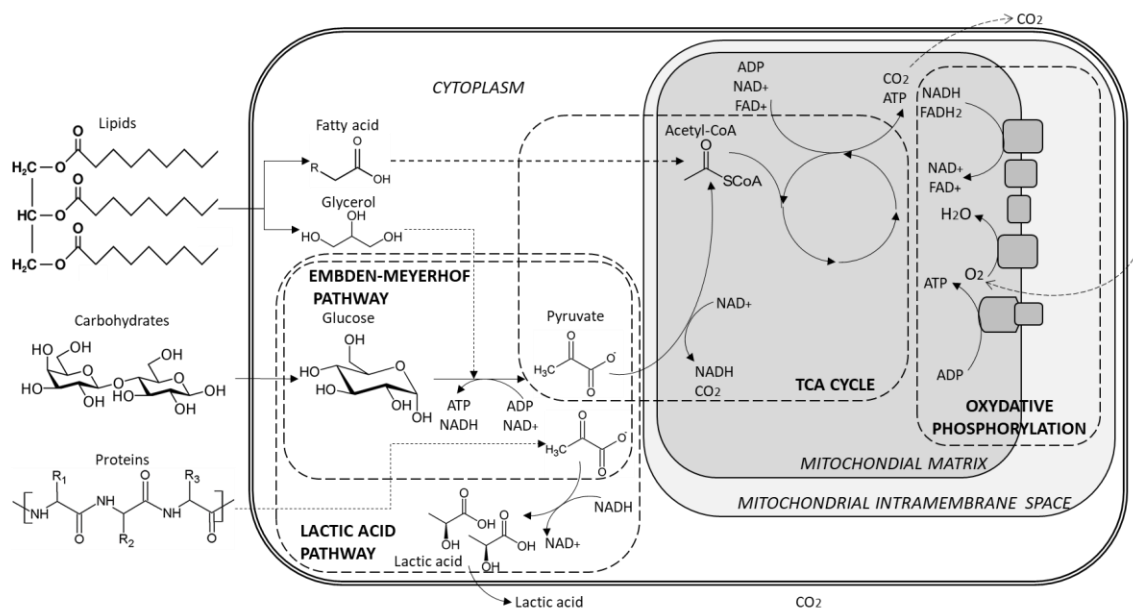


Figure 1-3 Aerobic and anaerobic (lactic acid) respiration pathways of a mammalian cell [96].

Respiration pathways can be classified according to the final electron acceptor into aerobic or anaerobic. The final electron acceptor is oxygen in aerobic respiration, while other molecules play this role in anaerobic respiration [96]. Therefore, mammalian cells count only with enzymatic

machinery for carrying out aerobic respiration. Still, they can produce ATP as a side-product of no oxygen-dependent metabolic pathways, such as reducing pyruvate to acid lactic, widely known as lactic fermentation [101]. In terms of ATP production rates, aerobic cell respiration has the highest efficiency since one glucose molecule can yield up to 38 ATP molecules. In contrast, ATP production is significantly lower in pathways with no oxygen involved. For instance, only two ATP molecules are synthesized in the lactic acid pathway [102].

Aerobic respiration is divided into three consecutive and interrelated stages: glycolysis, the tricarboxylic acid cycle (TCA), and oxidative phosphorylation, as shown in Figure 1-3 [103]. In glycolysis, glucose is incorporated into the cytoplasm and is converted to pyruvate through the Embden-Meyerhof pathway. During the first reactions of this pathway, corresponding to the conversion of glucose into two three-carbon sugar phosphates, 2 ATP molecules are consumed per glucose molecule. Nevertheless, a net gain of two pyruvates, 2 ATP and 2 NADH + H⁺ molecules, is obtained from one glucose molecule after the completion of glycolysis.

The obtained pyruvate molecules are then conducted into a mitochondria matrix and cleaved into an Acetyl-CoA molecule, receiving a CO₂ molecule and a NADH+ H⁺ molecule as well. Acetyl-CoA is then incorporated in the TCA cycle, where it is converted to 2 CO₂, a GTP (similar to ATP), 4 NADH, and FADH₂ and 3H⁺ [104]. Finally, NADH + H⁺ and FADH₂ produced in the previous stages can be transformed into ATP through oxidative phosphorylation. The oxidative phosphorylation is an enzymatic electron transport chain placed on the mitochondrial intermembrane, where NADH and FADH₂ molecules are oxidized to produce 5 ATP, NAD⁺, and FAD⁺ molecules. At the end of oxidative phosphorylation, the oxygen molecules receive the electrons, being consequently reduced into water [105].

Although oxygen is not directly related to neither the TCA cycle nor the Embden-Meyerhof pathway, its absence in oxidative phosphorylation limits the accomplishment of the two other stages because of the diminution in the reoxidation rate of NADH H⁺ into NAD⁺. Suppose oxygen is not present at the end of the electron transport chain. In that case, NADH H⁺ is accumulated, thus, restricts the completion of intermediate steps in the Embden-Meyerhof pathway and the conversion of pyruvate to Acetyl-CoA. [96].

As a response to the diminution of the ATP production rate due to oxygen lack in the mitochondria, mammalian cells resort to the intensification of the lactic fermentation, which leads to lethal

consequences for cells. In the first place, since the ATP production rate from this pathway is significantly lower than from aerobic respiration, the carbohydrate consumption rates necessarily have to rise drastically to fulfill the ATP demand [106]. This accelerated consumption reduces the availability of the carbon source in the medium proportionally, curtailing the culture time. Besides, the production of large quantities of lactic acid causes a diminution in the medium pH and an increase in osmolality, occasioning an imbalance in cell surroundings [107]. The summation of these conditions and the consequences of the ATP lack lead eventually to cell death.

Accordingly, higher energy availability would be associated with optimal use of nutrients, and therefore, with healthier cultures. Nevertheless, it is also necessary to consider some secondary products of oxidative phosphorylation, which have harmful effects on cells. These compounds are denominated Reactive Oxygen Species (ROS). They are a group of molecules derived from oxygen, which display high reactivity towards an extensive array of biomolecules due to their oxygen content or the presence of unpaired electrons [108]. In bioreactors, reactive species can be generated within the cell, mainly in the mitochondria or in the culture media, due to deterioration of media components by elevated oxygen concentration, light, or other components. Cells can activate a metabolic response for producing antioxidant substances that react with ROS, reducing their concentration in the cell environment. However, cells are submitted to oxidative stress when there is an imbalance between oxidant molecules accumulation and antioxidant response, which can negatively impact cell viability, productivity, and the integrity of the recombinant protein being produced.

Consequently, it is not advisable to have high oxygen concentrations that can trigger oxidative stress for the cells. To reduce oxidative stress on the cells, antioxidant agents have been added to the medium formulations to reduce the likelihood of degradation of the compounds and reduction of viability. In addition, dissolved oxygen can be controlled to limit oxidative stress. However, maintaining dissolved oxygen homogeneity in the bioreactor is complicated to study and requires particular attention during scale-up as large-scale bioreactors often present different geometries to those used during process development.

To sum up, adequate oxygen delivery to the mitochondrial membranes is vital for mammalian cell cultures. Oxygen plays the role of final electron acceptor in the aerobic respiration process, which is the most efficient metabolic pathway for ATP synthesis from carbohydrates, lipids, and proteins.

Cells require ATP for completing vital activities that allow them to proliferate. Otherwise, the synthesis of new cellular constituents and the maintenance of membrane integrity will not be possible. Moreover, the absence of oxygen promotes other metabolic pathways for obtaining energy, which is considerably less efficient and involves lethal side effects for the cell itself.

1.4.3 Oxygen-Water Phase equilibrium thermodynamics

Since all nutrients must be dissolved within the medium to be included in cell metabolism, the solubility of the substrates is a relevant factor to consider. In contrast to carbohydrates, lipids, amino acids, vitamins, and salts, oxygen solubility in water-based culture media is significantly lower. The maximum oxygen concentration in pure water in contact with saturated air at 37°C and 1 bar is 0.374 mmol O₂ l⁻¹, which is four orders of magnitude lower than the glucose solubility, that is, around 740 mmol glucose l⁻¹. Considering an imaginary experiment, where:

- CHO cells are inoculated at 1×10^9 cell l⁻¹ in 1L of fresh medium, previously saturated with air at 37°C.
- The culture medium has around 30 mmol Glucose l⁻¹, which corresponds to a commercial medium.
- After the inoculation, there is no oxygen input; that is, the only available oxygen source will be the previously dissolved oxygen.
- The specific glucose and oxygen consumption rates for a CHO cell are 0.15 pmol Glucose cell⁻¹h⁻¹ [109] and 0.16 pmol O₂ cell⁻¹ h⁻¹ [110].
- The duplication time is around 20h.
- Cells are not affected by low concentrations of metabolites; their specific consumption rate will be the same.

Under this hypothetical scenario, Oxygen would be depleted entirely after 2.3h, whereas the glucose concentration is practically the same after the same time. For this reason, the constant oxygen demand must be fulfilled by a continuous oxygen supply to the medium. This feature represents a technical challenge, which must be understood starting from analyzing the constraints imposed by thermodynamics for oxygen solubilization in a water-based media.

For describing phase equilibrium of the oxygen-water system at culture conditions, it is necessary to consider both the chemical nature of each component and the influence of culture conditions on how they interact.

On the one hand, oxygen is a non-polar molecule with two oxygen atoms united by a double covalent bond. It is commonly found as a colorless, odorless, tasteless gas occupying 21% of the atmosphere volume on average [111]. On the other hand, water is a colorless, odorless, and tasteless liquid at common culture conditions. Water molecules are strongly polar, which allows them to dissociate salts and other polar substances, such as acids, due to the action of hydrogen bonds.

The difference of polarities constrains the amount of oxygen that can be dissolved in water. Since critical oxygen temperature is 154.6 K, this system corresponds to dissolved gas in a liquid under temperature and pressure conditions. The presence of gas in the liquid has no significant impact on the liquid's physical properties [112]. Therefore, with the assumption of no excess properties, the Henry law is the most suggested model (1-2) for describing the solubility of oxygen in the water.

$$x_{O_2} = \frac{y_{O_2}P}{H} \quad (1-2)$$

Assuming that the system is in equilibrium, x_{O_2} is the solubility of oxygen in water, y_{O_2} is the oxygen composition in the gas phase, P is the total pressure, and H is the Henry parameter for this system. Henry parameter values are obtained experimentally and depend strongly on temperature and other dissolved components in the liquid, as shown in Figure 1-4.

Although equation (1-2) allows calculating oxygen solubility in water, mass transfer phenomena constrain the total quantity of dissolved oxygen in the bioreactor. Therefore, it is necessary to analyze how oxygen is transferred and the alternatives for increasing the rate of oxygen supply.

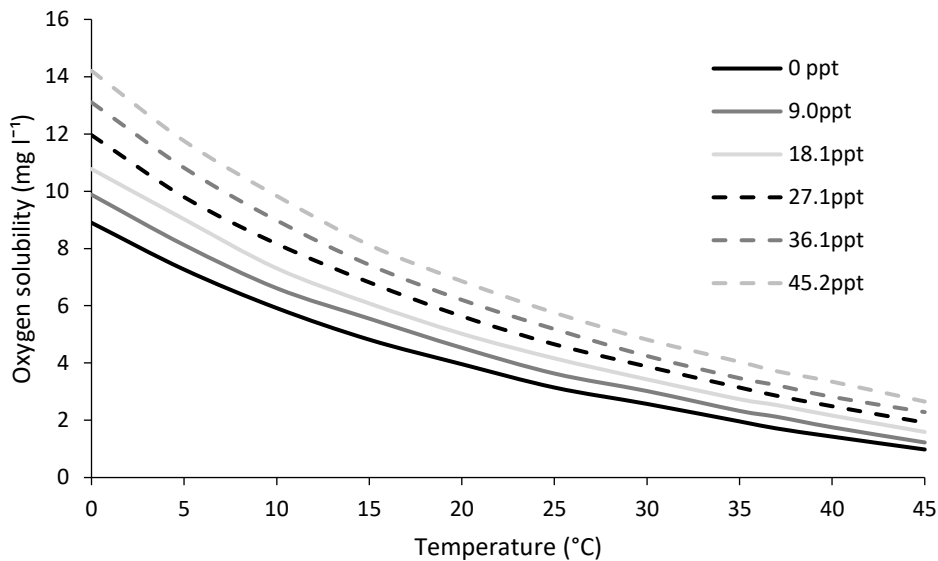


Figure 1-4: Oxygen solubility in NaCl aqueous solutions exposed to air at 1 bar with different temperatures [113].

1.5 Gas-liquid mass transfer in bioreactors

To estimate if the culture conditions limit cell growth, it is necessary to describe the path of oxygen molecules from the oxygen source to the mitochondria. Assuming that air is either bubbled or continuously renewed in the headspace and the absence of concentration gradients within the bubbles or the headspace, the oxygen source concentration corresponds to point A in Figure 1-5. Thus, although air is the most common oxygen source, air with higher oxygen concentrations than 21% can increase the oxygen transfer to the medium.

The two-films model for describing gas-liquid mass transfer [114] considers that the resistance to mass transfer in a given turbulent fluid phase is present in a thin layer adjacent to the interface, as shown in Figure 1-6. Thus, according to this model, two hypothetical, stagnant thin layers are present: the liquid region in contact with gas molecules and the gas region in touch with the liquid. Fick's law describes the flux through the films because mass transport is governed essentially by molecular diffusion within these hypothetical layers.

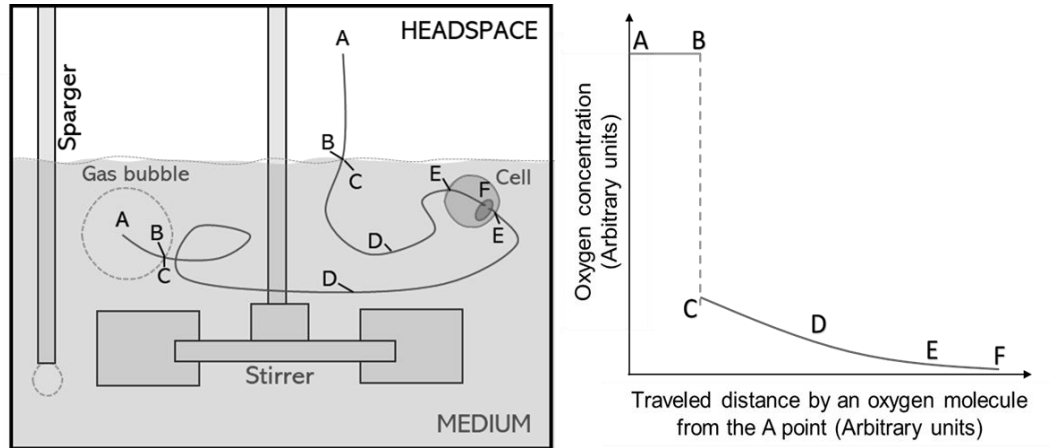


Figure 1-5: Scheme of the path of an oxygen molecule from the headspace to the mitochondria.

Equation (1-3) presents the flow of oxygen through the thin liquid layer, where J^0 is the oxygen molar flux through the gas-liquid interphase, D is the diffusivity of oxygen in medium, $C_L(z)$ is the concentration of oxygen as a function of the normal distance from the interphase, z .

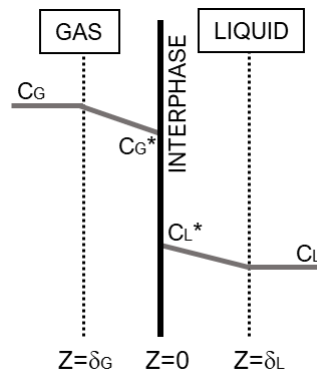


Figure 1-6: Two-films theory scheme.

$$J^0 = -D_{O_2L} \frac{\partial C_L(z)}{\partial z} \quad (1-3)$$

Suppose the thickness of the stagnant film is given by δ . In that case, the gradient can be approximated by (1-4), where C^*_L is the oxygen concentration in the liquid interphase, and C_L is the oxygen concentration in the bulk of the liquid:

$$\frac{\partial C_L(z)}{\partial z} \cong \frac{C_L^* - C_L}{\delta_L} \quad (1-4)$$

Usually, the ratio D/δ is unknown since the thickness of the films depends on the flow conditions and is replaced by a mass transfer coefficient k_L , which considers the mass transfer resistance of this film (1-5). Similarly, equation (1-6) presents the same development for the gas phase.

$$J^0 = -D_{O_2L} \frac{C_L^* - C_L}{\delta_L} = -k_L(C_L^* - C_L) \quad (1-5)$$

$$J^0 = -D_{O_2G} \frac{C_G - C_G^*}{\delta_G} = -k_G(C_G - C_G^*) \quad (1-6)$$

Considering that the saturation condition is achieved in the interphase, C_G^* and C_L^* are, in fact, the oxygen concentration at the equilibrium condition, which corresponds to Henry's Law (1-2). Therefore, employing (1-7) and overall mass transfer coefficient K_L can be defined as the difference between a hypothetical liquid concentration in equilibrium with the oxygen concentration in the gas bulk and the actual oxygen concentration in the liquid bulk.

$$J^0 = -K_L(C_G - C_L) \quad (1-7)$$

From (1-2), (1-5), (1-6), and (1-7), it is possible to define the resistance to mass transfer in equation (1-8).

$$\frac{1}{K_L} = \frac{1}{Hk_G} + \frac{1}{k_L} \quad (1-8)$$

Due to low oxygen solubility in water, the product Hk_G is significantly larger than k_L , allowing disregarding the gas phase's resistance and considering the overall mass transport coefficient as just the local liquid coefficient. Henceforth, C^* will be referred to as the oxygen solubility in the liquid.

$$J^0 = k_L(C^* - C_L) \quad (1-9)$$

Once oxygen crosses the interphase, it is referred to as dissolved oxygen (DO). Then, the oxygen molecule remains within the following liquid convective transport gradients (Figure 1-5-D) until, at some point, it is incorporated by the cell through a passive transport mechanism (Figure 1-5-E). Once within the cell, oxygen travels in the cytoplasm until finding a mitochondrion, where it is

eventually reduced to water at the end of the electron transport chain (Figure 1-5-F). Thus, the steps described from Figure 1-5-D to Figure 1-5-F represent no significant resistance to mass transfer, considering that liquid is in a continuous movement that prompts mass transfer and oxygen follows passive mechanisms for the crossing cell membrane.

Multiplying the term J^0 by the total interfacial area (a), oxygen transfer rate (OTR) can be defined as in Equation (1-10):

$$OTR = aJ^0 = k_L a(C^* - C_L) \quad (1-10)$$

Since the local liquid mass transfer coefficient and the total interfacial area are challenging to determine separately, these factors are measured as a single factor called volumetric mass transfer coefficient ($k_L a$). The presence of an oxygen concentration gradient was demonstrated within the liquid in bioreactors at a large scale [115], and thus, a gradient of $k_L a$ according to strictly to Equation (1-10). However, it is considered that the short mixing times in lab-scale scales as Spinner and Erlenmeyer flasks allow considering a single $k_L a$ value for a determined set of operating conditions [116]. The Annex summarizes the $k_L a$ values for different scales and bioreactor configurations, which evidence that the larger the scale is, the lower the vigorous conditions required for achieving a determined $k_L a$ value.

Estimating the quantity of oxygen that cells demand is usually done by calculating the Oxygen Uptake Rate (OUR), presented in Equation (1-11), where q_{O_2} is the cellular specific oxygen consumption and X is the cell concentration. OUR and specific oxygen consumption have been used to characterize fermentation productivity and cellular metabolism for various cell types. They have been considered as indicators of the cell state/function. Recently, OUR has also been suggested for quantifying the physiological state of anaerobic culture [117] or as a screening tool for identifying more productive or promising strains [118] [119].

$$OUR = q_{O_2} X(t) \quad (1-11)$$

According to the cell line, the specific cell consumption rate changes. Although the oxygen uptake rate of these cultures is at least two orders of magnitude lower than microbial cultures, mammalian cells are susceptible to shear stress and air bubbles. In

Table 1-7. Specific oxygen consumption rate for different microorganisms [120], [121]

Process	Specific oxygen consumption rate ($\text{kmol m}^{-3} \text{ h}^{-1}$)
Acetic acid	0.031
Antibiotic production	0.031
<i>Escherichia coli</i>	0.44
Mammalian cells	0.002

Finally, defining the culture medium as the control volume, the mass oxygen balance is defined as in Equation (1-12):

$$\frac{dC_L}{dt} = OTR - OUR \quad (1-12)$$

Equation (1-12) is equivalent in bioreactors to Equation (1-13):

$$\frac{dC_L(t)}{dt} = k_La(C^* - C_L) - q_{O_2}X(t) \quad (1-13)$$

The cell concentration can be expressed in terms of the duplication time (t_d) if the cells are in an exponential growth stage. The specific growth rate (μ) is defined as in equation (1-14).

$$\mu = \frac{\ln(2)}{t_d} \quad (1-14)$$

Thus, the exponential phase growth of the cells can be calculated as in equation (1-15):

$$X(t) = X_0 e^{\mu t} \quad (1-15)$$

By solving Equation (1-13) for DO concentration with the assumption of a constant k_La and q_{O_2} , a helpful expression is obtained for predicting the behavior of DO concentration during the exponential growth of a cell line. For example, when the culture achieves critical values of DO concentration or when the medium is depleted of oxygen. It is reiterated that the predictions made with this model will be valid if the cells are in exponential growth and are only limited by oxygen availability. However, if there is another substrate limiting the cells, such as the lack of the carbon or nitrogen source or the presence of a toxic compound, the model itself cannot make corrections for other deficiencies.

$$C_L(t) = C^* - \frac{q_{O_2} X_o}{k_L a + \mu} e^{\mu t} + \left(C_{Lo} - C^* + \frac{q_{O_2} X_o}{k_L a + \mu} \right) e^{-k_L a t} \quad (1-16)$$

To make predictions for a particular case, knowing the parameters for calculating OTR and OUR is necessary. A brief description of the bioreactor systems studied and how these parameters can be determined will be presented below.

1.6 Gas-liquid mass transfer in bioreactors

Determining the OTR and OUR of equation (1-12) is essential for establishing the effect of operating variables on oxygen supply. For example, once temperature, pressure, and medium are settled, the equation defines oxygen solubility (1-2). Since cell concentration (X) and DO concentration are commonly monitored variables, $k_L a$ and q_{O_2} are the estimated parameters.

Different methods have been developed to measure $k_L a$ and q_{O_2} from direct or indirect measurements of dissolved oxygen concentration in a liquid subjected to specific operating conditions in a bioreactor in a period. When selecting a method, the following factors should be considered: the aeration and homogenization systems used, the bioreactor type and its mechanical design, the composition of the fermentation medium, and the possible effect of the presence of microorganisms [122]. Measurement methods can be classified according to their nature into chemical or physical, whose features are summarized in Table 1-8.

Chemical methods are based on quantifying a chemical substance that reacts with the dissolved oxygen or even with other gas species dissolved in the liquid. Starting from a known work volume of a solution that has determined initial reactant concentration, the liquid is subjected to stirring or bubbling to allow oxygen (or gas) solubilization. Then, samples are obtained to select the remaining quantity of the reactant, and indirectly, the amount of reacted oxygen through time. These methods have mainly three drawbacks. First, culture media have components that may react with the reactant, occasioning a misestimation of the parameter. Second, some reactants are harmful to cells, which restricts their use just for $k_L a$ determination. Third, assumptions about the order of reaction kinetics may lead to misestimation.

Table 1-8: Methods of $k_L a$ and q_{O_2} determination

Method		Assay time	Scale applied	Assumptions / drawback	Ref.
Chemical	Sodium sulfite	Hours	Lab and pilot	Differences in fluid properties between sodium sulfite solutions and culture media, complex reaction kinetics. Not suitable for the microbial process. Fairly intensive labor.	[123]
	Absorption of Carbon dioxide	Minutes	Lab	Differences of fluid properties between alkaline solution and culture media. Complex reaction kinetics. Not suitable for microbial processes.	[124]
	Bio-oxidation of catechol	Minutes	Lab	Availability of oxidative enzyme. It is limited to a small scale.	[125]
	Measurements pH for CO ₂ solutions	Minutes	Any	Salt addition does not improve the mass transfer rate of CO ₂ . Unsuitable for the microbial process.	[126]
Physical	Mass balance	Hours	Any scale	Mixing times can be significant at large scales. Short air residence time in the bioreactor may not generate a considerable measure. The accuracy depends on the precision of the oxygen analyzer.	[72]
	Dynamic gassing in/out	Minutes	>100 mL	Probes are necessary. Probe response time must be considered. Mixing times can be significant at large scales. Dynamic changes in	[127]

Method		Assay time	Scale applied	Assumptions / drawback	Ref.
				dissolved oxygen along the test may disturb the microbial metabolism	
	Dynamic measurement of headspace	Minutes	<100 mL	Optical oxygen probes are necessary. Dynamic changes in dissolved oxygen along the test may disturb the microbial metabolism	[128]

The mass balance method is based on the direct measurement of oxygen composition of the inlet and outlet gas flows. Since the internal pressure in the bioreactor remains constant, it can be assumed that the inlet and gas flows are equal in quantity but differ in concentration. $k_L a$ can be determined starting from an oxygen saturated liquid and then subjected to a no-oxygen gas flow. The dissolved oxygen will be desorbed and will enrich with oxygen the outlet flow. The same can occur starting from an oxygen-depleted liquid that is subjected to airflow. Subsequently, q_{O_2} can be estimated employing the same methodologies as in the dynamic methods. This method is not invasive and entirely accurate. However, the equipment cost is the main reason for its scarce applications [119].

1.6.1 Dynamic gassing methods

Physical methods are based on the response of oxygen concentration in either the liquid, the headspace, or the inlet/outlet gas streams under non-stationary conditions; thus, they are also named dynamic methods. Since the measurement process has no direct impact on cell viability, these methods are preferred for oxygen transfer and q_{O_2} estimation. A determined calculation strategy is required according to the place in the bioreactor where oxygen is measured.

If the probe is placed in the bulk of the liquid, it is referred to as dynamic absorption/desorption or dynamic gassing out/in [127]. This technique is based on the system's response to a step-change in the concentration in the inlet gas. The typical case of dynamic desorption starts with an air-

saturated medium. Then, the air in the headspace and bubbling flow is replaced by gas with a lower concentration than the gas the medium was first saturated. It is usual to replace it with pure nitrogen or argon. This new condition results in a reduction of dissolved oxygen concentration, as shown in Figure 1-5A. Assuming that all the requirements for equation (1-12) are accomplished, the oxygen desorption rate can be expressed in equation (1-17), where C^* corresponds to the phase equilibrium concentration according to Henry's Law.

$$\frac{dC_L}{dt} = k_La(C^* - C_L) \quad (1-17)$$

Since C^* is lower than C_L , the change of dissolved oxygen concentration will decrease over time.

In case oxygen is replaced by pure nitrogen or argon, the oxygen desorption rate results in:

$$\frac{dC_L}{dt} = -k_LaC_L \quad (1-18)$$

Since the probe continuously measures the dissolved oxygen concentration, it is possible to determine k_La by solving equation (1-17) integrating two measurement times, as indicated in equation (1-19).

$$k_La = \frac{\ln\left(\frac{C_{L2}}{C_{L1}}\right)}{t_1 - t_2} \quad (1-19)$$

A similar procedure is obtained starting from an oxygen-poorly concentrated or depleted medium, known as dynamic gassing-in. The dissolved oxygen concentration would increase if an oxygen-containing gas were supplied, as shown in Figure 1-5B, following the absorption rate expressed in equation (1-20).

$$\frac{dC_L}{dt} = k_La(C^* - C_L) \quad (1-20)$$

Once again, k_La is obtained by solving equation (1-17) integrating two measured moments.

$$k_La = \frac{\ln\left(\frac{C^* - C_{L2}}{C^* - C_{L1}}\right)}{t_1 - t_2} \quad (1-21)$$

k_La values obtained by both methodologies should correspond to the same value since both describe the same phenomenon. Ideal measured curves are shown in Figure 1-7.

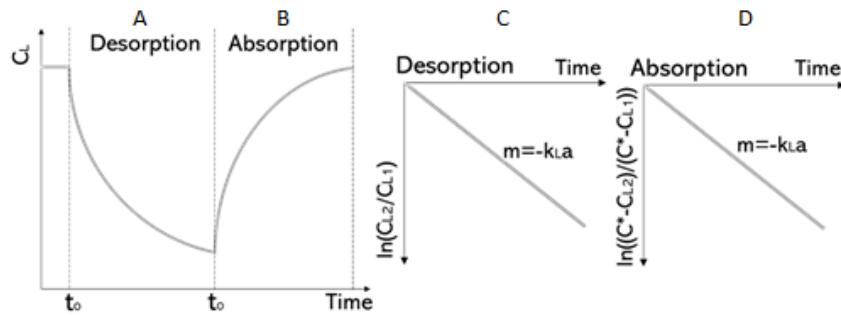


Figure 1-7: Expected measured data for A: dynamic gassing out and B: dynamic gassing in. Data analysis for $k_L a$ determination by C: dynamic gassing out and D: dynamic gassing out methods.

If q_{O_2} is the parameter to estimate, a combination of both desorption and absorption methodologies is usually employed [121]. After suspending mixing and aeration to an oxygen-saturated medium with a known cell concentration, oxygen concentration will decrease due to cell consumption, as shown in equation (1-22). As the system remains still, the change in oxygen composition will be attributed to cell consumption. It is necessary to consider that dissolved oxygen concentrations below certain levels can affect the cell culture irremediably. For mammalian cells, it is not recommended to achieve DO concentrations under 20% air saturation [129]; [130].

$$\frac{dC_L}{dt} = -OUR = -q_{O_2}X \quad (1-22)$$

After the desorption stage, mixing and aeration are turned on, increasing oxygen concentration according to equation (1-23). After integrating equations (1-12) and (1-23), a two equations system is obtained, where $k_L a$ and q_{O_2} are the variables. Since measurement times are orders of magnitude smaller than duplication times of mammalian cells (~ 24 h), it can be assumed that cell concentration remains constant during the experiment. q_{O_2} can also be estimated with a single gassing-in experiment and equation. However, the $k_L a$ value must be previously known.

$$\frac{dC_L}{dt} = k_L a(C^* - C_L) - q_{O_2}X \quad (1-23)$$

The same parameters can be estimated from similar procedures based on the oxygen concentration measurements of the headspace. Lab-scale equipment has been developed to analyze oxygen transfer in shaken Erlenmeyer flasks and well plates from measurements of the headspace [131], [132]. These devices count with an oxygen sensor for the headspace, a differential pressure sensor, and a valves system that allows or restricts the gas flow to or from the headspace.

During a measurement cycle without cells, k_La can be estimated by changes in the headspace concentration employing the valves system for supplying air or nitrogen. As the headspace is the oxygen source, oxygen absorption in or desorption out of the liquid will change composition in the headspace in a sealed system. Then, it is possible to relate oxygen transfer processes with the ideal gas state equation (1-24).

$$OTR = \frac{dp_{O_2}}{dt} \frac{V_g}{RTV_L} \quad (1-24)$$

Since the system is closed, the total oxygen moles remain constant, although oxygen can be dissolved in the liquid or the headspace. Hence, it is possible to relate the oxygen partial pressure and the dissolved oxygen concentration through equation (1-25). Consequently, k_La can be calculated as in equation (1-26).

$$C_L = \frac{mol_i O_2}{V_L} - \frac{p_{O_2} V_g}{RTV_L} \quad (1-25)$$

$$k_La = \frac{OTR}{C^* - \frac{mol_i O_2}{V_L} + \frac{p_{O_2} V_g}{RTV_L}} \quad (1-26)$$

The culture medium with cells is first placed within the device with an air atmosphere for determining OUR. When the oxygen concentration in the headspace is constant, the valves system seals the culture device, interrupting the airflow. The respiration of microorganisms induces a diminution in the partial pressure of oxygen and an increase in the carbon dioxide partial pressure in the headspace of the bioreactor. Since the system is sealed and mass transfer resistances are rejected, the change in oxygen concentration in the gas corresponds to the oxygen consumed by the cells [117]. If the system is still while cells consume the remaining oxygen, the OUR corresponds to equation (1-27). Nonetheless, if the system remains in movement, the OTR value in the medium without cells must be known in advance, as shown in equation (1-28).

$$OUR = -\frac{dp_{O_2}}{dt} \frac{V_g}{RTV_L} \quad (1-27)$$

$$OUR = OTR - \frac{dp_{O_2}}{dt} \frac{V_g}{RTV_L} \quad (1-28)$$

Although dynamic gassing methods are reliable and widely employed, the singularity of each system, the delay times associated with the measuring systems, and experimental mistakes could lead to the wrong estimation of the parameters (Koizumi and Aiba 1984). In general terms, it is

denoted that the characteristic response time of the probe must be much lower than the inverse of the intended k_La value to measure.

1.7 k_La as scale-up parameter

Stirred tanks are widely used in the industry because of the accumulated knowledge of this bioreactor configuration and its versatility [122]. Nevertheless, the presence of mobile parts that interacts out and inside the bioreactor increases the contamination risks. But also, the shear stress rates that can be achieved due to the impeller rotation can harm lethally the cultured cells, which will have a negative impact on bioreactor performance.

In terms of mass oxygen transfer, oxygen can be supplied from either the headspace or bubbles. Although volumetric mass transfer coefficients are improved employing bubbling, the presence of zones with high shear stress rates at bubble rupture concerns the use of this method for longer and healthier cultures. On the one hand, large bubble sizes reduce the frequency of high shear stress rates, but on the other, small bubble sizes improve the mass transfer by increasing the total interphase area.

Stirring is essential in cultures of suspended cell lines. Without medium movement, the cells would precipitate or aggregate among themselves, decreasing cell viability by flocs or cluster formation. In cell floc structures, cells are assembled so that surface cells are continuously supplied nutrients and oxygen. However, the surface cells limit the contact of the interior cells with the medium, causing possible hypoxia or the lack of other nutrients, and eventually, cell death. In addition, because internal cells are not programming their metabolism for death, proteases and other undesired cell products may be liberated, occasioning death in cascade reaction in the cell floc.

The fluid flow regime in stirred tanks is intimately related to the stirrer speed, diameter, and liquid properties. When the fluid is agitated under a turbulent regime, convective transfer rates dominate within the liquid. For that reason, heat, mass, and moment transfer parameters are intimately related to the stirring speed and bioreactor size. For instance, these parameters are the mixing time, convective heat coefficient, or the volumetric mass transfer coefficient.

The volumetric mass transfer coefficient in stirred bioreactors can be estimated by employing dimensional analysis or empirical equations. The dimensional analysis uses adimensional numbers

to establish similarities between the mass, momentum, and heat transfer mechanisms. However, this method is not widely used due to the inaccuracy associated with theoretical simplifications and estimates. In contrast, empirical equations are the most reported tool for k_La estimation. It is essential to mention that the perfect mixing condition is one crucial assumption for defining a single k_La value for a bioreactor under determinate operation conditions. Nevertheless, the larger the liquid volume is, the most difficult it is to assure absolute homogeneity. For that reason, the very last attempts for gas-liquid mass transfer determination are oriented to determine a k_La profile employing computational tools.

Empirical equations unconditionally require experimental validation. Generally, these models relate mathematically measurable variables with the desired operational parameter. One of the most used models for correlating operation conditions with k_La was presented by Cooper. The stirring and bubbling effect were standardized in this work in two variables: the power input per volume unit and the superficial gas velocity. The power input per volume unit is related to the momentum that is transferred to the liquid. Since liquid can be moved by the effect of the impeller or the bubbles that rise, total power input is considered the sum of two contributions. The superficial gas velocity is a parameter that relates the bubbling inlet flow with the transversal surface of the liquid.

The volumetric mass transfer coefficient is empirically related to equation (1-29), where K , α , and β are empirical parameters. K constant englobes the effects of other variables, such as medium composition and temperature, considered constant in a culture. Typical values for these parameters are between 0 and 1; the k_La value increases asymptotically as P/V or v_s values are more extensive.

$$k_La = K \left(\frac{P}{V} \right)^\alpha (v_s)^\beta \quad (1-29)$$

In the last decades, impeller design is an area that has been in continuous development. At first, it was thought that impeller shape did not influence mass transfer. Nevertheless, further studies demonstrated that it directly impacts the mixing times due to the formation of intern recirculation zones. Rushton impeller is widely used for bacterial and fungal cultures, especially for cultures that increase their viscosity as cells grow. In mammalian cells, marine impeller geometries are used. The main reason is that marine impeller geometries reduce the shear stress rates in the liquid.

Another typical parameter in mammalian cell cultures is the ratio between liquid height and bioreactor diameter (H/D), which is lower than microbial culturing bioreactors. Although mammalian cells are the cell lines that have the lowest specific oxygen consumption rates, these microorganisms are not facultative. In other words, they always require a minimum amount of dissolved oxygen in their surroundings. Otherwise, they get stressed or even dead. This requirement demands a bioreactor design that reduces the possibility of the presence of hypoxia and anoxia zones. As the liquid height increases, the probability of achieving zones with lower oxygen concentration than the critic is higher [133].

Bubbling must be carefully set on bioreactors for mammalian cell cultures. Bubbles undeniably help to increase the volumetric mass transfer coefficient. Nevertheless, they harm cells. On the one hand, the cell rupture procedure involves regions with higher shear stresses, which could cause a diminution of cell viability. Furthermore, the more frequent bubbles rupture, the more cells can be damaged. On the other hand, a low occurrence of bubbles will not significantly influence $k_L a$ values [88].

2. Improved experimental determination of the Volumetric Mass Transfer Coefficient for two bioreactor configurations and the specific oxygen consumption rate for a CHO cell line.

As the size of the bioreactor increases, Oxygen supply is often the limiting parameter that constrains the growth of cells that depend on aerobic respiration, such as mammalian cells. Since the volumetric mass transfer coefficient (k_{La}) is directly related to the Oxygen Transfer Rate (OTR) to the culture medium, keeping the k_{La} value among scales is one of the most used bioreactor Scale-up criteria. OTR and, therefore, k_{La} value depends on the physicochemical characteristics of the culture medium, bioreactor geometry, and operation conditions, such as temperature, stirring speed, or bubbling. Therefore, OTR is a critical parameter in bioreactor design. If this value is lower than the Oxygen Uptake Rate (OUR), the oxygen supply will be insufficient for the cells, eventually affecting the culture viability. OUR depends on the cell concentration and the specific consumption rate (q_{O_2}), a cell line-particular parameter. This work described the effect of two operation variables on the k_{La} value for two lab-scale bioreactor configurations: a shaken baffled Erlenmeyer and a Spinner flask. These bioreactor configurations have been modified from their standard commercial for online measurement of Dissolved Oxygen (DO) concentration within the medium, including a sparger accessory in the Spinner flask. The experiments were performed employing water and a commercial cell culture medium and varying the filling volume and the shaken speed for the Erlenmeyer bioreactor and the stirring speed and bubbling flow for the Spinner flask. An improved methodology for the dynamic Gassing in/out method was suggested, validated, and performed to determine the k_{La} value for both geometries. The improvements were derived considering the error caused by the characteristics of the probe, the change of Headspace, and the time for

conditions set up. Finally, the q_{O_2} for a suspended CHO cell line was determined through the improved dynamic Gassing in/out method. The obtained results for k_{La} are comparable with reported data and represent a helpful input for estimations of the behavior of CHO cells on larger scales.

2.1 Introduction

2.1.1 Bioreactor Scale-up

The term Process Development refers to creating economically viable means to manufacture a product with determining quantity parameters. At an initial stage, Process Development involves selecting and sequencing process steps from a repertoire of unit operations for transforming raw materials into the desired product. Subsequently, Process Development pursues establishing the multidimensional combination and interaction of input variables and process parameters demonstrated to assure quality. (Hejnaes and Ransohoff 2018; Łacki, Joseph, and Eriksson 2018)

Process Development for products that involve biochemical reactions is often more challenging because of the constraints imposed by the microorganism nature. (McDuffie 1991) Therefore, the cell line response description under different operation conditions is an unavoidable prerequisite for Bioprocess Development. (Doran 2013). Since culturing in small devices implies savings in terms of time and expenses, Bioprocesses Development generally starts in laboratory facilities, where the performance of the microorganisms at very controlled culture conditions is usually evaluated. Then, the most desirable conditions are transferred into larger reactors through a procedure called Scale-up. (Neubauer et al., 2013). Throughout an ideal Scale-up process, all physical and mechanical variables should remain the same; in this way, the microorganisms will behave as expected.

Nevertheless, the Scale-up procedure is not as trivial since several culture conditions depend on the transport phenomena within the bioreactor, which change as the culture volume increases. Likewise, changes in the culture environment inevitably alter microbial metabolism, compromising the expected yields and productivities. (Li et al. 2010) Therefore, the challenge of Bioreactor designers is to pursue devices that retain the optimum kinetics obtained at a smaller scale by assuring the most favorable conditions for cell proliferation and synthesize the product of interest, thus, achieving economically profitable processes. (Clarke 2013)

2.1.2 Oxygen mass transfer

In practice, one of the most used Scale-up strategies is to maintain a single parameter constant between scales, keeping a critical parameter constant among different bioreactor configurations, expecting that the microorganism behaves similarly. (Varley and Birch 1999) Oxygen is a crucial metabolite for aerobic cells in aerobic cell cultures due to its role in respiration. To be incorporated into cell metabolism, Oxygen must be dissolved within the culture medium. However, Oxygen cannot be massively supplied to the culture medium due to the constraint imposed by its low solubility in water; therefore, the bioreactor design must assure an adequate and continuous Oxygen transfer. The Oxygen Transfer Rate (OTR) or the rate with which Oxygen is dissolved within the medium can be described employing a convective mass transfer model as shown in Equation (2-1); where $k_L a$ is the volumetric mass transfer coefficient, C^* is the oxygen solubility in the culture medium at the operating conditions according to Henry's Law and C_L is the dissolved oxygen (DO) concentration in the liquid bulk.

$$OTR = k_L a (C^* - C_L) \quad (2-1)$$

Although Equation (2-1) model has certain limitations, especially at large scales, it evidences the direct relationship between OTR and $k_L a$. $k_L a$ is one of the most used as a Scale-up parameter for aerobic cells since $k_L a$ is a parameter that depends on the culture medium composition, the bioreactor shape, and operation conditions (Aroniada et al. 2020; Chisti 1993; Garcia-Ochoa and Gomez 2009).

An *a priori* design criterion based on Oxygen transfer dictates that the OTR should be greater than or equal to the cells' Oxygen Uptake Rate (OUR). Otherwise, the amount of Oxygen available for the cells to breathe will decrease until hypoxic/anoxic conditions are reached. Then, the cells will be forced to modify their metabolism by slowing down their growth. OUR is usually calculated as shown in (2-2), where X is the cell concentration, and q_{O_2} is the specific oxygen consumption, which corresponds to the amount of Oxygen consumed by a cell per unit of time. X depends on the inoculum and the replication rate, while q_{O_2} is a proper parameter of the cell line.

$$OUR = q_{O_2} X \quad (2-2)$$

Oxygen can be supplied to a medium in a bioreactor from either the Headspace or bubbles. The parameters that define how rapidly oxygen dissolves are the turbulence within the liquid and the

contact area between the headspace or bubble gas as the oxygen source and the medium. The higher the turbulence and the greater the surface area, the faster the liquid's Oxygen will enter. However, agitation will be limited by the resistance of the microorganism to shear stresses rates, since at very turbulent regimes, the likelihood of lethal regions within the bioreactor for the cells increases. In addition, the way the liquid is moved depends on the bioreactor configuration. For this work, a shaken Erlenmeyer and a Spinner flask were studied. Although they are widely used laboratory-scale geometries and have similar volumes, their shape and movement mechanism differ significantly from each other.

On the one hand, shaken flasks are widely used devices in research at a laboratory scale. This group is considered Erlenmeyer, conical, and well-plates, and other vessels that contain a liquid and are oscillatory moved by the action of an external shaking agent. These devices are frequently used because of their simplicity, the possibility of carrying out parallel experiments in a very cheap way, and the high gas-liquid transfer rates that can be easily achieved. (Büchs 2001; Andy A. Lin, Kimura, and Miller 1993; Zhu et al. 2017) On the other hand, Spinner flasks devices are conformed by a cylindrical glass or polymeric vessel with a stirring magnetic element located either at the bottom or anchored to a shaft. Fluid is moved by the action of an external magnetic field, creating a suitable environment for cell growth. These vessels also count on several accessories to improve their performance, like baffled sections or lateral outputs for sampling or gas transfer with the surroundings. The simplicity of spinner flasks has allowed their implementation in cultures of suspension-adapted and anchorage-dependent mammalian cell lines. (Hewitt et al. 2011; Liovic et al. 2012; Singh 1999; Sucosky et al. 2004) In addition, spinner flasks are an attractive alternative for screening and scale-down procedures due to their evident geometrical similarity with large-scale stirred tanks. (Karimi et al. 2013)

2.1.3 Dynamic Gassing in/out methods for k_{La} and q_{O_2} determination

Dynamic Gassing in/out or absorption/desorption method is based on the response of DO concentration under non-stationary conditions (Tribe, Briens, and Margaritis 1995); namely, this technique is based on the reaction of the system to a step-change in the concentration in the inlet gas. Depending on the inlet gas oxygen concentration and the DO concentration at the experiment start point, Oxygen is absorbed in or desorbed from the liquid. In this way, if the change in DO concentration is continuously measured, a model can be proposed for describing it is possible to

explain how Oxygen is transferred from or to the liquid medium. Furthermore, since the measurement process has no direct impact on cell viability if some cautions are followed, these methods can be used for $k_L a$ and q_{O_2} estimation.

The typical dynamic Gassing out or desorption starts with a saturated medium with air at the operating conditions. Then, the headspace and bubbling inlets are replaced with gas with a lower oxygen concentration than the air with which the medium was saturated. Nitrogen or argon are usually used as desorption gasses. This new condition results in a reduction of DO concentration. The change in DO concentration is expressed as in Equation (1-17).

$$\frac{dC_L}{dt} = k_L a (C^* - C_L) \quad (2-3)$$

Since C^* is lower than C_L , the change of DO concentration will decrease over time. In case oxygen is replaced by pure Nitrogen or argon, the oxygen desorption rate is Equation (2-4):

$$\frac{dC_L}{dt} = -k_L a C_L \quad (2-4)$$

Since the probe continuously measures the dissolved oxygen concentration, it is possible to determine $k_L a$ by solving Equation (1-17) integrating two measurement times, as indicated in Equation (1-19).

$$\ln\left(\frac{C_{L_2}}{C_{L_1}}\right) = k_L a (t_1 - t_2) \quad (2-5)$$

A similar procedure is obtained from an oxygen-poorly concentrated or depleted medium known as dynamic gassing-in. If an oxygen-containing gas were supplied, the dissolved oxygen concentration would increase, following the absorption rate expressed in Equation (1-20).

$$\frac{dC_L}{dt} = k_L a (C^* - C_L) \quad (2-6)$$

Once again, $k_L a$ is obtained by solving Equation (1-17) integrating two measured moments.

$$\ln\left(\frac{C^* - C_{L_2}}{C^* - C_{L_1}}\right) = k_L a (t_1 - t_2) \quad (2-7)$$

$k_L a$ values obtained by both methodologies should correspond to the same value since both describe the same phenomenon. Ideal measured curves are shown in Figure 1-7.

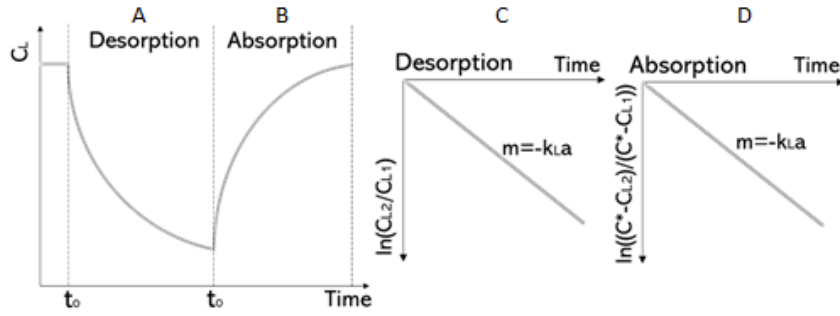


Figure 2-1: Expected measured data for A: dynamic Gassing out and B: dynamic Gassing-in. Data analysis for k_La determination by C: dynamic Gassing out and D: dynamic Gassing out methods.

When q_{O_2} is the parameter to estimate, a combination of both desorption and absorption methodologies can be employed as well (Garcia-Ochoa, Escobar, and Gomez 2015). After suspending mixing and aeration to an oxygen-saturated medium with a known cell concentration, oxygen concentration will decrease due to cell consumption, as shown in Equation (1-22). As the system remains still, the k_La value is despised, and oxygen composition changes will be attributed to cell consumption. It is necessary to consider that dissolved oxygen concentrations below certain levels may affect the cells irremediably. For mammalian cells, performing cultures under 20% air saturation is not recommended (Lin and Miller 1992); (Andy A Lin, Kimura, and Millert 1993).

$$\frac{dC_L}{dt} = -OUR = -q_{O_2}X \quad (2-8)$$

After the desorption stage, mixing and aeration are turned on, promoting the increase of oxygen concentration according to Equation (1-23). After integrating equations (1-12) and (1-23), a two equations system is obtained, where k_La and q_{O_2} are the variables. Since measurement times are orders of magnitude smaller than duplication times of mammalian cells ($\sim 24h$), it can be assumed that cell concentration remains constant during the experiment. q_{O_2} can also be estimated with a single gassing-in experiment and Equation. However, the k_La value must be previously known.

$$\frac{dC_L}{dt} = k_La(C^* - C_L) - q_{O_2}X \quad (2-9)$$

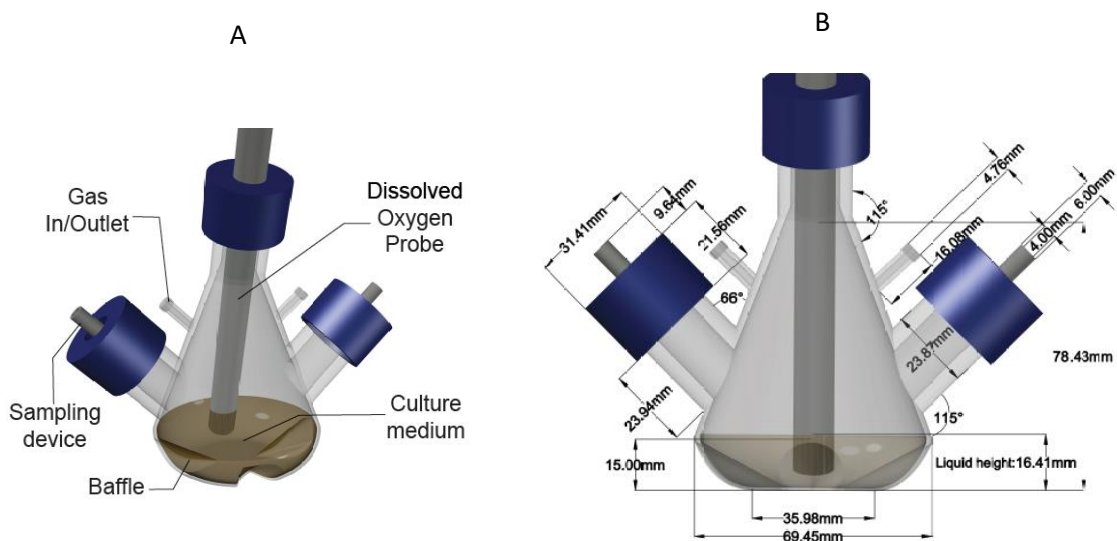
2.2 Materials and Methods

2.2.1 Bioreactor description

A glass Erlenmeyer flask and a glass Spinner flask bioreactor were employed. Their nominal commercial size was 100ml, and their measured total volumes were 148ml and 245ml \pm 1ml, respectively. In addition, both bioreactor configurations were modified from their commercial standard for allowing in-situ dissolved oxygen (DO) measurement.

Figure 2-2 presents the Erlenmeyer flask configuration. It had five nozzles: one is superior for placing a DO probe, and four are on the sides for gas exchange and sampling (Figure 2-2A). A detailed description and a cross-section of the Erlenmeyer flask bioreactor configuration are presented in Figure 2-2B and 1C, respectively. Three baffles were placed at the bottom of the vessel every 90°, leaving a no-baffled section where the DO probe tip rested (Figure 2-2D). In this way, the DO probe will be hydrodynamically equivalent to a fourth baffle. UNIMAX 1010 orbital shaker (Heidolph®, Schwabach, Germany) with a 10mm rotation diameter shook the Erlenmeyer flasks.

Figure 2-3 presents the Spinner Flasks bioreactor configuration (BellCo®, Neustadt Wied, Germany). In this case, the probe used for DO measurement also acted as the axis for the impeller rotation (Figure 2-3A). The impeller had three PTFE pieces: One covered magnet of 9mm diameter and 50mm long, one triangular paddle, and one perforated cylinder of 20mm diameter (Figure 2-3C). The side nozzles were employed for sampling and gas exchange.



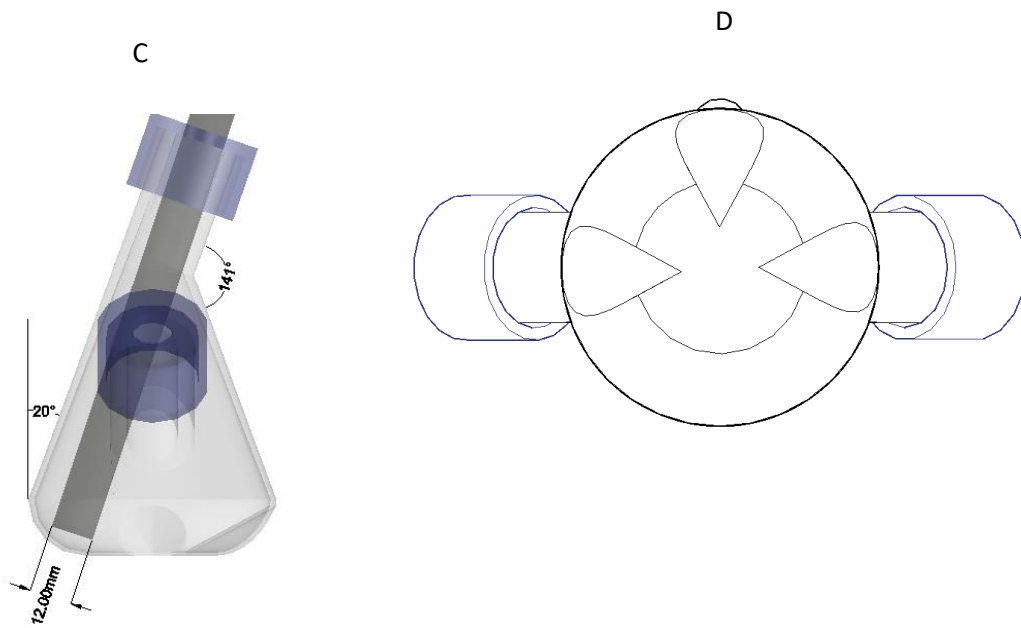


Figure 2-2: Description of Erlenmeyer flask bioreactor configuration: (A) 3D isometric view, (B) front view, (C) cross-section, and (D) 3-baffled bottom.

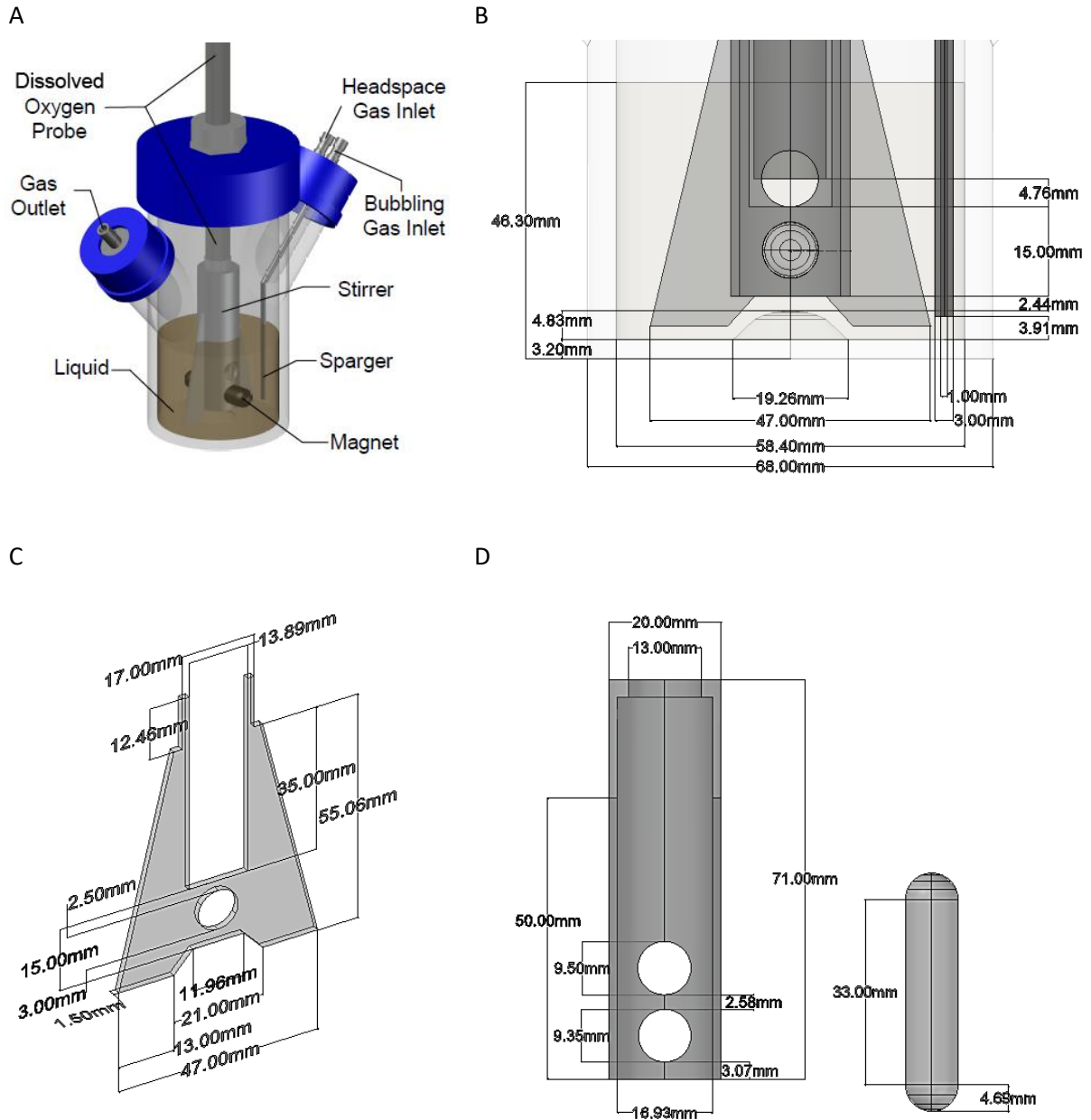


Figure 2-3: Description of Spinner flasks and impeller geometry: (A) 3D isometric view, (B) bottom geometrical disposition, (C) impeller, and (D) cylinder and magnetic stirrer bar.

DO monitoring was performed with an InPro 6820 Polarographic Oxygen Sensor (Mettler Toledo®, Greifensee, Switzerland) coupled with an Analytical Transmitter M300 (Mettler Toledo®, Greifensee, Switzerland). Before performing the $k_L a$ determination experiments, the characteristic time (τ) and response dead time (θ) of the DO measurement system were estimated through

dynamic measurements by submitting the probe to step-type disturbances. For this purpose, 100ml of distilled water were placed in two conventional 250ml Erlenmeyer flasks. First, one of the Erlenmeyer flasks was bubbled with air, while the other was bubbled with Nitrogen. Then, the sensor's tip was immersed in one of the Erlenmeyer flasks until the reported data was kept constant, i.e., with a variation of less than 0.01% saturation for 60 seconds. When this condition was met, the sensor was quickly immersed in the other Erlenmeyer flask. The reported data were recorded until achieving the stability criterion.

Five experiments were performed to find the transfer function's best parameters that describe the sensor's response to changes in the DO concentration. Since the experiments did not start from the same values of DO concentration, the responses were normalized employing the Equation, where N is the normalized response and y is the response as shown in Equation (2-10). In addition, although the manufacturer recommended a first-order transfer function with the characteristic time (τ) as a single parameter, a model was evaluated that also included a dead time (θ) as shown in Equation (2-11).

$$N(t) = \frac{y(t) - y(0)}{y(t_f) - y(0)} \quad (2-10)$$

$$\tau \frac{dN(t)}{dt} + N(t) = t - \theta \quad (2-11)$$

By solving the differential equation (2-12):

$$N(t) = 1 - \exp\left(\frac{-t + \theta}{\tau}\right) \quad (2-12)$$

A couple of parameters (τ , θ) was estimated for each experiment. In this case, both parameters were first supposed, and the expected normalized response was calculated. Then, an objective function was settled as the sum of the absolute value of all actual and estimated differences. Next, with a solver tool, the values of the parameters were changed until achieving a minimum of the objective function (2-13). The solution method of the solver tool was GRG Nonlinear with a convergence of 10^{-4} and forward derivatives. Finally, the arithmetic average of the values was defined as the parameters of the transfer function of the DO probe.

$$\text{Min} \left(\sum_{t=0}^t |N(t)_{Real} - N(t)_{Estimated}| \right) \quad (2-13)$$

2.2.2 Determination of the Volumetric Mass Transfer Coefficient (k_{La})

The study of the k_{La} value with different operating conditions was performed for both bioreactor geometries. The studied variable in the Erlenmeyer configuration was the stirring speed and the liquid volume, whereas the stirring speed and the bubbling flow were studied in the Spinner flasks. The available equipment constrained the operation range for the stirring speed. The maximum for the Erlenmeyer Shaker was 200 rpm and for the stirring plate for the magnets was 150 rpm. In addition, it was desired to maintain the bubble flow as lower as possible for bubbling since high shear stress zones are created during bubble exploiting. Thus, it was finally defined by the reliability of the available manometer and rotameter for airflow measurement. For the Spinner flask, four levels of each variable were evaluated: 0, 50, 100, and 150rpm, and 0, 0.24, 0.30, and 0.44ml s⁻¹. The measurements were performed randomly, but half had to be performed with the desorption method and the other half with the absorption method.

The dynamic absorption/desorption or Gassing in/out method was employed to determine the volumetric mass transfer coefficient. This technique is based on measuring the dynamic behavior of DO concentration within the bioreactor after a step-change in the oxygen concentration of the inlet gas. In this case, air and Nitrogen were employed as inlet gases at 15.8 psia, and the working liquids were deionized water and Dynamis AGT® culture medium (Gibco Life Technologies®, Carlsbad, USA) supplemented with solid L-Glutamine (Gibco Life Technologies®, Carlsbad, USA) to 8mM. By working with the culture medium, the bioreactor was previously sterilized. The experimental setup started by filling the liquid volume to evaluate 30 or 60ml for Erlenmeyer and 100ml for Spinner flasks. In the case of Erlenmeyer flasks, these values were set considering two technical restrictions. First, with volumes above 60ml, the height of the liquid exceeded the height at which the side outlets lids were located. Although the seal was verified, the probability of contamination would increase with medium reaching that level. While with values below 30ml, the sensor tip was not constantly submerged when the agitation was turned on. Liquid volumes were measured employing a ME204 analytical balance (Mettler Toledo®, Greifensee, Switzerland).

After that, the availability of air and pure Nitrogen in the gassing measurement system was checked. This system is represented in Figure 2-3 and consist of a circuit of hoses, pressure (PI) and flow (FI) indicators, 62mm PTFE filters with 0.22µm pore diameter (F) (Sartorius®, Göttingen,

Germany) and valves (V) manually manipulated for defining the gas that flows through the bioreactor.

Then, the bioreactor configuration was assembled to the gassing system with all valves set as closed, as shown in Figure 2-4 for the Spinner flask bioreactor configuration. Homologous, the Erlenmeyer flask bioreactor configuration was connected to the gassing system. The next step was verifying the system seal by opening valves V3, V5, V6, and V7. The pressure in the laboratory line of both gases is around 30psig. Next, the inlet pressure and airflow to the bioreactor were settled in 5psig and 1 ml s^{-1} with the valves V5 and V6. By letting air flowing to the bioreactor and covering the outlet of filter F3 (V11 closed), the pressure reported by the PI5 PSA-01 (Autonics®, Mundelein, IL, USA) would increase in a correctly sealed system; if not, it would remain constant because air leaks.

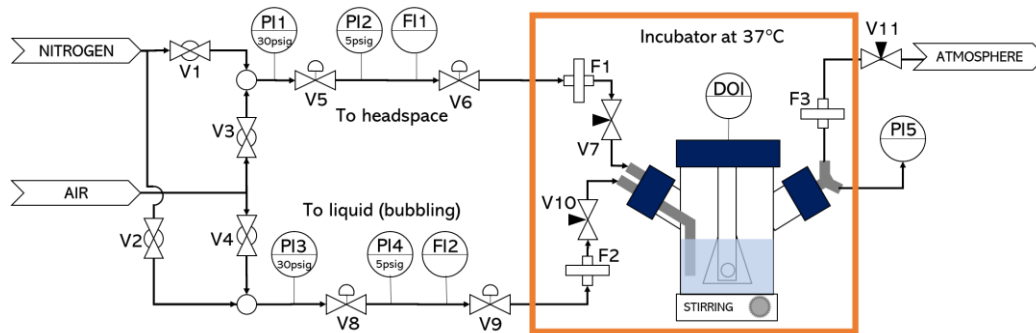


Figure 2-4: Diagram of the equipment for dynamic gassing k_{La} determination. V: Valve, PI: Pressure indicator, FI: Flow indicator, F: $0.22\mu\text{m}$ filter, DOI: Dissolved oxygen indicator.

Once an adequate seal is verified, the DO sensor was polarized for 6 hours by leaving the system in a controlled temperature chamber. If the studied liquid were water, the measurement cycle could start once the liquid temperature is 37°C . Otherwise, the plan was left for a day at 37°C with 1 ml s^{-1} airflow at 5psig to the Headspace, and V11 opened. If no contamination was observed, the procedure continued.

According to the recommendations of the DO probe manufacturer, One Point calibration was always performed before starting k_{La} measurement cycles. The zero value was kept according to factory settings. 100% value was defined with air flowing at 1.5 ml s^{-1} to the Headspace and 0.1 ml s^{-1} to bubbling at 5psig and stirring at 100rpm for both the shaker and the magnets motor. After two hours, it was expected that the system was Oxygen saturated. Thus, the DO reported

concentration was settled as 100% saturation. When the transmitter was fixed with the new 100% value, all valves are closed except V9, which was subsequently opened. After finishing this step, the system was prepared for k_La or q_{O_2} determination.

Given that one of the considerations of the model is to have an atmosphere inside the reactor of constant concentration and that we will be working with two gases (Air 21% O_2 v/v and pure Nitrogen 0% O_2), it is necessary to have a time in which the oxygen concentration in the headspace changes from one gas to the other. If this step was not carried out, the obtained results might not correspond to the actual k_La value of the system. Therefore, the complete k_La measurement cycle consisted of six stages, explained as follows and outlined in Figure 2-5.

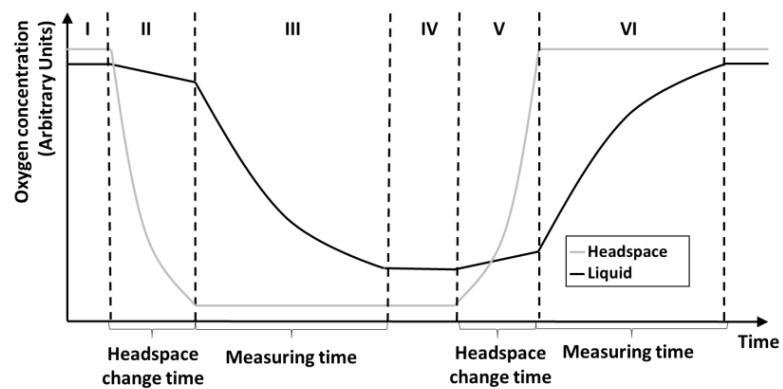


Figure 2-5: k_La measurement cycle: (I) Stabilization of Headspace and liquid oxygen concentration, (II) reduction of headspace oxygen concentration with Nitrogen, (III) dynamic gassing out k_La measurement, (IV) stabilization of Headspace and liquid oxygen concentration, (V) increase of the headspace oxygen concentration with air and (VI) dynamic gassing-in k_La measurement.

- I) Stabilization of initial oxygen concentration: In this stage, valves V1 and V2 were closed, stirring was settled at 100rpm, and airflow of 1.5 ml s^{-1} to the Headspace was fixed with valves V3, V5, V6, and V7. According to the sensibility of the system reported by the manufacturer, the DO-reported concentration medium should correspond to a stable value between 95% and 105% of saturation with air (Figure 2-5 I).
- II) Air to Nitrogen headspace change: Once the DO concentration-response was stable after 60s, the inlet gas to the Headspace was replaced by Nitrogen. For this purpose, stirring was turned off, valves V3 and V4 were closed, and V1 was opened to change the flowing gas from Air to Nitrogen. A Nitrogen flow of 1.6 ml s^{-1} at 5psig to the Headspace was settled with valves V5, V6, and V7. The time is measured after the

Nitrogen flow was fixed. After 400s, the O_2 concentration in the Headspace of the Spinner Flask Bioreactor configuration was expected to be under 1% v/v. In the case of the Erlenmeyer Flask, 200 s were awaited since the Nitrogen flow was settled. This time will correspond to the Headspace change time in Figure 2-5II. The criterion for defining the headspace change time follows the mass oxygen balance in the Headspace with a gas inlet and outlet, as schematized in Figure 2-6 and presented in Equation ((2-14).

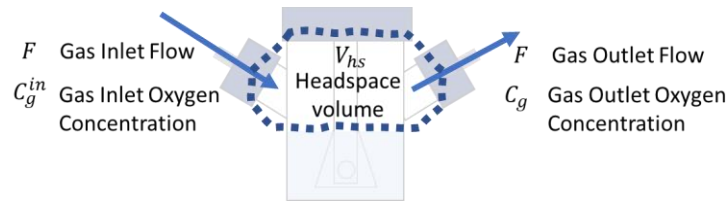
$$\frac{dC_g}{dt} = \frac{F}{V_{hs}} (C_g^{in} - C_g) \quad (2-14)$$


Figure 2-6: Considerations for oxygen mass balance for determining Headspace change time.

Three assumptions were considered for the Equation (2-6) model, which was experimentally validated by performing headspace changes with the tip of the DO sensor placed in the Headspace at three different heights from the liquid surface. First, since there is no pressure increase in the Headspace while the gas passed through the bioreactor, the inlet and outlet flow are the same. Second, since the liquid is immobile, diffusion is a mass transfer mechanism that controls the amount of Oxygen that escapes from the liquid phase. Third, the magnitude order of the diffusive flux during the Headspace change time is not enough for depleting all the Oxygen of the medium. After solving Equation (2-14), the expression of Equation (2-15) was obtained for calculating the Headspace change time (t_{hsc}) or the time in which the headspace oxygen concentration is reduced by 95% concerning the initial value:

$$t_{hsc} = \frac{3V_{hs}}{F} \quad (2-15)$$

During this stage, part of the initial Oxygen gets inevitably desorbed. Nevertheless, the final concentration after the Headspace change time was enough for achieving reproducible results.

- III) Measurement by decreasing DO concentration: After the headspace change, the Nitrogen inlet flow to the Headspace was reduced to 0.1 ml s^{-1} . Then, desired stirring and Nitrogen bubbling conditions were settled. Whether 1000s of measurement passed or the DO concentration reached values below 10%, stirring and bubbling were turned off, and valves V1, V2, and V8 were closed (Figure 2-5 III).
- IV) Stabilization of initial oxygen concentration: This stage consisted of waiting until the liquid's oxygen concentration remained with a difference below 0.1% during 60s (Figure 2-5 IV).
- V) Change of the Headspace from Nitrogen to air: Once the DO concentration was stable after 60s, the inlet gas to the Headspace was replaced from Nitrogen to Air. For this purpose, stirring was turned off, and V3 was opened for air flowing. Then, the headspace oxygen concentration is augmented with an airflow of $1,5 \text{ ml s}^{-1}$ at 5psig, fixed employing valves V4 and V5 during 200s or 400s, following the headspace change time criteria defined through the following Equation (2-15). Inevitably, the DO concentration started to increase due to the solubilization through diffusion. Nevertheless, the final concentration after the Headspace change time was enough for achieving reproducible and replicable results (Figure 2-5 V).
- VI) Measurement by increasing DO: Finally, the air headspace flow was reduced to 0.2 ml s^{-1} . Desired stirring and Nitrogen bubbling conditions were settled. After 1000s or reaching a measured value over 90% DO concentration, stirring and bubbling were turned off, and valves V1, V2, and V8 were closed. Subsequently, the measurement cycle was repeated by stabilizing the measured saturation value (Figure 2-5 VI).

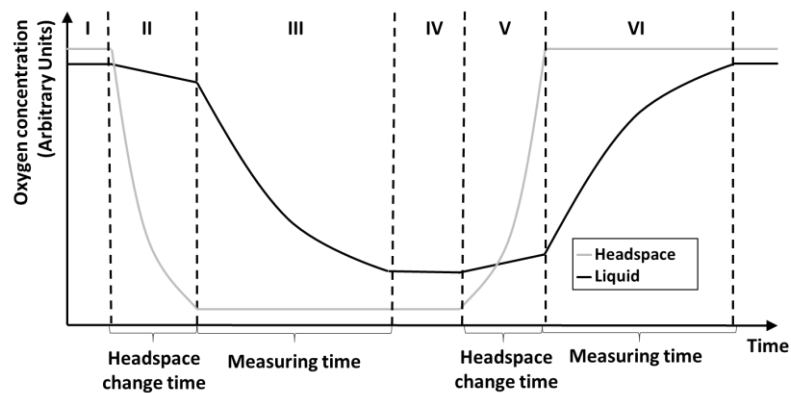


Figure 2-7: k_{La} measurement cycle: (I) Stabilization of Headspace and liquid oxygen concentration, (II) reduction of headspace oxygen concentration with Nitrogen, (III) dynamic gassing out k_{La} measurement, (IV) stabilization of Headspace and liquid oxygen concentration, (V) increase of the headspace oxygen concentration with air and (VI) dynamic gassing-in k_{La} measurement.

The state of each valve during measurement stages in k_{La} is summarized in Table 2-1

Table 2-1: Valve state during measurement stages in k_{La} determination.

Valve	Stage					
	I	II	III	IV	V	VI
V1						
V2						
V3						
V4						
V5	C	C	C	C	C	C
V6	C	C	C	C	C	C
V7						
V8	C		C	C		C
V9	C		C	C		C
V10						
V11						

	Closed
	Open
C	Control

2.2.3 Determination of the specific oxygen consumption (q_{O_2}) for a CHO cell line

After determining the correlation between the operation parameters and the k_{La} , the value of the specific oxygen consumption rate (q_{O_2}) of a suspended CHO cell line was determined. For this purpose, an initial culture was performed from a 2ml cryovial with approx. 1×10^7 cells. The content of the cryovial was thawed and diluted in a 100ml glass Erlenmeyer with 40ml of Dynamis® culture medium. The culture was incubated in a 5% v/v CO₂/air atmosphere at 37°C and stirred at 100rpm with a UNIMAX 1010 orbital shaker (Heidolph®, Schwabach, Germany). After four days, 30ml of culture was extracted from the Erlenmeyer, placed in four 15ml centrifuge tubes, and centrifuged at 230g for 10min. The supernatant was discarded, the cell pellet was resuspended in 15ml Trypsin (Gibco Life Technologies®, Burlington, Canada) and incubated for 5min at 37°C. Although the employed CHO cell line is adapted to grow in suspension, cells come from being thawed, which

may stress the cells and influence some clusters to form. Since it is impossible to know the number of cells in a cluster, it was pertinent to perform the trypsinization procedure for separating cells, thus establishing the exact cell concentration in the culture.

After the incubation, 15ml of 1:9 Bovine Fetal Serum: Dynamis® culture medium was added to the centrifuge tubes and centrifuged at 230g for 5min. The supernatant was discarded, and the cell pellet was resuspended in a fresh Dynamis® culture medium with an aim concentration of 2.5×10^9 cells l^{-1} . Cell concentration and viability were measured with 20 μ l of a 1:1 solution of culture sample and 0.4% w/v Trypan blue. With this inoculum, three dilutions of 30ml with fresh medium and known cell concentration were prepared (2.5×10^9 cells l^{-1} , 1.0×10^9 cells l^{-1} , 5.0×10^8 cells l^{-1}). The bioreactor was previously sterilized, and the DO probe was calibrated with fresh medium at 37°C.

After verifying the seals, the bioreactor was plugged into the $k_L a$ measurement system, stirred at 150rpm, and incubated in a 5% CO₂ atmosphere until the DO probe reports 37°C. The DO concentration was expected to be above 90% saturation with air when 37°C was achieved. Then, the system was ready for the measurement cycle, which is explained as follows and similarly outlined in Figure 2-8:

- I) Reaching a high initial oxygen concentration: In this stage, valves V1 and V2 were closed, stirring was settled at 150rpm, and airflow of 1.5 ml s^{-1} to the Headspace was fixed with valves V3, V5, V6, and V7. According to the sensibility of the system reported by the manufacturer, the DO-reported concentration medium should correspond at least to a 90% saturation (Figure 2-8 I).
- II) Air to Nitrogen headspace change: Once the DO concentration-response was stable after 60s, the inlet gas to the Headspace was replaced by Nitrogen. For this purpose, stirring was turned off, valves V3 and V4 were closed, and V1 was opened to change the flowing gas from Air to Nitrogen. A Nitrogen flow of 1.6 ml s^{-1} at 5psig to the Headspace was settled with valves V5, V6, and V7. The time is measured after the Nitrogen flow was fixed. After 200s, the Oxygen concentration in the Headspace of the Spinner Flask Bioreactor configuration was expected to be under 1% v/v. This time will correspond to the Headspace change time in Figure 2-8 II. In comparison to the Stage II of the $k_L a$ measurement procedure, it was expected that the DO concentration dropped faster in this case because

the cells will start consuming the available Oxygen and inevitably desorbed DO by diffusion.

- III) Measurement by decreasing DO concentration: After the headspace change, the Nitrogen inlet flow to the Headspace was reduced to 0.2 ml s^{-1} . Then, the stirring was settled on 100 rpm , and the DO measurement was registered until it reached values below 30%. Then, stirring and bubbling were turned off, and valves V1, V2, and V8 were closed (Figure 2-8 III).
- IV) Change of the Headspace from Nitrogen to air: The inlet gas to the Headspace was replaced from Nitrogen to Air (Figure 2-8 IV). For this purpose, stirring was turned off, and V3 was opened for air flowing. Then, the headspace oxygen concentration is augmented to the airflow of 1.6 ml s^{-1} at 5 psig , fixed employing valves V4 and V5, during 200s or 400s, following the headspace change time criteria defined through the following Equation (2-15). The DO concentration inevitably started to decrease due to cell consumption.
- V) Measurement by increasing DO: Finally, the air headspace flow was reduced to 0.2 ml s^{-1} . Desired stirring and Nitrogen bubbling conditions were settled. After 1000s or reaching a measured value over 90% DO concentration, stirring and bubbling were turned off, and valves V1, V2, and V8 were closed. Subsequently, the measurement cycle was repeated.

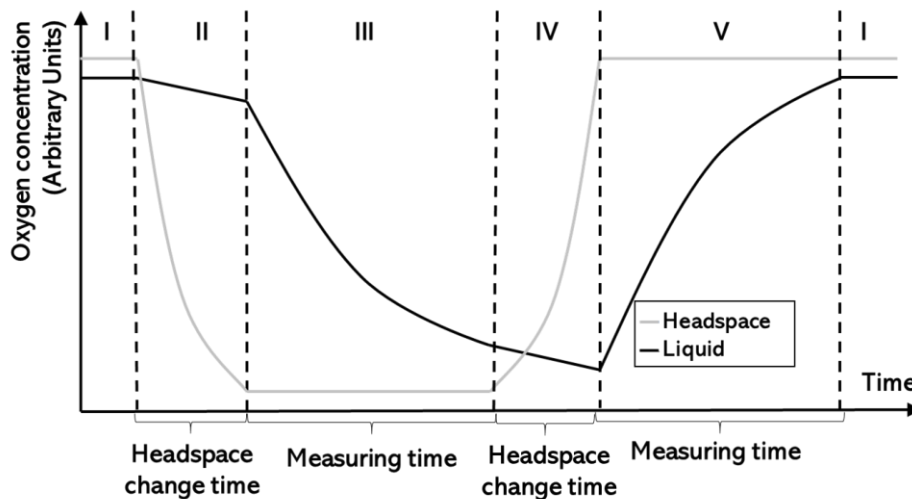


Figure 2-8: q_{O_2} measurement cycle: (I) Stabilization of headspace oxygen concentration, (II) reduction of headspace oxygen concentration with Nitrogen, (III) dynamic gassing out k_{La} measurement, (IV) change of headspace oxygen concentration, (V) increase of the headspace oxygen concentration with air and (VI) dynamic gassing-in k_{La} measurement.

The state of each valve during the q_{O_2} determination referred to in Figure is summarized in Table 2-2.

Table 2-2: Valve state during measurement stages in q_{O_2} determination.

Valve	Stage				
	I	II	III	IV	V
V1	■	□	□	■	■
V2	■	□	□	■	■
V3	□	■	■	□	□
V4	□	■	■	□	□
V5	C	C	C	C	C
V6	C	C	C	C	C
V7	□	□	□	□	□
V8	C	■	C	■	C
V9	C	■	C	■	C
V10	□	□	□	□	□
V11	□	□	□	□	□

■	Closed
□	Open
C	Control

According to the mass oxygen balance, the experimental measurements of Stage III were treated following the model presented in Equation (2-16). It is considered that the cell concentration corresponded to a value measured before the bioreactor is placed in the incubator, and it remained constant since the duplication time of the cell line is around 23h. The cell concentration time of the experimentation for each dilution did not exceed two hours. The supposed duplication time was validated with data from cultures before these experiments, which were performed with the same CHO cell line in unmodified Spinner-type reactors with 40ml of Dynamis® medium 8mM l-glutamine supplemented, and cultured at 37°C, 5% CO₂ and 115rpm.

$$\frac{dC_L(t)}{dt} = -k_L a C_L(t) - q_{O_2} X \quad (2-16)$$

Solving this equation with the initial condition: $C_L(t=0) = C_{L_0}$

$$C_L(t) = \frac{1}{k_L a} \left((k_L a C_{L_0} + q_{O_2} X) e^{-k_L a t} - q_{O_2} X \right) \quad (2-17)$$

The expected q_{O_2} value was expected by order of 5 mg cell⁻¹ h⁻¹. Then, the difference between the measured and the expected DO concentration was calculated for each experiment. Then, the objective function was settled using a solver tool as shown in Equation (2-18) changing the q_{O_2}

value. The solution method of the solver tool was GRG Nonlinear with a convergence of 10^{-4} and forward derivatives.

$$\min \left(\sum_{t=0}^t |C_L(t)_{Real} - C_L(t)_{Estimated}| \right) \quad (2-18)$$

In parallel, an alternative procedure for measuring q_{O_2} was proposed based on the mass oxygen balance. Since k_{La} is zero in the absence of fluid motion, the OTR term will also be zero. This condition makes the drop in DO concentration dependent on cell consumption, as presented in Equation (2-19).

$$\frac{dC_L}{dt} = -OUR = -q_{O_2}X \quad (2-19)$$

In this case, the expression for the DO concentration during the experiment where the headspace concentration was already changed is expressed as in Equation (2-20):

$$C_L(t) = C_{L_0} - q_{O_2}X t \quad (2-20)$$

This expression does not depend on the oxygen concentration of the inlet gas; thus, it is valid for both Gassing in and gassing out experiments. Plotting the DO concentration values during the culture time, a straight line is obtained, whose slope is the OUR. Given a known cell concentration, the q_{O_2} value can be obtained.

2.3 Results and discussion

2.3.1 Characteristic and dead time

The normalized response to the probe to step changes in the measured DO concentration is presented in Figure 2-9, and the obtained parameters are summarized in Table 2-3.

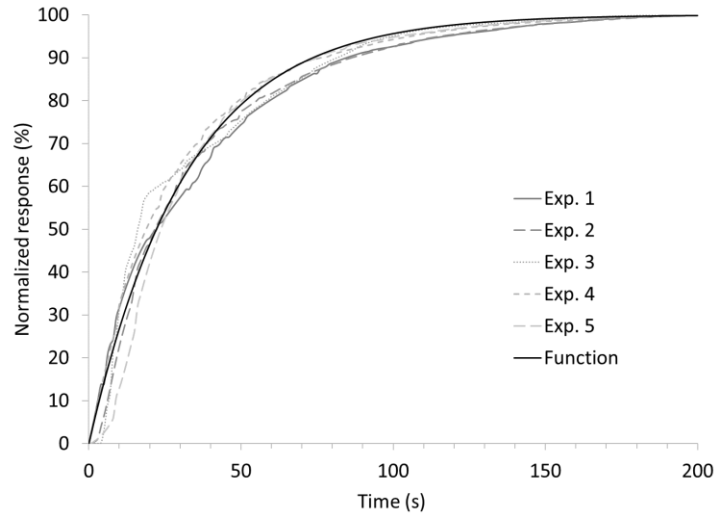


Figure 2-9: Measurement of the probe response to a step change. The darkest continuous line is the first-order transfer function with an average of the parameters obtained from Experiments 1 to 5.

Table 2-3: Summary of parameters for step perturbation for the DO probe

Parameter	Exp1	Exp2	Exp3	Exp4	Exp5	Average
θ	1.506	0	2.074	0	1.201	0.956
τ	33.81	32.37	31.72	30.58	35.83	32.86

From this data, it can be concluded that the model suggested by the manufacturer is the most appropriate since the found dead time is less than the sensitivity of the system; that is, the measurements cannot be taken in times lower than a second. Likewise, the characteristic time will be considered as 33s for the following experiments.

2.3.2 Relevance of headspace change time and delay due to DO probe response for the $k_L a$ measurement.

Knowing the value of the characteristic time within the DO sensor response transfer function, the following mathematical model is proposed to evaluate the relevance of the time of change in gas

concentration in the Headspace included in stages II and V of the protocol mentioned. Here, the Stage II scenario will be evaluated, where at the beginning, the liquid is saturated with Oxygen, and the gas is replaced from the air (21% v/v O₂) to Nitrogen. Therefore, the first model to consider is the mass oxygen balance in the Headspace, which was already presented in Equation (2-21).

$$\frac{dC_g(t)}{dt} = \frac{F}{V_{hs}} (C_g^{in} - C_g(t)) \quad (2-21)$$

By solving Equation (2-21), the analytic expression for the oxygen concentration of the Headspace can be found with the initial condition $C_g(t=0) = C_{g0}$

$$C_g(t) = C_g^{in} - (C_g^{in} - C_{g0}) e^{\frac{-F}{V_{hs}} t} \quad (2-22)$$

Since in Stage II the inlet gas is Nitrogen, the model is presented in Equation (2-23):

$$C_g(t) = C_{g0} e^{\frac{-F}{V_{hs}} t} \quad (2-23)$$

Since oxygen solubility in the medium depends on the Henry constant and the oxygen concentration in the gas, as the temperature and medium composition remained constant during the headspace change, the solubility was the only function of the oxygen concentration in the gas. Thus, the difference in solubility with time can be calculated as proposed in Equation(2-24), where P corresponds to the absolute pressure of the system (560mmHg at experiment conditions).

$$\frac{dC^*}{dt} = \frac{P}{H} \frac{dC_g(t)}{dt} \quad (2-24)$$

Replacing Equation (2-23) in (2-24), and rearranging:

$$\frac{dC^*(t)}{dt} = \frac{F H}{P V_{hs}} (C_g^{in} - C_g(t)) \quad (2-25)$$

For the Stage II:

$$\frac{dC^*(t)}{dt} = - \frac{F H}{P V_{hs}} C_{g0} e^{\frac{-F}{V_{hs}} t} \quad (2-26)$$

The mass oxygen balance for the liquid phase was already defined as in Equation (2-1), but in this case, the oxygen solubility (C^*) changes with time due to the headspace change:

$$\frac{dC_L(t)}{dt} = k_L a (C^*(t) - C_L(t)) \quad (2-27)$$

Finally, the dynamic response of the DO probe is considered with the first-order transfer function presented in 37, where C_m corresponds to the DO concentration reported by the measurement device.

$$\frac{dC_m(t)}{dt} = \frac{1}{\tau} (C_L(t) - C_m(t)) \quad (2-28)$$

It is essential to consider that, so far, the model can be applied for any reactor geometry since it does not directly consider restrictions due to the shape of the reactor. Therefore, the next step evaluated two scenarios considering a $k_L a$ value of 10h^{-1} , corresponding to a typical value expected for Spinner bioreactors. This value was achieved for the studied case and detailed further.

- Scenario A: The three set of equations (2-26), (2-27), and (2-28) is considered and solved for obtaining a function that describes the expected concentration (C_m) through time with initial conditions:
 - $C^*(t=0) = C^*(21\% \text{ v/v } \text{O}_2 \text{ at } 37^\circ\text{C and } 560\text{mmHg})$
 - $C_L(t=0) = C_m(t=0) = C_{L0}$
- Scenario B: Equation (2-24) is not considered; the experiment's headspace oxygen concentration is zero. In this case, the Equations (2-26) y (2-27) can be simplified with equations (2-29) and (2-30).

$$\frac{dC^*(t)}{dt} = 0 \quad (2-29)$$

$$\frac{dC_L(t)}{dt} = -k_L a C_L(t) \quad (2-30)$$

The results of the two scenarios are compared and presented in Figure 2-10, where the experimental data is collected by setting the conditions for a $k_L a$ of 10h^{-1} by avoiding Stage II from the measurement procedure. Since the variation between the experimental data and the measured DO concentration prediction of scenario A is less than 1%, the discussion continues from the model's data. Not considering headspace change represents a significant deviation of scenario B from the actual DO concentration value. Additionally, the delay involved in using the sensor is evident by comparing Real and Scenario A curves. In addition to delaying reporting the actual DO

concentration of the liquid, the shape of the curves of the exact scenario change over time, especially in the first few seconds. This change in the curve shape has consequences in determining the k_{La} value since this parameter is calculated from a linearization of the experimental data.

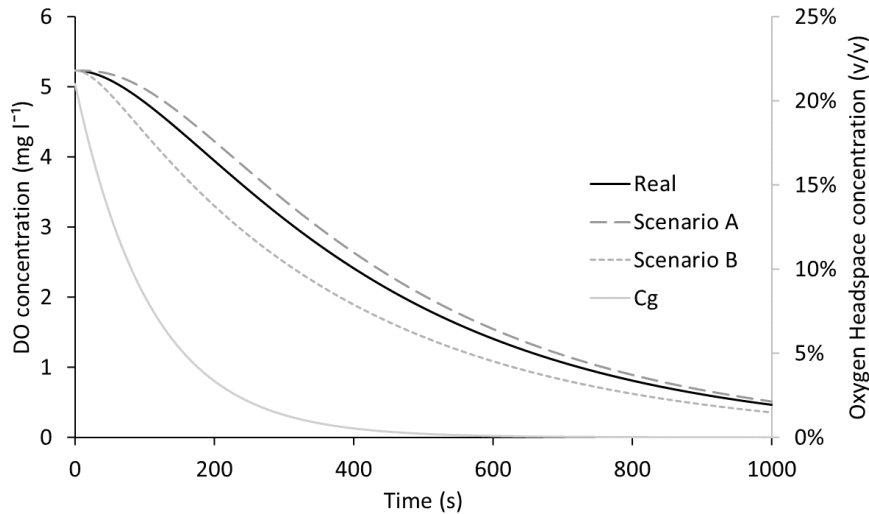


Figure 2-10: Real (C_L and C_g) and expected (C_m) DO concentration for Scenario A: the change of oxygen solubility is considered, and Scenario B: the gas oxygen concentration is regarded as zero.

In *Figure 2-10*, the experimental measurements, which correspond to the expected values from Scenario A, are linearized and plotted against the ideal curve of $k_{La}=10h^{-1}$. The difference between the measured and actual k_{La} value is below 5% after the 450s. According to the above, it would not be necessary to turn off the agitation or suspend the bubbling to determine the k_{La} value since the k_{La} value obtained after the 450s would be very close to the actual value. Nonetheless, it is pertinent to note that the dissolved oxygen concentration after the 450s will be below 40%, so the Oxygen available is to be desorbed for k_{La} measuring. Experimentally, it was verified that the amount of Oxygen in the static liquid after the Headspace Change is at least 90% saturation, starting from 100%. Therefore, it is suggested to follow the proposed experimental procedure. The relative error is calculated considering as $k_{La}=10h^{-1}$ as the actual value.

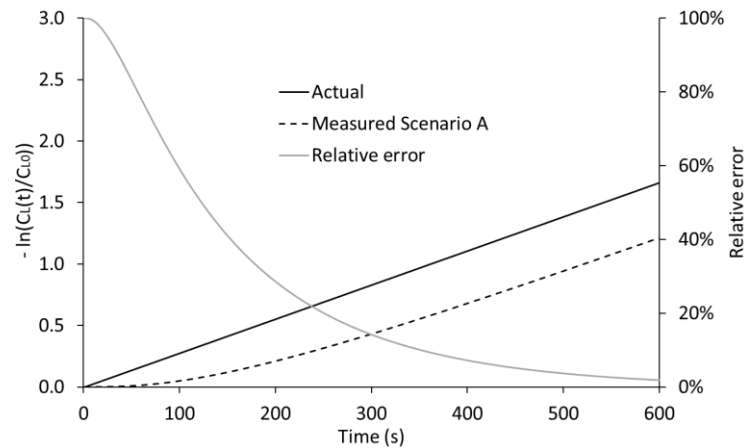


Figure 2-11: Actual and measured linearized values of DO concentration for Scenario A.

It should also be noted that this exercise was performed with a typical value of $k_L a$ obtained from the literature for the employed bioreactor geometries (Monteil et al., 2013). If the system reaches higher $k_L a$ values, Oxygen will desorb faster during Gassing, reducing the time available to measure the parameter. Besides, not only is having available Oxygen essential to have sufficient information for the proper estimation of $k_L a$, but also when measuring q_{O_2} of a cell line that may be affected under conditions of hypoxia or anoxia, or that consumes Oxygen so rapidly that insufficient information is obtained to describe OUR accurately. A similar analysis could be performed for Stage V, where the liquid is poorly Oxygen concentrated, and the headspace gas is changed from Nitrogen to air. However, similar results can be obtained.

Figure 2-12 shows the sensor's delay concerning the actual concentration estimated in the liquid. This delay certainly affected Stages III and VI, which are the core of the measurement procedure. For avoiding misestimations due to the nature of the DO measurement system, the dynamic response of the probe was modeled from differential equations. In Stage VI, the air is supplied to the medium; equations represent a system of differential equations by the mass oxygen balance for the liquid considering perfect mixing and the first-order model for a probe response.

By solving the system of equations (1-17) and (2-28), the explicit functions for C_m and C_L are equations (2-31) and (2-32).

$$C_m(t) = \left(\frac{C_o - C^*}{1 - k_L a \tau} \right) e^{-k_L a t} + \left(C_o - C^* - \frac{C_o - C^*}{1 - k_L a \tau} \right) e^{-\frac{t}{\tau}} + C^* \quad (2-31)$$

$$C_L(t) = (C_o - C^*) e^{-k_L a t} + C^* \quad (2-32)$$

If oxygen concentration diminishes, the solutions for the differential equation system are presented in Equations (2-33) and (2-34).

$$C_m(t) = \frac{C_o}{1 - k_L a \tau} e^{-k_L a t} + C_o \left(1 - \frac{1}{1 - k_L a \tau}\right) e^{-\frac{t}{\tau}} \quad (2-33)$$

$$C_L(t) = C_o e^{-k_L a t} \quad (2-34)$$

With the functions for the measured DO concentration, it is possible to estimate the time from which the linearization of the reported DO values is suitable for determining $k_L a$. *Figure 2-12* presents the relative error for bioreactors at operational conditions with $k_L a$ values 1.0 and 100 h^{-1} . It was established that the data for the estimation of $k_L a$ would be considered after 100s from the start of agitation or bubbling. In this way, both the error induced by the delay in the reporting of the measurement by the DO sensor and the error caused by the researcher while adjusting the conditions of the experiment are reduced.

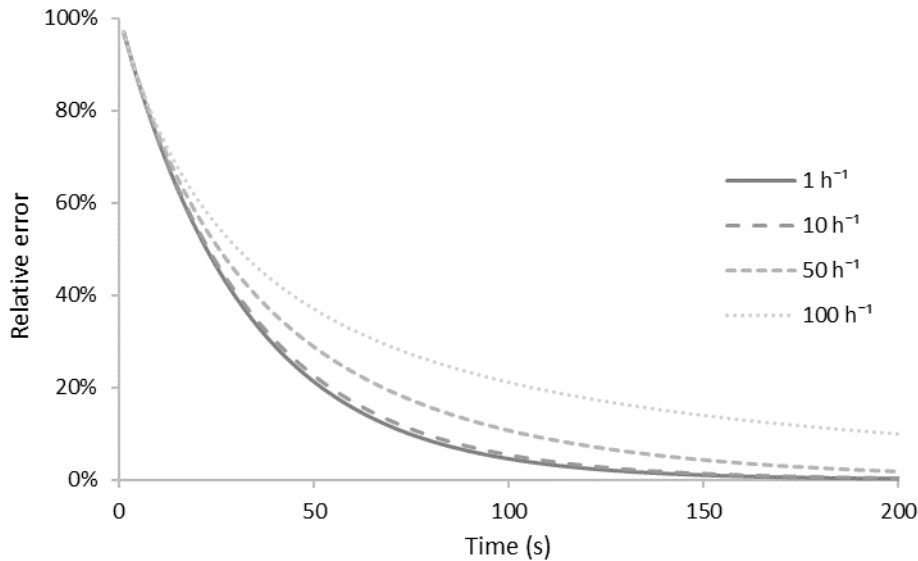
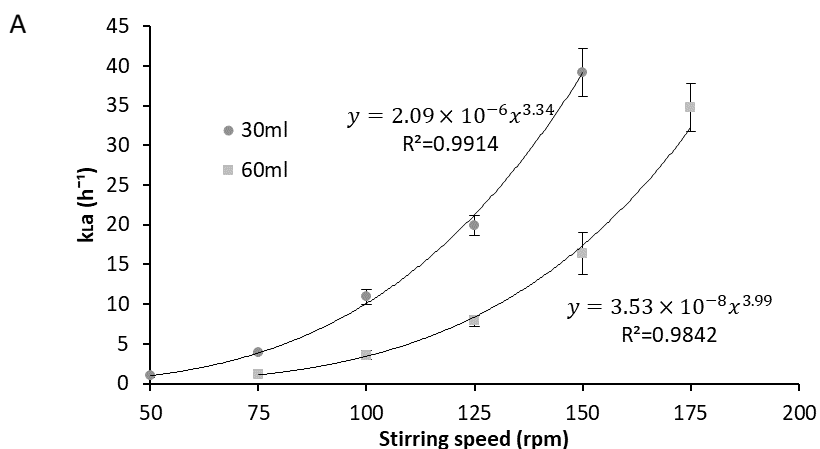


Figure 2-12: Relative error in $k_L a$ determination during the first 200s of the measurement stage with a sensor characteristic time of 33s.

2.3.3 k_{La} values for two bioreactor configurations.

As described in the methodology, it was planned to calibrate the electrode before starting any k_{La} measurement. However, a recalibration of the 100% saturation point was not performed unless the membrane was changed. Even on working days, when starting with one fluid and switching to another, the current generated by the redox reaction inside the sensor appeared to be the same at saturation. The first explanation could be attributed to the fact that the difference in composition did not affect dissolved Oxygen at equilibrium. Nonetheless, the actual variable being measured with the sensor is the dissolved oxygen activity, given the nature of the chemical equilibrium. More detailed tests are needed to determine if the solubility of Oxygen in the two liquids is the same. This brief discussion is necessary since the value to be considered for solubility will henceforth correspond to the same value as for water, even though the authors often assume that the saturation in the medium is 90% of the value in water.

In *Figure 2-13* and *Figure 2-14*, the measured k_{La} values are presented. Again, the results are consistent with expectations. The k_{La} values rise as the agitation increases in both the Spinner and the Erlenmeyer bioreactor. In the case of the Erlenmeyer bioreactor, similar k_{La} values were obtained for water and medium at the same conditions, which is evidenced by the order of magnitude of the regression parameters for the accepted potential models similar for both liquids. However, this is not the case with the Spinner bioreactor, where the trend depends on the liquid evaluated.



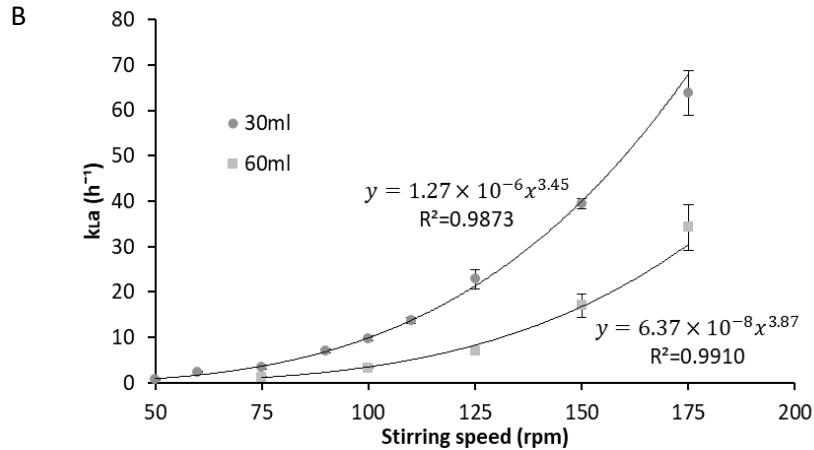


Figure 2-13: k_{La} values for the Erlenmeyer bioreactor configuration with A: Distilled water / B: Dynamis® cell culture. $N=3$. Error bars: σ .

For water, k_{La} increases as the bubbling flow and agitation speed increases with a trend like that found for Erlenmeyer-type reactors. Therefore, the model for describing the k_{La} for water in the Spinner bioreactor should be like the potential model for Erlenmeyer, whose accuracy can be verified in Figure 2-13 A. Although k_{La} values also rise with the stirring speed in the culture medium, the increasing trend is not the same. The increase between the no bubbling condition and the one with the lowest bubbling flow (0.25ml s^{-1}) is more significant than higher bubbling values at the same stirring speed. It could even be said that the curve has an asymptotic behavior, while in the other studied cases, the increase was exponential. In Figure 2-13 B, it can also be seen that a potential model is not suitable for the prediction of the oxygen transfer parameter. Additionally, the achieved k_{La} values are higher than for water, which differs from those obtained in the Erlenmeyer bioreactor. The values were similar for the two fluids at the same conditions.

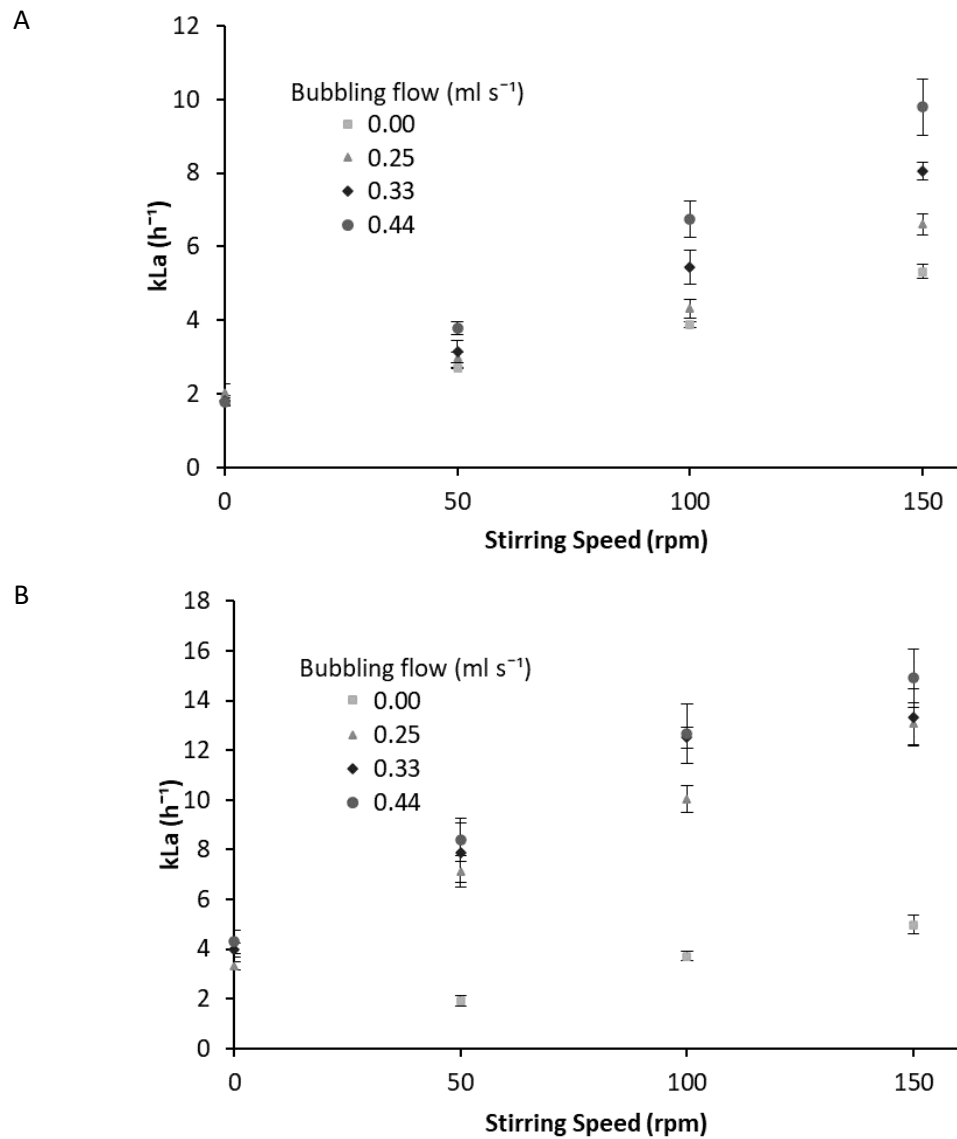


Figure 2-14: k_La values for the Spinner bioreactor configuration with A: Distilled water / B: Dynamis® cell culture. $N=4$. Error bars: σ . The thicker error bar corresponds to the bubble flow of 0.33ml s^{-1} .

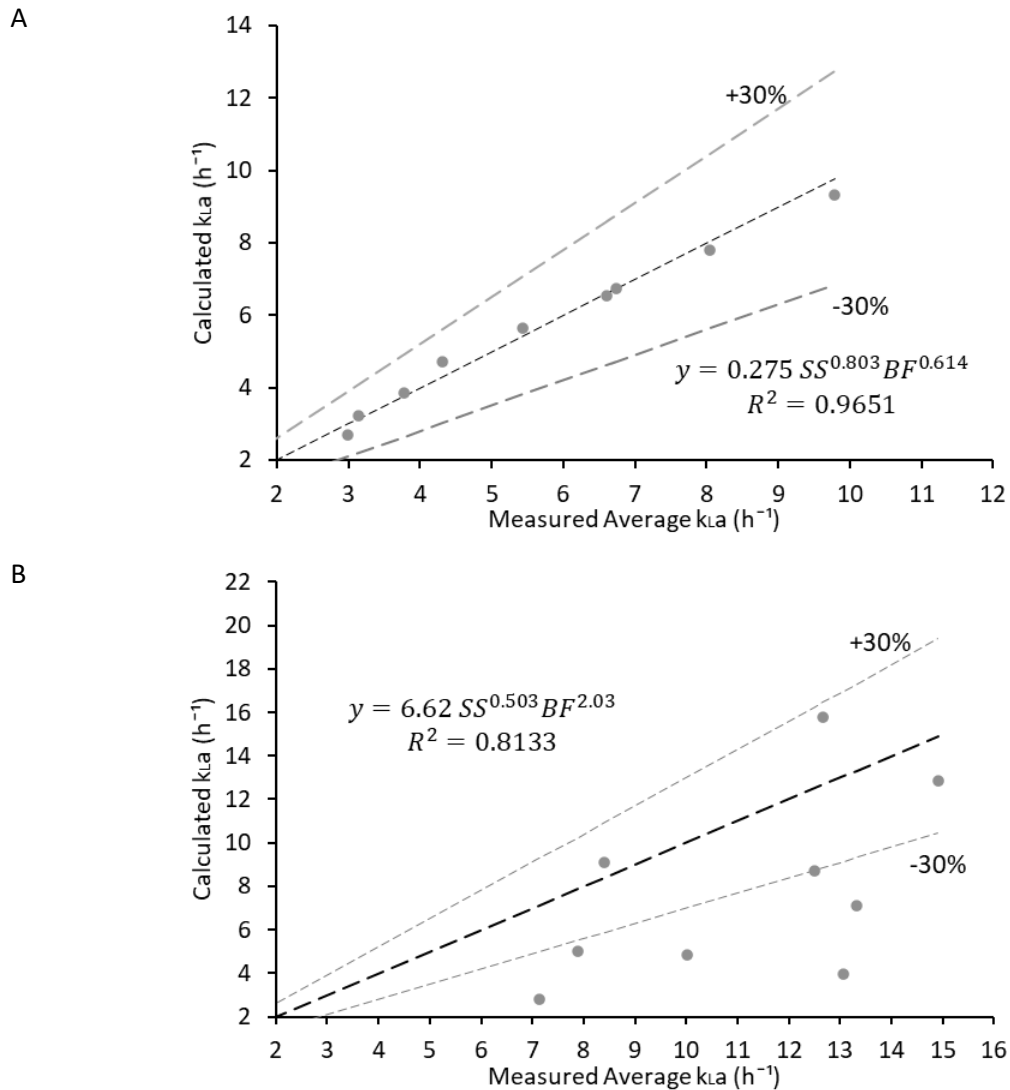


Figure 2-15: Potential model and its comparison with experimental data for calculating k_{La} in the Spinner flask for A: Water and B: Dynamis[®] Culture Medium. Stirring speed (SS in rpm) and bubble flow (BF in ml s⁻¹).

It should also be considered that the models presented in Figure 2-15 only include the non-zero parameter levels, i.e., those experiments whose stirring speed was 50, 100, or 150rpm and bubbling was present. Therefore, a potential model that includes two variables would not be adequate to predict k_{La} . When any of these variables is zero, the model response does not match the experimental evidence.

It is supposed that an increase in k_La is due to the bubble layer on the medium surface, as seen in *Figure 2-16*. This phenomenon did not occur in water, where bubbles on reaching the surface lasted less than 5 seconds in the liquid, which can be attributed to the fact that the composition of the liquid is different, particularly in surfactants content. The presence of these molecules in the medium leads to further surface tension compared to water, which leads to more stable bubbles within the medium. Since k_La is a parameter that integrates the mass transfer coefficient and the gas-liquid interfacial area, the bubble column would increase the contact area. This hypothesis would also explain the similarity between the k_La values in the Erlenmeyer for the two fluids, given that there is no bubbling. It was sought to standardize the bubble size by any quantifiable variable, but the shape of the bubbles was heterogeneous and complex due to stirring. Moreover, further studies are required to validate this hypothesis.



Figure 2-16: Bubble layer in Spinner flask Bioreactor with 100ml Dynamis® culture medium at 37°C, 100rpm, and 0.44ml s⁻¹.

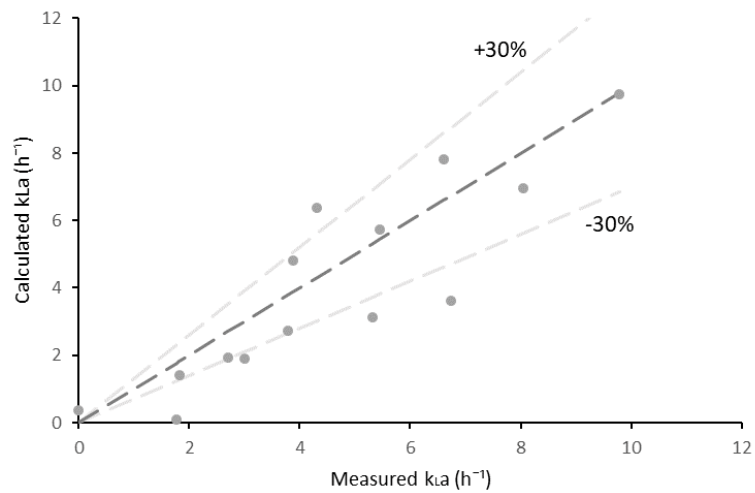
The poor predictability of the model in *Figure 2-15 B* for k_La in the Spinner with culture medium, and the incapability of predicting k_La values when one of the parameters is zero in the potential model, motivate to propose another type of model to correlate the operating conditions studied. The shape of the potential model does not allow predicting the value of k_La when one of the variables, bubble flow or stirring speed, is zero, which is not valid, as can be evidenced by *Figure 2-14*. The proposed model is a polynomic presented in Equation (2-35), where the Greek characters are parameters to determine.

$$k_La = \alpha SS + \beta BF + \gamma SS \times BF + \delta SS^2 + \epsilon BF^2 + \theta \quad (2-35)$$

The values for each parameter are presented as follows:

Parameter	Water	Culture medium
α	0.02637	10.56
β	-0.7567	26.37
γ	0.1271	0.0661
δ	-1.072×10^4	-4.651×10^4
ϵ	-1.481	-0.3221
θ	0.3883	-1.369
R^2	0.9781	0.9117

A



B

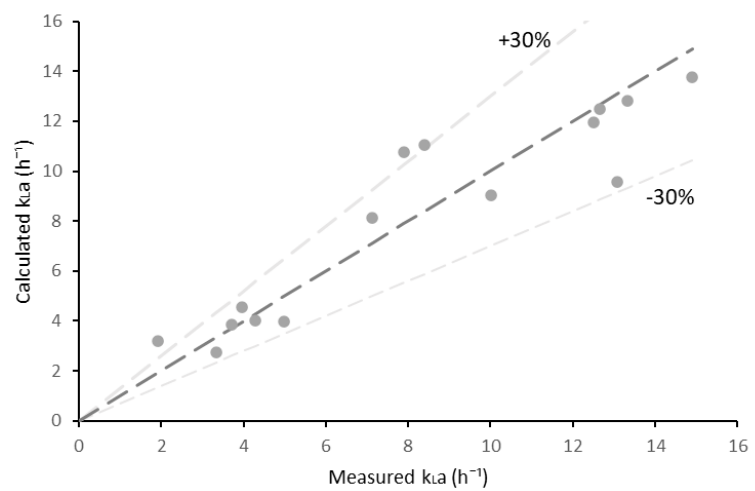


Figure 2-17: Polynomial model and its comparison with experimental data for the calculation of k_La in the Spinner flask for A: Water and B: Dynamis® Culture Medium. Stirring speed (SS in rpm) and bubble flow (FB in $ml\ s^{-1}$).

Finally, the absorption and desorption methods were compared to determine whether the indiscriminate use of one or the other model is valid for the determination of k_La . On the contrary, there is a bias when using a determined method. *Figure 2-18* shows the error relative to the average for the measurements employing the dynamic Gassing in the technique for all the pair of values of the evaluated parameters in the Spinner bioreactor. "First" and "Second" are related to which measurement was performed chronologically first.

However, it does not mean that obligatory two measurements were performed, one followed by the other. According to the experimental planning, it could happen that a pair of values of the parameters were evaluated first using the gassing-in method, and then one by gassing out and then one by gassing in. In this case, this third measurement would correspond in the Figure to "Second." From this information, it is possible to affirm that there is no evidence that the method is biased towards any value tendency since there are values above and below the average. Nor does it appear to be influenced by the performance moment of the experiment. This would confirm that the proposed determination methods correspond to reality and that despite the oxygen flux direction going in opposite directions, both approaches are helpful to describe the oxygen transfer phenomenon in a bioreactor, and in general, for any vessel with fluid in motion.

First, it was validated that the cell concentration can be considered constant during the experiment of q_{O_2} determination. In *Figure 2-19*, it is presented the cell concentration during the exponential growth stage from cultures before these experiments that were performed with the same CHO cell line in unmodified 100ml Spinner-type bioreactors with 40ml of Dynamis® medium 8mM l-glutamine supplemented and cultured at 37°C, 5% CO₂, and 115rpm. According to the regression, the specific growth rate for the CHO line is $0.0303h^{-1}$, corresponding to a duplication time of 22.87h. This means that after two hours at favorable conditions for cell proliferation, the cell concentration would increase around 6%.

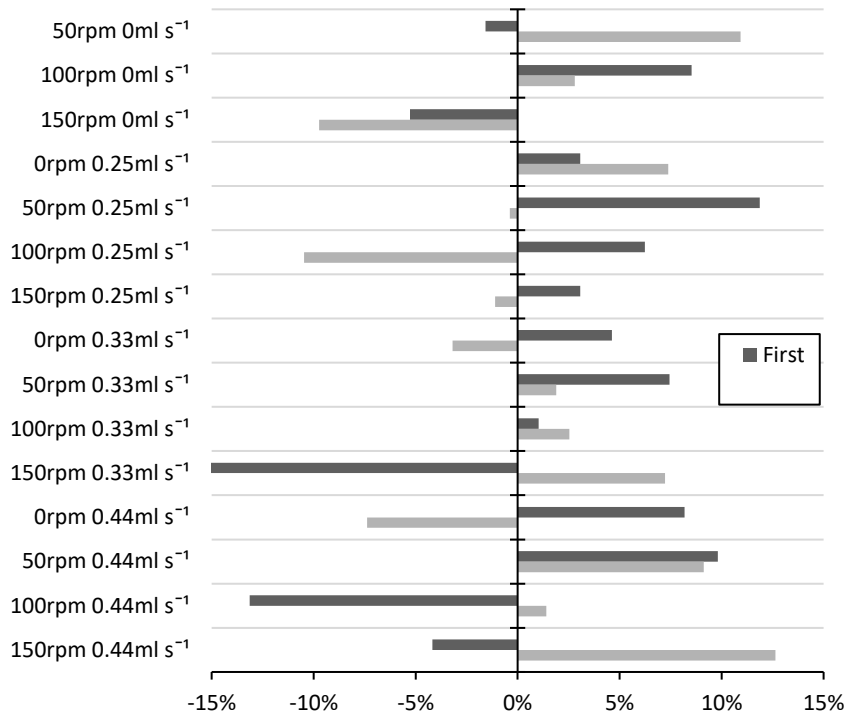


Figure 2-18: Relative error of two k_{La} measurements employing the gassing-in method.

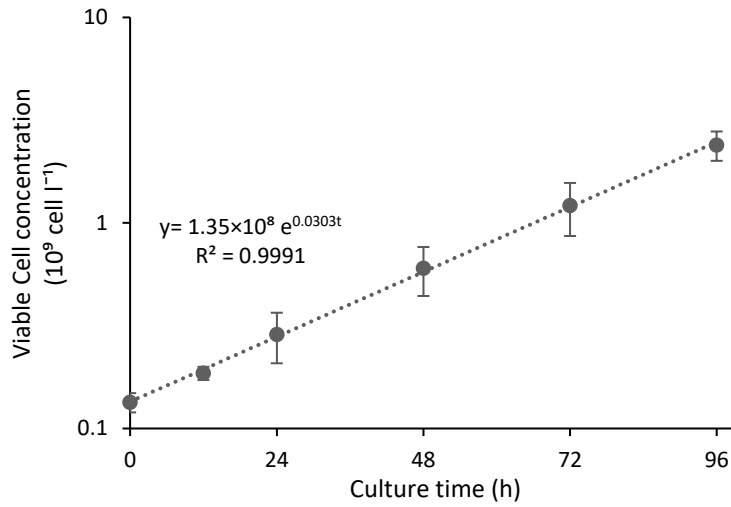


Figure 2-19: CHO cell growth kinetic during exponential stage in 100ml Spinner-type bioreactors with 40ml of Dynamis® medium 8mM l-glutamine supplemented, and cultured at 37°C, 5% CO₂ and 115rpm. N=3. Error bars=σ.

From a technical point of view, the OUR determination is more demanding than k_{La} since the conditions before and during the experiment require more preparation and dexterity. First, the two

measurement methodologies are compared. The obtained results for the q_{O_2} determination with stirring values are shown in *Figure 2-20*, which corresponds to $6.68 \times 10^{-9} \text{ mg O}_2 \text{ cell}^{-1} \text{ h}^{-1}$. In contrast, the values obtained with static liquid were different according to the inlet gas. This should not have happened since the mathematical model for this methodology is independent of how Oxygen flows, from or to the liquid. Therefore, the linear regression does not cross the experimental points, nor is the range given by the standard deviation. Besides, the OUR value for 10^9 cell l^{-1} was higher than for the $2.5 \times 10^9 \text{ cell l}^{-1}$ concentration, which could be explained if the cells had changed their metabolism. However, this explanation loses validity since q_{O_2} measurements were performed with the same culture using the other method before and after the experiments with the immobile fluid. It is also possible to justify this behavior given the presence of a concentration gradient. In the absence of agitation, the cells would precipitate. Therefore, there will be a boundary condition imposed by the cells at the bottom of the reactor. However, it would be expected that the magnitude of the gradient is proportional to the number of cells in the medium, which is not the case here. The sensor manufacturer's recommendation can be reaffirmed from these results, where it is suggested to have the fluid well mixed before any measurement.

According to the literature, a q_{O_2} value of $6.68 \times 10^{-9} \text{ mg O}_2 \text{ cell}^{-1} \text{ h}^{-1}$ is of the same order of magnitude, and in fact, it is very close to the values reported for similar cell lines. This verifies that the model and the methodology used are adequate for determining the parameters related to the supply and consumption of Oxygen for mammalian cell line cultures (Fleischaker Jr and Sinskey 1981).

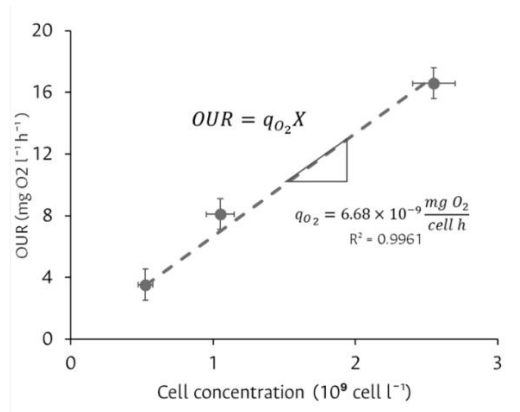


Figure 2-20: OUR as a function of cell concentration for the stirred experiments. N=8. Error bars:

σ .

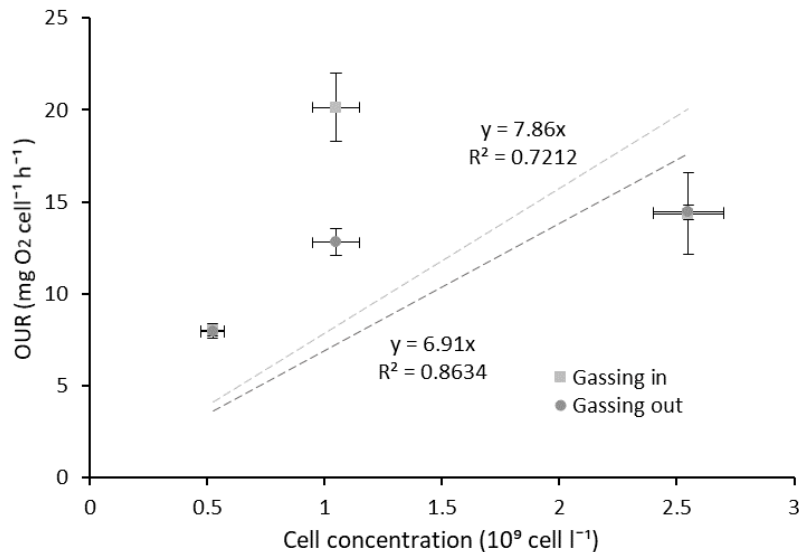


Figure 2-21: OUR as a function of cell concentration for the stirred experiments. $N=3$. Error bars: σ .
The darkest error bars correspond to gassing out experiments.

Therefore, the accepted value is the one obtained by the experiments of the liquid in motion. This value has the same magnitude order as the reported by other authors. It is relevant to mention that the measurements were performed at different values of agitation speed to verify that the k_{La} value did not affect the q_{O_2} . Additionally, the q_{O_2} measurement cycle was completed with a freshly inoculated culture performed in a Spinner bioreactor at 100rpm and no bubbling with a cell concentration of $1.00 \times 10^{10} \text{ cell l}^{-1}$. The obtained value corresponded with a 5% relative error compared to the obtained with the Equation for Erlenmeyer. As in k_{La} , the OUR deals were not biased by the Gassing in or out method.

2.4 Conclusions

The dynamic absorption/desorption method was used to determine the volumetric mass transfer coefficient in two different bioreactor configurations and measure the specific oxygen consumption of a CHO cell line. Given the dynamic nature of this method, possible sources of error that can delay the follow-up of the variable of interest, that is, the percentage of oxygen saturation, affect the accuracy of the estimated value, were studied. Furthermore, within the times that can delay the follow-up variable's report, the sensor's operation, times to obtain the desired conditions

according to the calculation model, and dead times inherent to the experimental process were considered.

In response, a measurement protocol was presented that can be applied to any geometry, a commercial sensor for measuring DO and cell line. Likewise, a model based on the dependence on dissolved Oxygen was proposed to define the operating and bubbling conditions required in a bioreactor.

Once the parameters of Equation (2-35) are known for the study case, it is possible to make predictions about the behavior of the DO concentration in a culture over time. In *Figure 2-22*, the comparison between three k_La values achieved in a bubbled spinner bioreactor starting from 100% air saturation can be appreciated. After the first day of culture, the cell demand at the lowest values of k_La cannot be fulfilled. Therefore, it is expected that after the first day of culture, the cells will have either died or modified their metabolism for living under this critical condition. The same behavior would be expected with a k_La value of 8 h^{-1} after the second day of culture, while the oxygen demand in the culture at the higher k_La is still satisfied by the OTR. As mentioned, this estimate assumes the fulfilling of other requirements of cells, the no-generation of toxic compounds, or avoiding stressful conditions, such as a lower temperature.

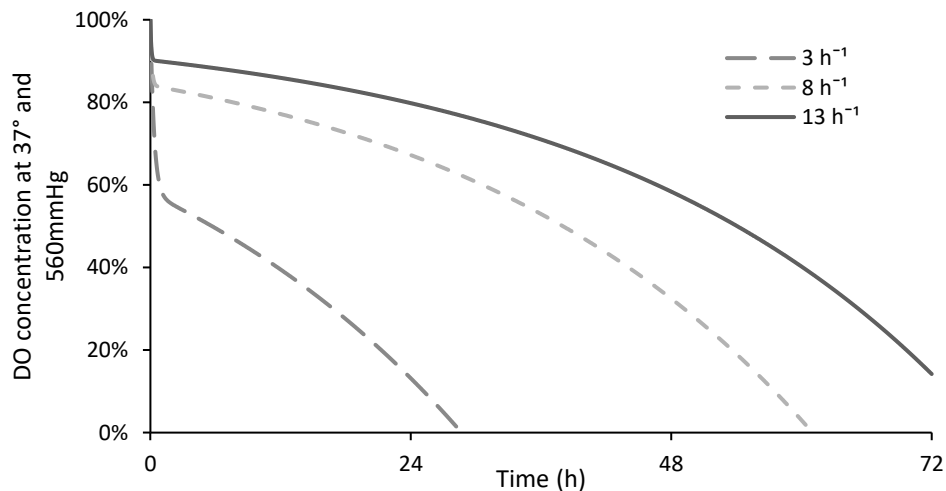


Figure 2-22: DO concentration in terms of air saturation at operation conditions during the culture of the CHO cell line.

3. CHO cells cultures at determined k_{La} values in two bioreactor geometries.

3.1 Introduction

Biopharmaceuticals are substances obtained from biological sources and used for diagnosing, healing, treating, or preventing a disease [146]. While conventional medications are risk-associated due to their non-selectivity and intrinsic toxicity, biopharmaceuticals feature a complex structure that induces a specific response in the patient. Thus, they are more effective in treating a variety of illnesses [147].

Because of a higher percentage of success of biopharmaceuticals in several medical trials [148], [149], in comparison with conventional medicines, their demand has increased in the last thirty years, representing the fastest growing sector in the biotechnology industry [13]. Essentially, the biopharmaceuticals' market is dominated by recombinant proteins, which are molecules produced due to a genetic modification of the genome of a host cell [150]. Some examples of these proteins with currently approved market license are hormones (such as insulin and somatostatin), growth factors, cytokines, and monoclonal antibodies (mAb). The lasts are widely used to treat different diseases, including cancer, rheumatoid arthritis, multiple sclerosis, and Alzheimer's disease [49]. Since mAbs entered the market in 1986, they have become the dominant product of biopharmaceutics. In 2016, mAbs contributed approximately 50% of the biopharmaceutical market worldwide, with a volume of close to 80 billion USD, while by 2020, sales of these products are projected at more than 120 billion USD.

Typical bacterial hosts, such as *Escherichia coli* lack the required cellular machinery for monoclonal antibody synthesis because they cannot carry out glycosylation reactions, which are fundamental for forming this type of recombinant protein. For this reason, cell lines derived from rodents or humans, namely Chinese Hamster Ovary (CHO), Mouse Myeloma (NS0, Non-Secreting Murine Myeloma), Kidney Baby Hamster (BHK), Human Embryo Kidney (HEK), and Human Retina (PER-C6) cells, are used in both biomedical research and industrial production. For example, in 2012, it was shown that 51% of the approved licenses to produce biopharmaceuticals used mammalian cells as host cells [151].

CHO cells are the most used mammalian host cells in the large-scale commercial production of biopharmaceuticals [3], which can be attributed to four reasons: first, they are a GRAS organism (Generally Recognized as Safe), and the genome of the CHO-K1 cell line was recently sequenced [52]. Second, the productivity achieved with gene amplification is highly specific [53]. Third, CHO cell lines show efficient post-translational processing of complex proteins, maintaining high similarity between native recombinant and CHO-derived proteins [51]. And finally, there are several reports of successful adaptation to advanced cultivation strategies, which facilitate their culture in conventional bioreactor configuration, facilitating scale-up and improving productivity.

In this section of the work, the relevance of the selection of oxygen transfer rate as a parameter to establish analogies between shaker-stirred and impeller-stirred bioreactors was studied. In this way, it will be possible to confirm if this parameter is adequate to continue the process of scaling up to larger bioreactors.

3.2 Materials and Methods

3.2.1 Cells and culture medium

The cell source was a frozen 2ml cryovial containing approximately 1×10^7 cells from a parental CHO-S line pass five adapted to growth in suspension. First, the cryovial was submerged in 70% ethanol solution at 70°C until thawed. Then, the content of the cryovial was transferred to a four-baffled glass 100ml Erlenmeyer bioreactor with 30ml of Dynamis® culture medium (Gibco Life Technologies®, Carlsbad, USA) supplemented with 8mM of l-glutamine (Gibco Life Technologies®,

Carlsbad, USA), and incubated for four days at $37^{\circ}\text{C} \pm 0.1$, $5\% \pm 0.1$ of CO_2 and $130\text{ rpm} \pm 1$. After that, the culture was centrifuged at $230g$ for 10min . Next, the supernatant was discarded, and the cells were transferred into three Erlenmeyer flasks with the same mentioned characteristics, medium volume, and incubation conditions. The resulting cultures were centrifuged at $230g$ for 10min . According to the medium manufacturer, cells were then resuspended in 30ml of freezing medium, which consists of $46.25\% \text{ v/v}$ fresh medium, $46.25\% \text{ v/v}$ used medium and $7.5\% \text{ v/v}$ DMSO (Sigma-Aldrich, Buchs, Switzerland). Then, the 30ml of cell suspension was distributed in 26 cryovials, stored for 24h at -80°C , and later in liquid nitrogen until its use. Five days before starting an experiment at determined k_{La} , one of the cryovials was thawed and was inoculated in an Erlenmeyer flask with the same conditions as mentioned. The required cells for start cultures of $1 \times 10^9 \text{ cell l}^{-1}$ were extracted from this culture, and the remaining cells were cultured as backup cultures at the mentioned culture conditions. The culture was finally suspended when cell viability was under 75% .

3.2.2 Bioreactor configuration and operation conditions

The two used bioreactor configurations were already detailed explained. The employed medium volumes were 30ml and 100ml for the Erlenmeyer and Spinner bioreactors, respectively. The sterilization was performed following the DO probe manufacturer instructions. Since only one DO measurement system was available, a glass replica of the sensor was built. In this way, two parallel cultures with cells coming from the same culture could be grown at the same operating conditions.

After inoculation and seal verification, the culture was stirred at 150rpm in the Erlenmeyer bioreactor or 150rpm and bubbled with air at 5psig and 0.44ml s^{-1} at 5psig until achieving a DO concentration higher than 95% of saturation. After that, the operation conditions for a determined k_{La} value were settled as shown in Table 3-1. Image of the real aspect of the culture environment is presented in Figure 3-1 and Figure 3-2.

These values were chosen to consider the prediction made by the model represented in (2-35). According to this prediction, we expect to have the following scenarios: cultures with a k_{La} value of 13 will be in exponential phase even three days after the inoculation, those with a k_{La} value of 8 will start to oxygen starve before reaching day three, and cells cultured at the lowest k_{La} will not get the exponential growth phase.

Table 3-1: Operation conditions for cultures at determined k_{La} values.

k_{La} (h^{-1})	Erlenmeyer	Spinner
3	73rpm	100rpm / $0ml\ s^{-1}$
8	86rpm	-
13	96rpm	150rpm / $0.33ml\ s^{-1}$



Figure 3-1. Picture of the real culture environment for the Erlenmeyer bioreactors.

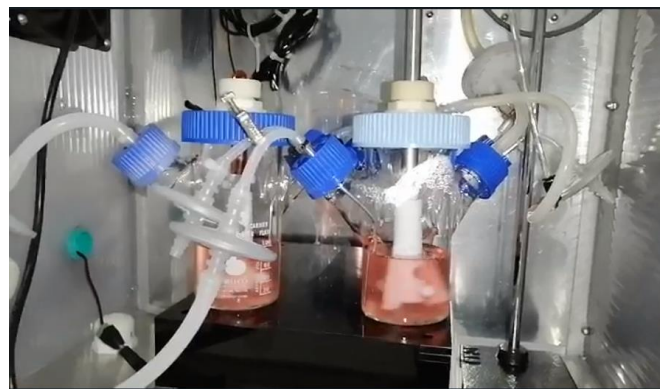


Figure 3-2. Picture of the real culture environment for the Spinner bioreactors.

3.2.3 Culture monitoring

Eight variables were followed for describing the cell culture behavior: Cell concentration, viability, glucose, acid lactic, free LDH concentration, percentage of DO saturation, pH, and Osmolality. Since the inoculation, 500 μ l of samples are obtained from the cultures each 24h. However, if the reported DO concentration is under 20% of air saturation, the sampling interval changes to 12h. This criterion is set considering that in the literature, it is reported that mammalian cells are negatively affected when exposed to hypoxic environments below 20% [144], [152]. After sampling, cell density and viability were immediately determined by counting in a Neubauer chamber (Bright-line, Boeco®) and trypan blue exclusion test. The counts were accomplished on a microscope at 10X. After counting, the sample was centrifugated at 1000g for 5min. The supernatant was stored at -20°C, and the cell pellet was discarded. The protocols and calibration curves for glucose, acid lactic, and free LDH concentration determination are detailly explained in the Annex material. pH was measured with a HI10832 HALO® microelectrode (Hanna Instruments, Woonsocket, US) calibrated with the supplied buffers by the manufacturer (4.01, 7.01, and 10.01) and under atmospheric conditions. Finally, Osmolality was measured with an Osmomat 3000® (Gonotec, Berlin, Germany) calibrated with the patrons supplied by the manufacturer (0, 250, and 500 mOsm l⁻¹).

3.3 Results and discussion

The following is the follow-up to the cell concentration and metabolites mentioned to analyze cell behavior at different oxygen transfer rates.

3.3.1 Cell growth and Viability

From Figure 3-3, there is a correlation between the k_{La} value and the maximum cell concentration reached in both the Erlenmeyer and the Spinner. This means that oxygen transfer rate does have an influence on the performance of the cultured CHO cell line. At first glance, it is possible to relate the growth rate to the k_{La} , i.e., the cells grow faster in the exponential phase and reach higher cell concentrations in the experiments with higher oxygen transfer rate values. However, the maximum concentration achieved in the two reactors operating at the same highest k_{La} value is not the same. In the Erlenmeyer type reactor, a concentration of 1.1×10^7 cell ml⁻¹ was reached, while in the

Spinner reactor, the maximum was 9.0×10^6 cell ml^{-1} . This difference can be attributed to bubbling, and shaker agitation can induce higher shear stress rates in the cells.

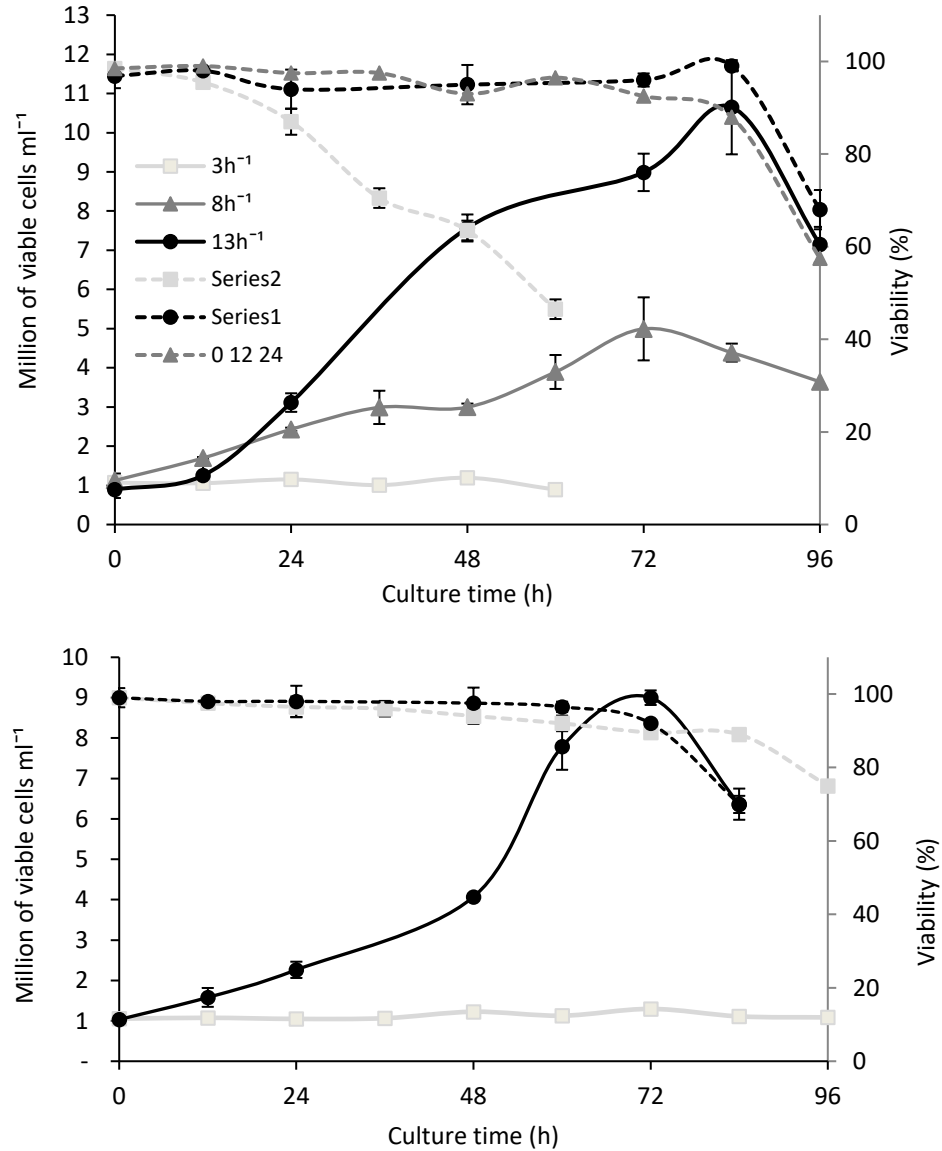


Figure 3-3. Cell concentration (continuous) and viability (dotted) in a 30ml(top)/100ml(bottom) batch culture of CHO cells performed in an Erlenmeyer(top)/Spinner(bottom) bioreactor. $n=4$ and Error bars= σ .

Furthermore, when comparing the behavior of the growth curves at lower k_{La} values, it was observed that the Spinner culture lasted longer, even though the cell concentration did not increase. In contrast, the culture in the Erlenmeyer bioreactor configuration had a shorter culture time with a progressive drop in viability. By qualitative assessment of the cultures during the experiments, it was observed that an orbital stirring speed of 73rpm was not sufficient to keep the cells in suspension. This is reflected in the presence of a precipitate that increased during the culture time, which is suspected to be non-suspended cells. When analyzing a sample of the precipitate under the microscope, it became clear that these were indeed CHO cells and not from another organism that had entered the bioreactor, and that they were also in clusters or already dead. In this way, it was also ruled out that it was contamination. Because of the presence of these dead cells, enzymes, and other compounds harmful to the still suspended cells were likely released. For this reason, the cells cultured in the Erlenmeyer at the lower k_{La} value did not grow.

The significant difference between the behavior of the cultures at lower k_{La} values in the two geometries used would imply that although in terms of oxygen transfer, the two geometries are similar, there are other alien parameters to the respiration that must be considered for a successful scale-up or scale-down process.

3.3.2 Monitoring of Dissolved oxygen concentration

Regarding the monitoring of dissolved oxygen, it can be affirmed that the expected results were obtained qualitatively; that is, the DO concentration drops as the culture progresses, as shown in *Figure 3-4*. However, this did not happen for the Erlenmeyer culture at the lowest k_{La} value, which was also evidenced in the growth curves. The low agitation speed means that the cells are not well agitated to maintain their growth condition in suspension. Besides, a remarkable fact is the behavior of the dissolved oxygen concentration at advanced stages of the culture. It was expected that at some point, the DO concentration reached zero value and remained at this value until the cells died. However, this was not the case. Depending on the experiment, the value of the DO concentration in advanced times of the culture oscillated between 10 and 5% saturation. The moments in which this stabilization occurs correspond to the arrival of the culture to the stationary phase.

Concerning the higher k_{La} value, it can be observed that there is a more significant drop in the DO concentration at the beginning than expected. Despite this, the behavior from then on is very similar, considering that the experiment had a higher driving force due to a higher concentration difference between the interface and the liquid bulk. However, in this case, the model cannot predict the behavior after the second day.

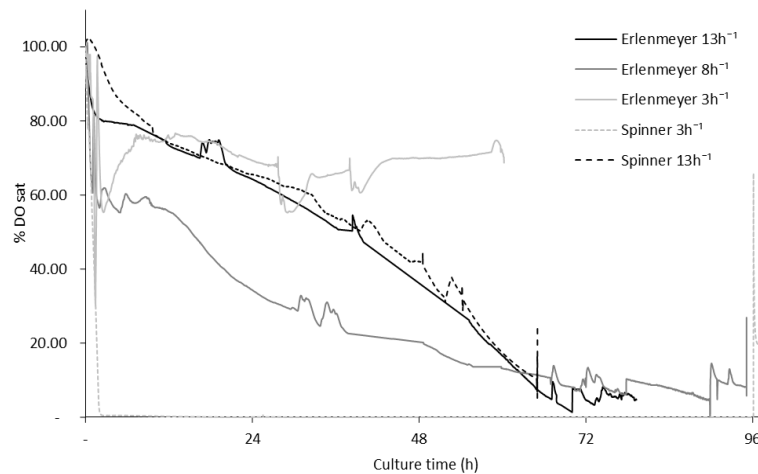


Figure 3-4. Monitoring of DO concentration in a 30ml/100ml batch culture of CHO cells performed in an Erlenmeyer(continuous)/Spinner(dotted) bioreactor. $n=1$.

A further comparison for the Erlenmeyer cultures is presented in Figure 3-5.

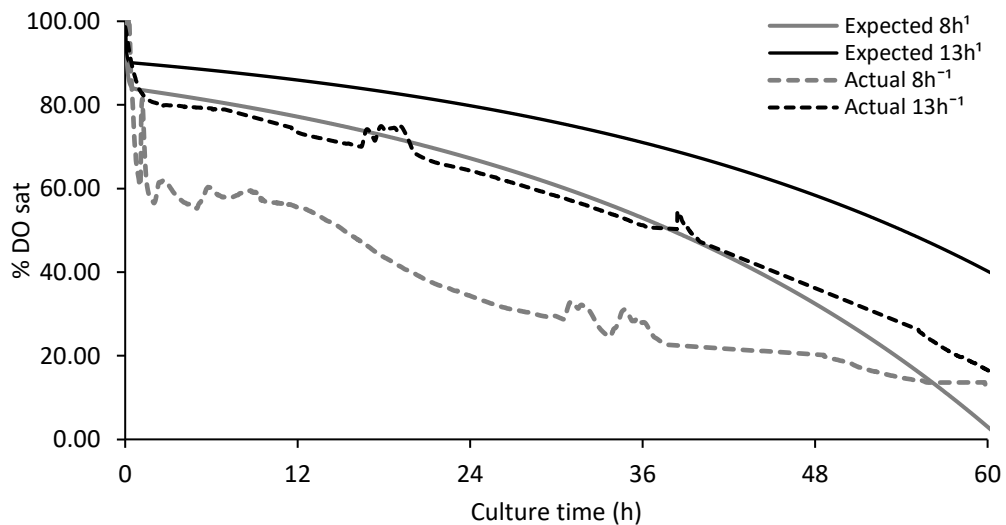


Figure 3-5. Comparison of actual and expected DO concentration for Erlenmeyer bioreactor.

In the case of the lowest k_{La} in the Spinner, a dramatic drop in dissolved oxygen concentration is observed. Although it does not confirm the predictions made by the model, it highlights that it is not appropriate to perform cultures at this k_{La} value if it is expected to obtain cell concentrations greater than 1×10^6 . Moreover, the similarity between the importance of the dissolved oxygen drop at the highest value of k_{La} between the two culture geometries is evident. However, it should be noted that the cell concentrations achieved in the Spinner-type reactor are lower than those obtained in the Erlenmeyer. By calculating the replication times during the exponential phase following the equation (1-14), it can be found that the cells in the Erlenmeyer (23h) duplicates two hours faster than those in the Spinner (21h).

These variations could be attributed to the fact that the value of the specific oxygen consumption determined by the methodology described above is not the same as that of cells cultured at given values of k_{La} . Therefore, as a recommendation for future work, the protocol for determining q_{O_2} should consider using a culture that has already had inoculation in the exponential phase at most minuscule one doubling time. This will provide a more appropriate culture in terms of the metabolic state of the cells since the cells are in the lag phase immediately after centrifugation, trypsinization, and final inoculation in the reactor. Therefore, the metabolic state does not correspond to what happens during the exponential growth stage.

Despite this, the relevance of the model in qualitative terms is relatively good since it predicts that at the low value of k_{La} , the cells will not replicate and gives an idea of the time at which the cells enter the stationary phase.

3.3.3 Monitoring of metabolites

Regarding glucose consumption and lactic acid production in Figure 3-6, the expected behavior is observed. The glucose concentration decreases as the culture progresses, while lactic acid increases and then decreases due to the reincorporation of lactate as a substrate in the metabolic cycle of the cells. Again, here the behavior of the culture in the Erlenmeyer with the lowest k_{La} value is evident. Although the cells did not reproduce, they did consume glucose to stay alive. However, the viability of the culture begins to drop when there is still glucose in the medium. Therefore, growth is inhibited by a factor other than the availability of the carbon source.

Nevertheless, if the cells were stressed by lack of oxygen, the lactic acid concentration would increase faster than in the other cultures. This would lead us to think that the cells under these conditions modified their metabolic patterns, such that they do not require as much oxygen to stay alive, but still, the conditions do not allow them to replicate. In the Spinner case, at the lowest k_{La} , it is observed that the cells consumed the glucose available in the medium but did not reproduce.

A DOT of 10% resulted in the lowest viable cell and product concentration. The lower viable cell yield resulted from a reduced cultivation time and the early entry of cells into the death phase. This would confirm the ability of cells to regulate their oxygen demand. Also, oxygen deficiency may influence the rate of production of a possible monoclonal antibody. According to some literature reports, culture at hypoxic conditions, or under 10%, has negative consequences on viability and speed of antibody production. Therefore, it would not be advisable to work in this region if the objective is to synthesize a recombinant mAb-like protein [153]–[155].

Comparing Figure 3-3 and Figure 3-6, the cells still have glucose availability when the stationary phase of the growth kinetics begins in the cultures with k_{La} values of 8 and 13h^{-1} . For this reason, it could be inferred that the cells are not suffering from a lack of carbon source when their growth is truncated, i.e., the cells have other limitations of another substrate or an inhibitor that prevents them from continuing their growth exponential. This limiting factor is probably oxygen since the DO concentration at that point is less than 15%.

Lactic acid could be used as a parameter to determine the oxygen starvation stress the cell is subjected to since the presence of lactic acid in the medium indicates that the cell must have taken alternative metabolic routes to oxidative phosphorylation to obtain energy. In this order of ideas, the cells were less stressed with the highest k_{La} conditions in the Erlenmeyer and the Spinner-type reactor. Also, it could be observed that less glucose is converted into lactate at the most elevated k_{La} conditions.

With respect to pH, it should be clarified that the measurements were made in the laboratory atmosphere and not inside the incubator; for this reason, the values reported in Figure 3-7 were higher than those to which the cells had been subjected during the culture. However, the direct relationship between pH and lactic acid concentration is evident. This confirms that as the culture progresses, the cells begin to secrete lactic acid as a side product of their metabolism, thus

decreasing the pH of the medium. While during the re-consumption of lactic acid in the advanced stages of the culture, when glucose is scarce, the pH value rises.

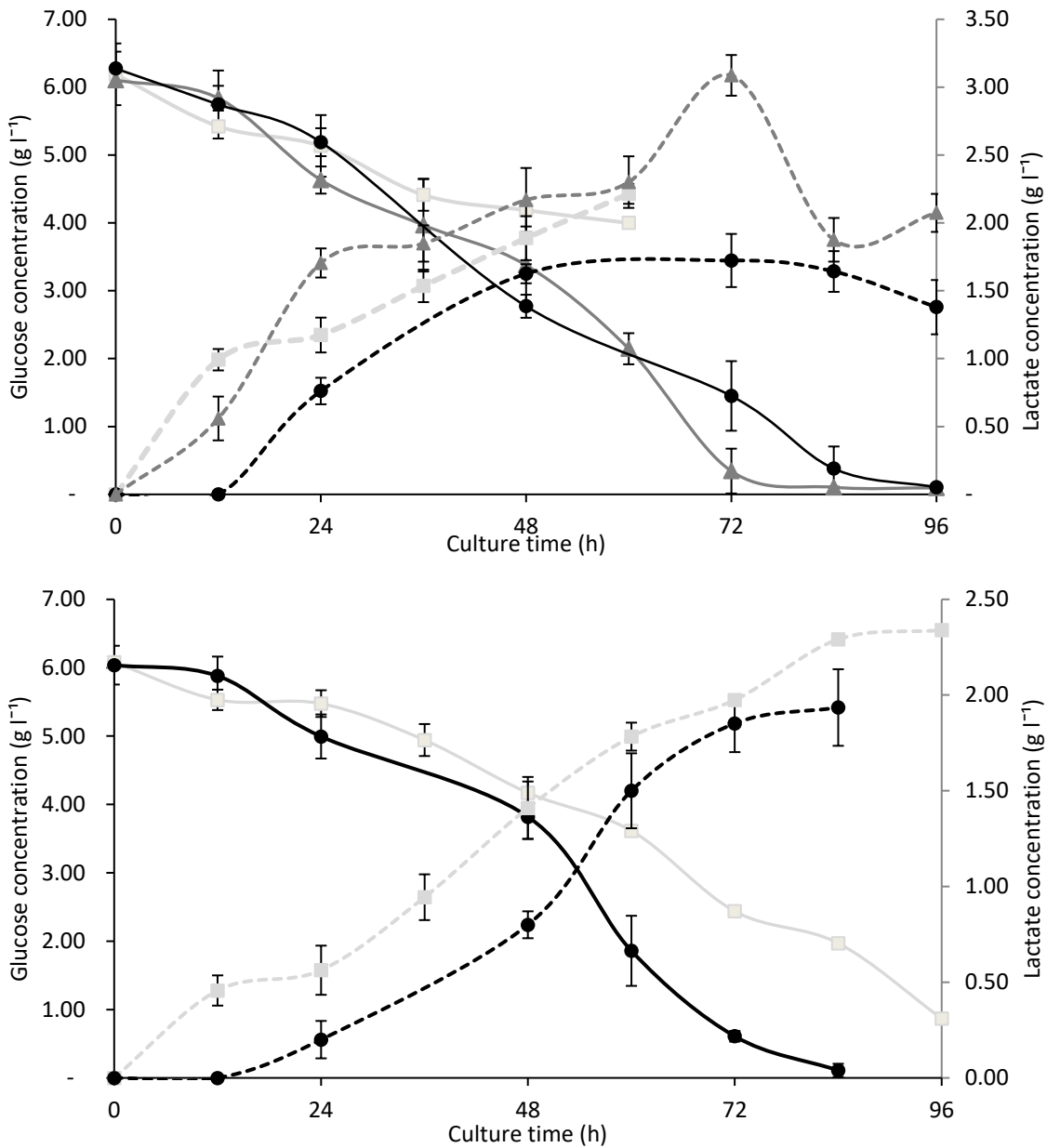


Figure 3-6. Glucose (continuous) and lactic acid concentration (dotted) in a 30ml(top)/100ml(bottom) batch culture of CHO cells performed in an Erlenmeyer(top)/Spinner(bottom) bioreactor. $n=4$ and Error bars= σ .

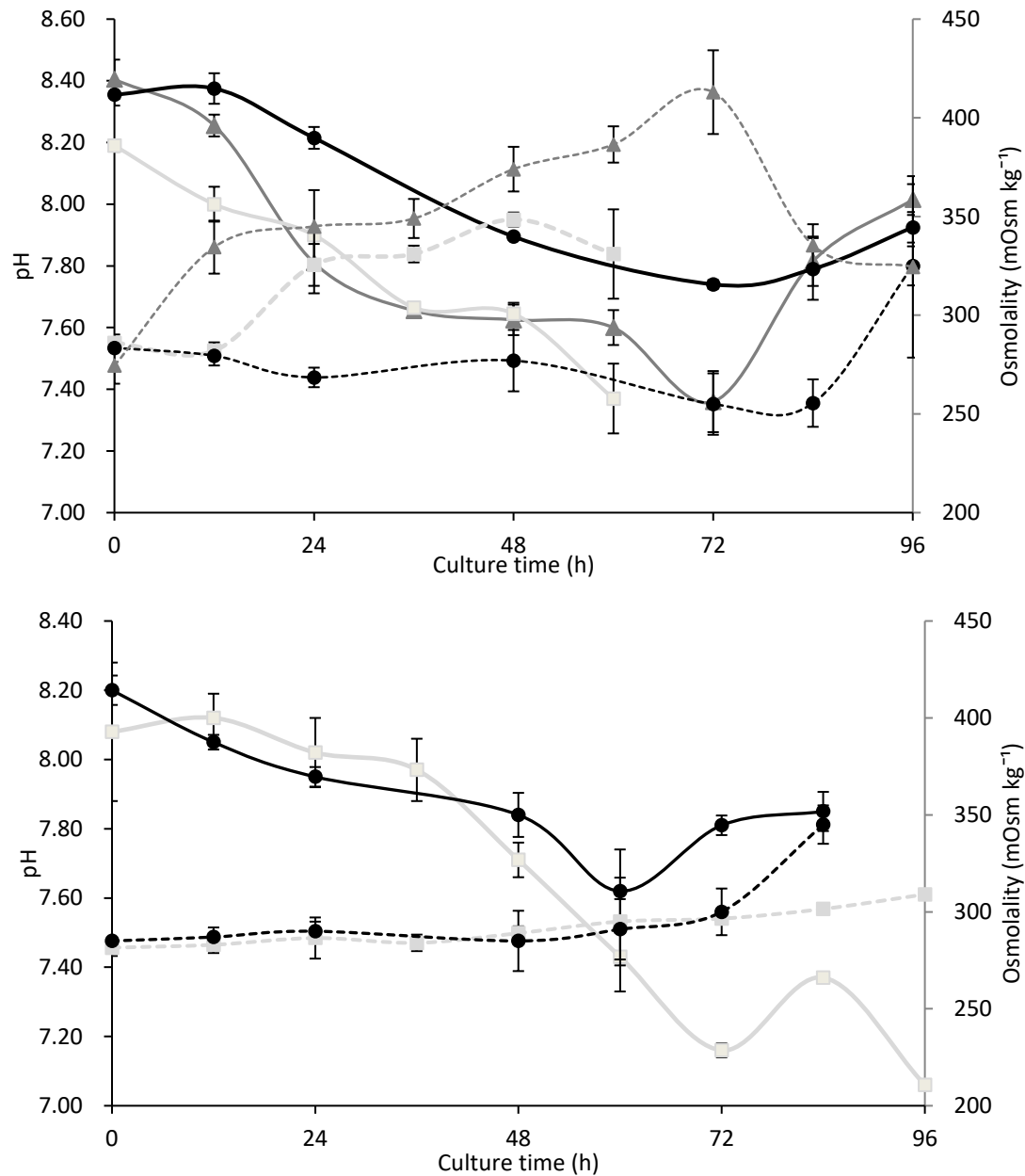


Figure 3-7. pH (continuous) and osmolality (dotted) in a 30ml(top)/100ml(bottom) batch culture of CHO cells performed in an Erlenmeyer(top)/Spinner(bottom) bioreactor. $n=4$ and Error bars= σ .

It is essential to highlight that the most acidic values are reached when the cultures at lower kLa values are near the end of the culture. With respect to osmolality, it is a criterion that does not provide a clear trend with respect to the analysis of the performance of these cultures. Since in certain cultures, it increases as the culture progresses, while in others, it decreases. This is mainly

since other reactions are taking place. It would be helpful to count with other monitoring tools, like HPLC columns, for amino acid quantification. In this way, more detail on the dynamics of cell metabolism would be available.

Finally, it is presented in Figure 3-8 the monitoring to free LDH enzyme in the medium. As LDH is an intracellular enzyme, its detection in the surrounding culture medium is only possible when non-programmed cell death has occurred. In consequence, extracellular LDH is an indicator of cell membrane rupture or apoptosis in mammalian cell culture.

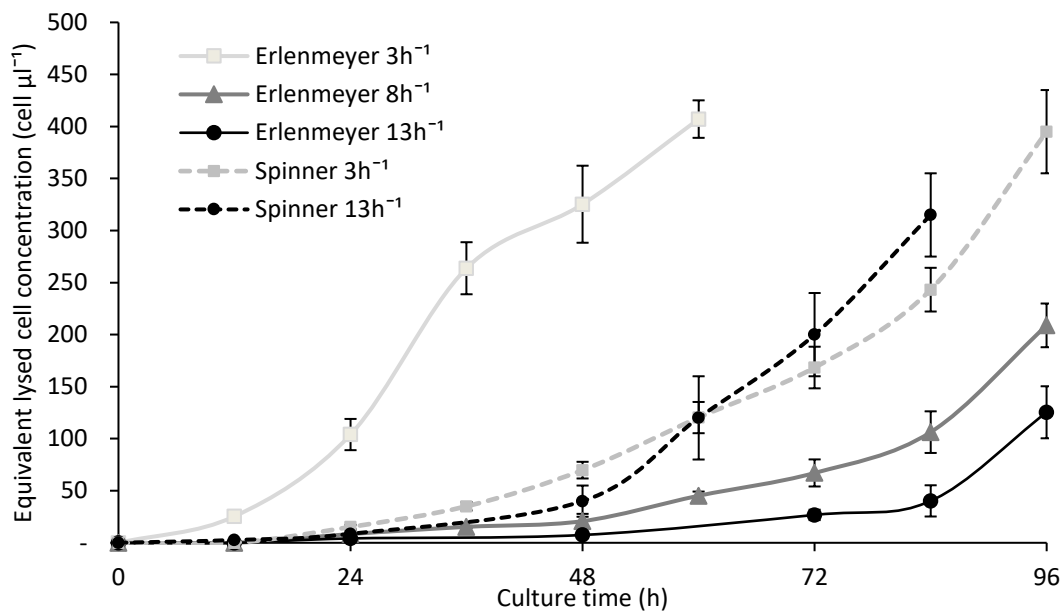


Figure 3-8. Free LDH concentration in a 30ml/100ml batch culture of CHO cells performed in an Erlenmeyer/Spinner bioreactor. $n=4$ and Error bars= σ .

The most suitable conditions for cell growth were achieved in the Erlenmeyer type reactor. The rapid release of LDH in the Erlenmeyer case at the lowest k_{La} value confirms that the cells were undergoing some stress resulting in necrotic death. It is also observed that there is a higher rate of death by necrosis in the spinners than in the Erlenmeyer.

This may be due to the presence of two opposite boundary conditions that limit the fluid control volume in the spinners. On the one hand, there is a wall with zero relative velocity, and on the other hand, a stirrer at a certain speed. The simulated presence of these two conditions necessarily leads to a velocity gradient along with the entire fluid, and therefore to increased turbulence and shear stress.

This is not the case in Erlenmeyer, where the fluid moves simultaneously with the vessel. And although waves are present because of inertia, this homogeneity in the velocity profile means that the gradients are lower, and thus, the cells are not subjected to stresses that put their integrity at risk. To reach a more detailed study of the fundamental behavior of the fluid in a bioreactor, computational fluid dynamics tools can be used to show areas where shear stresses can irreversibly affect the cells.

Because the bubbling flow rate being used was higher than recommended, it was expected that the cells would experience higher shear stress. However, the values reported evidence that the bubbles, in this case, were not causing a significant increase in the rate of cell death compared to the reactor that was only being agitated. It is likely that there are two overlapping effects. On the one hand, there will be cells dying from the bubbling effect, while in the other reactor, they are affected by the lack of oxygen. But to be able to answer this question, further tests at different operating conditions would be necessary.

3.4 Conclusions

- CHO cell cultures were performed at the same oxygen transfer conditions in two laboratory-scale bioreactor geometries. One stirred by a magnetic bar and other moved by action of an orbital shaker.
- Similar results were obtained for cultures grown at a k_La value of $13h^{-1}$, however, that did not occur for those grown at $3h^{-1}$. The agitation conditions in the shaker were not enough for keep the cells in suspension. Therefore, It is possible to affirm that although oxygen transfer is a critical parameter in the performance of the culture, other parameters other than oxygen transfer must also be taken into account, such as the minimum fluidization speed.
- The scale-up process production process should be performed in a larger bioreactor employing a k_La value of $13h^{-1}$.

4. Conclusions and suggestions

4.1 Conclusions

CHO cells were selected for this project, as they are the favorite mammalian cell model employed worldwide to produce recombinant proteins, specifically for therapeutic mAbs. Besides low immunogenic risk and the ability for post-translational processing of complex proteins, CHO cells were selected due to their high specific growth and productivity rates and ease adaptation to CDM, suspension growth, and advanced culture strategies.

The dynamic absorption/desorption method was used both for the determination of the volumetric mass transfer coefficient in two different bioreactor configurations and for the measurement of the specific oxygen consumption of a CHO cell line. Given the dynamic nature of this method, possible sources of error that can delay the follow-up of the variable of interest, that is, the percentage of oxygen saturation, affect the accuracy of the estimated value, were studied. Within the times that can delay the follow-up variable's report, the sensor's operation, times to obtain the desired conditions according to the calculation model, and dead times inherent to the experimental process were considered.

In response, a measurement protocol was presented that can apply to any geometry, a commercial sensor for the measurement of DO and cell lines. Likewise, it was proposed a model based on the dependence on dissolved oxygen for the definition of the operating and bubbling conditions that are required in a bioreactor.

CHO cell cultures were performed at the same oxygen transfer conditions in two laboratory-scale bioreactor geometries. Similar results were obtained for cultures grown at a kLa value of $13h^{-1}$. However, that did not occur for those produced at $3h^{-1}$. The agitation conditions in the shaker were not enough to keep the cells in suspension. Therefore, it is possible to affirm that although oxygen

transfer is a critical parameter in the performance of the culture, other parameters other than oxygen transfer must also be considered, such as the minimum fluidization speed.

4.2 Suggestions

- The scale-up process production process should be performed in a larger bioreactor employing a k_{La} value of 13h^{-1} .
- Employ models based on computational fluid dynamics to know what is happening within the culture medium. In this way, predictions can be made with more rigorous criteria to avoid areas of hypoxia, conditions with lethal shear forces for cells, and other pertinent ones related to the design of bioreactors.
- Perform the protocol for determining q_{O_2} with a culture that has already had inoculation in the exponential phase at most minuscule one doubling time. This will provide a more appropriate culture in terms of the metabolic state of the cells. Since it is likely that the cells immediately after centrifugation, trypsinization, and final inoculation in the reactor are in the lag phase, and therefore, the metabolic state does not correspond to what happens during the exponential growth stage.

A. Annex: Values for k_La for Shaken Flasks

INN	Commercial Name	Company(s)	Type	Cell model	Approved application	Approval year
Denosumab	Prolia®	Amgen, GlaxoSmithKline, DaiichiSankyo, AstraZeneca	Human IgG2	CHO	Osteoporosis	2010
Belimumab	Benlysta®	Human Genome Sciences, GlaxoSmithKline	Human IgG1 λ	NS0	Systemic lupus erythematosus	2011
Ipilimumab	Yervoy®	Lonza Biologics, Inc., Bristol-Myers Squibb, Medarex	Human IgG1 κ	CHO	Metastatic melanoma	2011
Brentuximab vedotin	Adcetris®	Seattle Genetics, Inc.	Chimeric IgG1 κ/λ + MMAE	CHO	Hodgkin lymphoma	2011
Pertuzumab	Perjeta®	Genentech, Inc., Roche	Humanized	CHO	Breast cancer	2012
Raxibacumab	Abthrax®	Human Genome Sciences, GlaxoSmithKline	Human IgG1 λ	NS0	Anthrax infection	2012
Ado-trastuzumab emtansine	Kadcyla™	Genentech, Inc., Roche, Lonza Ltd.	Humanized IgG1 κ + DM1	CHO	Metastatic breast cancer	2013
Vedolizumab	Entyvio®	Millenium Pharmaceuticals Inc., Takeda Pharmaceuticals, AbbVie Bioresearch	Humanized IgG1 κ	CHO	Ulcerative colitis, Crohn's disease	2014
Ramucirumab	Cyramza®	Eli Lilly & Co.	Human IgG1 κ/λ	NS0	Gastric, lung and colorectal cancer	2014

INN	Commercial Name	Company(s)	Type	Cell model	Approved application	Approval year
Obinutuzumab	Gazyva™	Genentech, Inc., Roche	Humanized IgG1k	CHO	CLL	2013
Siltuximab	Sylvant®	Jansen Biotech, Inc.	Chimeric IgG1	CHO	Castleman's disease	2014
Secukinumab	Cosentyx™	Novartis	Human IgG1k	CHO	Plaque psoriasis	2015
Nivolumab	Opdivo®	Bristol-Myers Squibb, Lonza Biologics	Human IgG4k	CHO	Metastatic melanoma	2015
Pembrolizumab	Keytruda®	Merck & Co.	Humanized IgG4k	CHO	Metastatic melanoma	2015
Dinutuximab	Unituxin™	United Therapeutics Corp., Penn Pharmaceutical Services	Chimeric IgG1k	Sp2/0	Pediatric neuroblastoma	2015
Daratumumab	Darzalex®	Jansen Biotech, Inc.	Human IgG1	CHO	Multiple myeloma	2015
Ixekizumab	Taltz®	Eli Lilly & Co.	Humanized IgG4	CHO	Plaque psoriasis	2016
Olaratumab	Lartruvo™	Eli Lilly & Co.	Human IgG1	NS0	STS	2016
Necitumumab	Portrazza®	Eli Lilly & Co.	Human IgG1k	NS0	Metastatic squamous non-small cell lung cancer	2015

B. Annex: Values for k_La for Shaken Flasks

<i>Device</i>	<i>Liquid medium</i>	<i>Temperature (°C)</i>	<i>Volume Range (L)</i>	<i>Agitation range (rpm)</i>	<i>Shaking diameter (cm)</i>	<i>Range k_La (h^{-1})¹</i>	<i>Method</i>	<i>Ref.</i>
Shaken bioreactors with wide conical bottom	Water	20 ¹	1-2.5	50-80	No reported	2-8	CFD	[156]
5L cylindrical glass bottles with a vented cap having a 1.5cm polyether sulfones membrane. 5cm Shaking diameter	Pro-CHO5 medium	37	<5	125	No reported	9.3	Static gassing-out	[157]
Five-liter cylindrical glass bottles	Pro-CHO5 medium	37	5	125 rpm	5	9.5	No reported	[157]
250 - 1000mL bottles	Deionized water	37	0.05-0.6	110	No	4-20	Dynamic gassing-out	[158]

¹ The author reports "Room temperature".

Device	Liquid medium	Temperature (°C)	Volume Range (L)	Agitation range (rpm)	Shaking diameter (cm)	Range k_{La} (h^{-1})	Method	Ref.
1-L polycarbonate Erlenmeyer shake flasks with a vented cap. 50mm shaking diameter.	UHP deionized water	20 ²	0.3	70-220	No	2-20	Dynamic gassing-out	[140]
1-L cylindrical glass bottles with a vented cap having a 1.5 cm polyether sulfones membrane. 50mm shaking diameter.	UHP deionized water	20 ²	0.3	70-220	No	5-30	Dynamic gassing-out	[140]
TubeSpin [®] bioreactor 600 polypropylene tubes. 50mm shaking diameter.	UHP deionized water	20 ²	0.3	70-220	No	1-40	Dynamic gassing-out	[140]
500ml unbaffled orbital shaken bioreactor	Glucose and maltodextrin medium	35	0.10-0.25	100-250	No	45-110	No reported	[159]
Cylindrical orbital shaken bioreactors	Sodium sulfate solution	-	2.5-37.5	80-220	No	2-80	Sodium sulfite oxidation	[160]
TubeSpin [®] conical bottom bioreactor 50 modified with a vented cap, featuring five ventilation holes.	Sodium sulfate solution	37	0.01-0.05	100-300	No reported	20-120	Sodium sulfite oxidation	[161]

C. Annex: Values for k_La for Stirred/Bubbled vessels

<i>Device</i>	<i>Impeller</i>	<i>Gas sparger</i>	<i>Liquid medium</i>	<i>Temp (°C)</i>	<i>Working Volume (L)</i>	<i>Vessel diameter (m)</i>	<i>Power inlet parameter</i>	<i>Aeration parameter</i>	<i>Range k_La (h^{-1})</i>	<i>Method</i>	<i>Ref.</i>
Biostat A Plus bioreactor (chemostat).	Rushton and marine with outside diameters 45mm	Air supply is enriched in oxygen (41%)	Supplemented HyClon serum-free	33-37	0.5	0.13	100 rpm	0.010 L/min	0.0203 - 0.0451	Dynamic gassing-in	[162]
2.5L UniVessel SU® Sartorius Disposable Bioreactor.	Two 3-blade segment (30°) impeller. D/T=0.41	No	Water	37	2.5	0.13	50-200 rpm 1-100 W/m ³	No	0.30-0.75	Dynamic gassing-out	[163]

<i>Device</i>	<i>Impeller</i>	<i>Gas sparger</i>	<i>Liquid medium</i>	<i>Temp p(°C)</i>	<i>Working Volume (L)</i>	<i>Vessel diameter (m)</i>	<i>Power inlet parameter</i>	<i>Aeration parameter</i>	<i>Range k_La (h^{-1})</i>	<i>Method</i>	<i>Ref.</i>
3L UniVessel® Sartorius Glass Bioreactor	3-blade segment (45°) impeller. D/T=0.42	No	Water	37	3	0.13	50-200 rpm 1-100 W/m ³	No	0.30-0.75	Dynamic gassing-out	[163]
5L CelliGen® New Brunswick Disposable Bioreactor.	A pitched blade impeller. D/T=0.59	No	Water	37	5	0.17	50-200 rpm 1-100 W/m ³	No	0.30-0.75	Dynamic gassing-out	[163]
3L Mobius CellReady® Millipore Disposable Bioreactor.	A Marine type impeller. D/T=0.53	No	Water	37	3	0.14	50-200 rpm 1-100 W/m ³	No	0.25-0.80	Dynamic gassing-out	[163]
5L Biostat® baffled stirred bioreactor	Stir bar with or without paddle. D/T=0.35	-	Deionized water	37	4.5	0.17	60-300 rpm	-	0.23-0.88	Dynamic gassing-out	[94]

<i>Device</i>	<i>Impeller</i>	<i>Gas sparger</i>	<i>Liquid medium</i>	<i>Temp (°C)</i>	<i>Working Volume (L)</i>	<i>Vessel diameter (m)</i>	<i>Power inlet parameter</i>	<i>Aeration parameter</i>	<i>Range $k_L a$ (h^{-1})</i>	<i>Method</i>	<i>Ref.</i>
5.0L Four-baffled, cylindrical vessel	Three identical A100 marine impellers	Pipe sparger with 1.8 mm diameter holes.	Chemical defined medium – CHO culture	34	3000-4400	1.2	4.5-125.4 W/m ³	0.014-0.214 mm/s	0.06-3.00	Dynamic gassing-in	[164]
1L Spinner flask bioreactor	Stir bar with or without paddle. D/T=0.625	-	Deionized water	37	0.3-1.0	0.128	60-140 rpm	-	1.05-4.79	Dynamic gassing-out	[94]
500L Four Baffled Stainless-Steel Vessel	Two pitched blades (D/T=0.56) or a marine impeller (D/T=1.26)	Single drilled 1mm hole sparger	Chemical defined medium – CHO culture	36.5	500 ²	1.33	20-40 W/m ³	0.003-0.07 vvm.	0.2-4.0	Dynamic gassing-in	[90]

² This value was obtained from System specifications for XDR-500[®] Single Use Bioreactor by Xcellerex

<i>Device</i>	<i>Impeller</i>	<i>Gas sparger</i>	<i>Liquid medium</i>	<i>Temp p(°C)</i>	<i>Working Volume (L)</i>	<i>Vessel diameter (m)</i>	<i>Power inlet parameter</i>	<i>Aeration parameter</i>	<i>Range k_La (h^{-1})</i>	<i>Method</i>	<i>Ref.</i>
Three-baffled and six-blades torispherical-bottomed cylindrical vessel	Four six- blade Rushton turbines	Ring sparger with six orifices (1 mm).	PBS with 1g/L Pluronic F69	37	80	0.36	70-123 rpm	1-20 L/h Bubble size: 6.1-9.3 mm	1.5-5.5	Dynamic gassing-in	[165]
Unbaffled four-blades cylindrical stirred tanks with probes and sampling pipe.	Three four- blade impellers.	Straight tube sparger with four holes (0.3 mm)	PBS with 1g/L Pluronic F69	37	2.3	0.11	140-260 rpm	1-20 L/h Bubble size: 2.23-3.80 mm	0.3-5.5	Dynamic gassing-in	[165]
250mL Spinner flask bioreactor	Stir bar with or without paddle. D/T=0.65	-	Deionized water	37	0.1-0.25	0.08	60-140 rpm	-	1.59-6.85	Dynamic gassing-out	[94]

<i>Device</i>	<i>Impeller</i>	<i>Gas sparger</i>	<i>Liquid medium</i>	<i>Temp (°C)</i>	<i>Working Volume (L)</i>	<i>Vessel diameter (m)</i>	<i>Power inlet parameter</i>	<i>Aeration parameter</i>	<i>Range $k_L a$ (h^{-1})</i>	<i>Method</i>	<i>Ref.</i>
2L glass bioreactor	A 3-segment blade impeller. Air with 74% oxygen	Air with 74% oxygen	Chemical defined medium – CHO culture	-	2		10-90 W/m ³	0.05-0.4 mm/s	1-8 ³	Dynamic gassing-out	[166]
A cylindrical cultivation chamber, two impellers mounted on a rigid shaft and a submerged sparger.	2 × 3- blade segment impeller and 6-blade disk + 3-blade segment (top) impeller combinations	A combi sparger, which consists of a ring sparger part (hole diameter 0.8 mm) and a micro sparger part (hole	PBS	20	500	-	1-100 W/m ³	0.1 vvm.	8-16	Dynamic gassing-out	[167]

³ This value was estimated from the presented equation by the authors.

<i>Device</i>	<i>Impeller</i>	<i>Gas sparger</i>	<i>Liquid medium</i>	<i>Tem p(°C)</i>	<i>Working Volume (L)</i>	<i>Vessel diameter (m)</i>	<i>Power inlet parameter</i>	<i>Aeration parameter</i>	<i>Range k_La (h^{-1})</i>	<i>Method</i>	<i>Ref.</i>
		diameter 0.15 mm)									
A cylindrical cultivation chamber, two impellers mounted on a rigid shaft and a submerged sparger.	2 × 3- blade segment impeller and 6-blade disk + 3-blade segment (top) impeller combinations	A combi sparger, which consists of a ring sparger part (hole diameter 0.8 mm) and a micro sparger part (hole diameter 0.15 mm)	PBS	20	200	-	1-100 W/m ³	0.1 vvm.	6-15	Dynamic gassing-out	[167]
200L stirred tank	Pitched-blade impeller D/T=0.36	1 mm drilled hole sparger	Merck proprietary basal medium	36.5	200	0.564	140 rpm 25.2 W/m ³	0.8-1.6 L/min 0.004-0.008 vvm	0.8-10	Steady-state	[92]

<i>Device</i>	<i>Impeller</i>	<i>Gas sparger</i>	<i>Liquid medium</i>	<i>Temp (°C)</i>	<i>Working Volume (L)</i>	<i>Vessel diameter (m)</i>	<i>Power inlet parameter</i>	<i>Aeration parameter</i>	<i>Range k_La (h^{-1})</i>	<i>Method</i>	<i>Ref.</i>
Three-vertical baffled glass bioreactor	A 6-blade Rushton impeller and a 3-blade Marine type propeller. 4.5cm	7-hole sparger	Pro-CHO5 medium	37	3.0	0.012	120 rpm 6 kW/m ³	0.77 L/min	9.3	Static gassing-out	[157]
10L glass bioreactor	One 3-segment blade impeller.	Air with 90% oxygen	Chemical defined medium – CHO culture	-	10		20-130 W/m ³	0.05-0.4 mm/s	1-11	Dynamic gassing-out	[166]
3L stirred tank	A Marine type impeller D/T=0.54	500 or 20µm drilled hole sparger	Merck proprietary basal medium	36.5	1.5-2.0	0.130	260-450 rpm 20.5-106.4 W/m ³	0.01-0.15 vvm	0.5-11	Steady-state	[92]
1000L Thermo Scientific	3-blade segment (45°) impeller.	Drilled hole sparger	PBS	37	650-1000	0.959	1-40 W/m ³	5.75-11.5 m/s	1-12	-	[168]

<i>Device</i>	<i>Impeller</i>	<i>Gas sparger</i>	<i>Liquid medium</i>	<i>Temp p(°C)</i>	<i>Working Volume (L)</i>	<i>Vessel diameter (m)</i>	<i>Power inlet parameter</i>	<i>Aeration parameter</i>	<i>Range k_{La} (h^{-1})</i>	<i>Method</i>	<i>Ref.</i>
Hyclone Single-use Bioreactor (S.U.B.)											
3L New Brunswick Bioflo110® Bioreactor	Rushton-style impellers	Sparring tube	0.5g/L xylose, 1.7g/l yeast nitrogen base and 2.27g urea	-	1.50	0.29	250-450 rpm	0.196 L/min	7.2- 21.6	Dynamic gassing- out	[169]
1000L Xcellerex Single-use Bioreactor (XDR®)	3-blade segment (40°) impeller.	Drilled hole sparger	PBS	37	650-1000	0.965	1-40 W/m ³	5.75-11.5 m/s	1-18	-	[168]

<i>Device</i>	<i>Impeller</i>	<i>Gas sparger</i>	<i>Liquid medium</i>	<i>Tem p(°C)</i>	<i>Working Volume (L)</i>	<i>Vessel diameter (m)</i>	<i>Power inlet parameter</i>	<i>Aeration parameter</i>	<i>Range $k_L a$ (h^{-1})</i>	<i>Method</i>	<i>Ref.</i>
3L Four-baffled Glass bioreactor	A single marine impeller. D/T=0.54	Single drilled 0.5mm hole sparger	Chemical defined medium – CHO culture	36.5	3.0	0.016 ⁴	200-260 rpm 20-40 W/m ³	0.018-0.2 vvm.	1.4-20	Dynamic gassing-in	[90]
2000L Stainless Steel Vessel	A pitched blade or a single marine impeller and a drilled hole sparger.	Single drilled 2 or 3mm hole sparger	Chemical defined medium – CHO culture	36.5	2000 ⁵	1.82	20-40 W/m ³	0.002-0.01	0.4-20	Dynamic gassing-out	[90]
A cylindrical cultivation chamber, two impellers	2 × 3- blade segment impeller and 6-blade disk + 3-blade	A combi sparger, which consists of a ring sparger	PBS	20 ⁶	50	-	1-100 W/m ³	0.1 vvm.	4-24	Dynamic gassing-out	[167]

⁴ This value was calculated based on Surface to Volume ratio presented by [90] and the supposition of 3L as effective culture volume

⁵ This value was obtained from System specifications for XDR-2000® Single Use Bioreactor by Xcellerex

⁶ The authors reported room temperature.

<i>Device</i>	<i>Impeller</i>	<i>Gas sparger</i>	<i>Liquid medium</i>	<i>Tem p(°C)</i>	<i>Working Volume (L)</i>	<i>Vessel diameter (m)</i>	<i>Power inlet parameter</i>	<i>Aeration parameter</i>	<i>Range k_La (h^{-1})</i>	<i>Method</i>	<i>Ref.</i>
mounted on a rigid shaft and a submerged sparger.	segment (top) impeller combinations	part (hole diameter 0.8 mm) and a micro sparger part (hole diameter 0.15 mm)									
A cylindrical cultivation chamber, two impellers mounted on a rigid shaft and a submerged sparger.	2 × 3- blade segment impeller and 6-blade disk + 3-blade segment (top) impeller combinations	A combi sparger, which consists a ring sparger part (hole diameter 0.8 mm) and a micro sparger part (hole	PBS	20	1000	-	1-100 W/m ³	0.1 vvm.	10-30	Dynamic gassing-out	[167]

<i>Device</i>	<i>Impeller</i>	<i>Gas sparger</i>	<i>Liquid medium</i>	<i>Tem p(°C)</i>	<i>Working Volume (L)</i>	<i>Vessel diameter (m)</i>	<i>Power inlet parameter</i>	<i>Aeration parameter</i>	<i>Range k_La (h^{-1})</i>	<i>Method</i>	<i>Ref.</i>
		diameter 0.15 mm)									
80L glass bioreactor	Two elephant ear impellers.	Air with 30% oxygen	Chemical defined medium – CHO culture	-	80		5-80 W/m ³	0.2-1.2 mm/s	1-26	Dynamic gassing-out	[166]
A cylindrical cultivation chamber, two impellers mounted on a rigid shaft and a submerged sparger.	2 × 3- blade segment impeller and 6-blade disk + 3-blade segment (top) impeller combinations	A combi sparger, which consists of a ring sparger part (hole diameter 0.8 mm) and a micro sparger part (hole	PBS	20	2000	-	1-100 W/m ³	0.1 vvm.	12-38	Dynamic gassing-out	[167]

<i>Device</i>	<i>Impeller</i>	<i>Gas sparger</i>	<i>Liquid medium</i>	<i>Tem p(°C)</i>	<i>Working Volume (L)</i>	<i>Vessel diameter (m)</i>	<i>Power inlet parameter</i>	<i>Aeration parameter</i>	<i>Range k_La (h^{-1})</i>	<i>Method</i>	<i>Ref.</i>
		diameter 0.15 mm)									
5L Unbaffled, cylindrical vessel	Stirring due to the application of a rotating magnetic field.	Membrane sparger on the bottom	Herstin-Schramm medium	20	4.0	0.13	No stirring 60-160 kW/m ³	1-5 L/min Bubble size: 0.5-3.0	20-50	Dynamic gassing-in	[170]
5 L Unbaffled, cylindrical vessel	Stirring due to the application of a rotating magnetic field.	Membrane sparger on the bottom	Distillated water	20	4.0	0.13 ⁷	No stirring 60-160 kW/m ³	1-5 L/min Bubble size: 0.5-3.0	30-70	Dynamic gassing-in	[170]
Stirred tank reactor with four flat baffles	Two-disk turbine stirred type D/T=0.33		BSM	30	2	0.12	150-650 rpm	2.5 mm/s 2 L/min 1 vvm	18-70	Dynamic gassing-in-out	[121]

⁷ This value was calculated assuming that liquid height is 0.3m

<i>Device</i>	<i>Impeller</i>	<i>Gas sparger</i>	<i>Liquid medium</i>	<i>Temp (°C)</i>	<i>Working Volume (L)</i>	<i>Vessel diameter (m)</i>	<i>Power inlet parameter</i>	<i>Aeration parameter</i>	<i>Range $k_L a$ (h^{-1})</i>	<i>Method</i>	<i>Ref.</i>
500L Four Baffled Stainless-Steel Vessel	A pitched blade D/T=0.33	Single drilled 0.5mm hole sparger or dual with a Frit sparger	Chemical defined medium – CHO culture	36.5	500 ⁸	0.7556	20-40 W/m ³	0.0035-0.08 vvm.	7.0-60	Dynamic gassing-in	[90]
4.0 L Concentric draft tube airlift bioreactor.	No	Circular perforated plate with 0.05m diameter with 90 equidistant holes with 0.001m diameter.	Glycerol 65%	25	3.5	0.12	No stirring 0-70 W/m ³	0.50-1.50 vvm. 1.28-3.85 mm/s	50-120	Dynamic gassing-in	[171]

⁸ This value was obtained from System specifications for Thermo Scientific® HyClone Single-Use Bioreactor (S.U.B.) 500 L

<i>Device</i>	<i>Impeller</i>	<i>Gas sparger</i>	<i>Liquid medium</i>	<i>Temp p(°C)</i>	<i>Working Volume (L)</i>	<i>Vessel diameter (m)</i>	<i>Power inlet parameter</i>	<i>Aeration parameter</i>	<i>Range k_La (h^{-1})</i>	<i>Method</i>	<i>Ref.</i>
4.0 L Concentric draft tube airlift bioreactor.	No	Circular perforated plate with 0.05m diameter with 90 equidistant holes with 0.001m diameter.	Xanthan gum 0.25%	25	3.5	0.12	No stirring 0-70 W/m ³	0.50-1.50 vvm.	55-150	Dynamic gassing-in	[171]
3L New Brunswick Bioflo110® Bioreactor	Rushton-style impellers	Sparring tube.	Cereal milling byproduct in distilled water	30	1.50	0.29	340-500 rpm	0.033-1.0	7.2-106.2	Static gassing-out	[172]

<i>Device</i>	<i>Impeller</i>	<i>Gas sparger</i>	<i>Liquid medium</i>	<i>Temp (°C)</i>	<i>Working Volume (L)</i>	<i>Vessel diameter (m)</i>	<i>Power inlet parameter</i>	<i>Aeration parameter</i>	<i>Range $k_L a$ (h^{-1})</i>	<i>Method</i>	<i>Ref.</i>
PMMA made cylindrical stirred tank	A six bladed Rushton turbine with D/T= 0.33; a six bladed Rushton turbine" with D/T=0.5; a Pitched Blade Turbine (PBT) with D/T=0.33; a Lightning turbine A310 with D/T=0.33; a Lightning turbine A310 with D/T=0.45	No	Deionized water	20-21	0.5 ⁹	0.19	60-2000 rpm 2-2000 W/m ³	No	0.1-100	Simplified dynamic pressure method	[173]

⁹ This value was calculated from H=T=0.19m

<i>Device</i>	<i>Impeller</i>	<i>Gas sparger</i>	<i>Liquid medium</i>	<i>Tem p(°C)</i>	<i>Working Volume (L)</i>	<i>Vessel diameter (m)</i>	<i>Power inlet parameter</i>	<i>Aeration parameter</i>	<i>Range k_La (h^{-1})</i>	<i>Method</i>	<i>Ref.</i>
	or a Marine propeller with D/T=0.37 Stirrer										
5.0 Benchtop bioreactor.	Rushton turbine impeller with six blades. D/T=0.33	Circular perforated plate with 0.05m diameter.	Glycerol 65%	25	3.5	0.17	400-800 rpm 75-800 W/m ³	0.50-1.50 vvm. 1.28-3.85 mm/s	90-250	Dynamic gassing-in	[171]
Four-baffled semi-circle bottom vessel	One or two impellers (Rushton turbine, pitched 4 Blades, Pitched 2 Blades)	Orifice and nozzle	Deionized water	28	1.77	0.90	0-1000 rpm	1-5 L/min	3-180	Dynamic gassing-out	[174]
4.0 L Concentric draft tube	Rushton turbine impeller with	Circular perforated plate with	Glycerol 65%	25	3.5	0.12	400-800 rpm 0.2-3.20 kW/m ³	0.50-1.50 vvm.	90-300	Dynamic gassing-in	[171]

<i>Device</i>	<i>Impeller</i>	<i>Gas sparger</i>	<i>Liquid medium</i>	<i>Temp (°C)</i>	<i>Working Volume (L)</i>	<i>Vessel diameter (m)</i>	<i>Power inlet parameter</i>	<i>Aeration parameter</i>	<i>Range $k_L a$ (h^{-1})</i>	<i>Method</i>	<i>Ref.</i>
stirred airlift bioreactor.	six blades. D/T=0.33	0.05m diameter with 90 equidistant holes with 0.001m diameter.						1.28-3.85 mm/s			
4 L stirred tank bench bioreactor	Seven different dual-impeller combinations with three-blade	-	Xanthan solutions	32	4.0	-	600-1000 rpm	0.4-1.2 vvm	70-280	Dynamic gassing-out	[175]
4 L stirred tank bench bioreactor	Elephant Ear and classical Rushton turbine.	-	Glycerol solutions	32	4.0	-	600-1000 rpm	0.4-1.2 vvm	50-280	Dynamic gassing-out	[175]

<i>Device</i>	<i>Impeller</i>	<i>Gas sparger</i>	<i>Liquid medium</i>	<i>Tem p(°C)</i>	<i>Working Volume (L)</i>	<i>Vessel diameter (m)</i>	<i>Power inlet parameter</i>	<i>Aeration parameter</i>	<i>Range k_La (h^{-1})</i>	<i>Method</i>	<i>Ref.</i>
240L Bubble column - 2m in height	No	Tree type sparger with 0.5mm diameter holes	Sodium sulfate solution	25	120	0.39	No	0.14-0.28 m/s Bubble size: 3-5 mm	650-900	Sodium sulfite oxidation	[115]
5.0 Benchtop bioreactor.	Rushton turbine impeller with six blades. D/T=0.33	Circular perforated plate with 0.05m diameter.	Xanthan gum 0.25%	25	3.5	0.17	400-800 rpm 1.70-0.13 kW/m ³	0.50-1.50 vvm. 1.28-3.85 mm/s	140-415	Dynamic gassing-in	[171]
Four-baffled Ellipsoid-bottom stirred tank.	Three blade impellers.	A ring sparger with 18 equally spaced orifices (1.5 mm in diameter).	Tap water	25	30	0.28	100-550 rpm 3-2000 W/m ³	0.2-2 vvm 1.625-16.25 mm/s	20-325	Dynamic gassing-out	[176]
4.0 L Concentric draft tube	Rushton turbine impeller with	Circular perforated plate with	Xanthan gum 0.25%	25	3.5	0.12	400-800 rpm 0.05-0.5 kW/m ³	0.50-1.50 vvm.	55-450	Dynamic gassing-in	[171]

<i>Device</i>	<i>Impeller</i>	<i>Gas sparger</i>	<i>Liquid medium</i>	<i>Temp (°C)</i>	<i>Working Volume (L)</i>	<i>Vessel diameter (m)</i>	<i>Power inlet parameter</i>	<i>Aeration parameter</i>	<i>Range $k_L a$ (h^{-1})</i>	<i>Method</i>	<i>Ref.</i>
stirred airlift bioreactor.	six blades. D/T=0.33	0.05m diameter with 90 equidistant holes with 0.001m diameter.									
20L one-baffled vessel	A Rushton turbine (D/T=0.4) and a pitched-blade turbine (D/T=0.4)	Ring sparger	Water	30	13	0.14	500-1200 rpm	5-33 L/min 0.2-2 vvm	50-450	Dynamic gassing-out	[177]
550 L Baffled, torispherical-bottomed cylindrical vessel	B2-45 D/T=0.488	A two-head sparger at the bottom of the vessel	Xanthan gum solutions	25	150-300	0.68	400 rpm	96-400 L/min 0.32-2.66 vvm. 4.41-18.4 mm/s	125-800	Oxygen mass balance	[178]

<i>Device</i>	<i>Impeller</i>	<i>Gas sparger</i>	<i>Liquid medium</i>	<i>Tem p(°C)</i>	<i>Working Volume (L)</i>	<i>Vessel diameter (m)</i>	<i>Power inlet parameter</i>	<i>Aeration parameter</i>	<i>Range k_La (h^{-1})</i>	<i>Method</i>	<i>Ref.</i>
								Bubble size: 1-16mm			
3L five-baffled vessel	Double flux-specific impeller D/T=0.56	Sparger tube	Water	30	2.5	0.14	500-1000 rpm	1 L/min	100-1000	Dynamic gassing-out	[177]
3L five-baffled vessel	Double flux-specific impeller D/T=0.56	Sparger tube	Xanthan solutions (0.25, 0.5, 1%)	30	2.5	0.14	400-1000 rpm	1 L/min	5-1000	Dynamic gassing-out	[177]

D. Annex: Values for $k_L a$ for Stirred/Bubbled vessels

Device	Liquid media	Equation	$C \times 10^3$	α	β	χ	Range	Ref.
Four-baffled Ellipsoid-bottom stirred tank, three blade impellers.	Tap water	$C \left(\frac{P}{V_L}\right)^\alpha v_s^\beta P_{OG}^\gamma$	0.0082	0.430	0.438	- 0.0467	30L 100-550rpm 0.2-2 vvm	[176]
10L glass bioreactor with one 3-segment blade impeller. Air with 90% oxygen	Chemical defined medium CHO culture	$C \left(\frac{P}{V_L}\right)^\alpha v_s^\beta$	0.011	0.55	0.67	-	10L 20-130 W m^{-3} $0.5-4.0 \cdot 10^{-4}$ $m s^{-1}$	[166]
80L glass bioreactor with one 3-segment blade impeller. Air with 30% oxygen	Chemical defined medium CHO culture	$C \left(\frac{P}{V_L}\right)^\alpha v_s^\beta$	0.016	0.72	0.77	-	80L $5-80 W m^{-3}$ $0.2-1.2 \cdot 10^{-3}$ $m s^{-1}$	[166]
2L glass bioreactor with one 3-segment blade impeller. Air with 74% oxygen	Chemical defined medium	$C \left(\frac{P}{V_L}\right)^\alpha v_s^\beta$	0.018	0.25	0.59	-	2L $10-90 W m^{-3}$ $0.5-4.0 \cdot 10^{-4}$ $m s^{-1}$	[166]

Device	Liquid media	Equation	$C \times 10^3$	α	β	χ	Range	Ref.
	CHO culture							
Four-baffled cylindrical vessel with a standard Rushton turbine	Deionized water	$C \left(\frac{P}{V_L} \right)^\alpha v_s^\beta$	0.077	0.67	0.58	-	1.77L 0-1000 rpm 0.56-2.82 vvm	[174]
Four-baffled cylindrical vessel with two Rushton turbines	Deionized water	$C \left(\frac{P}{V_L} \right)^\alpha v_s^\beta$	0.091	0.68	0.58	-	1.77L 0-1000 rpm 0.56-2.82 vvm	[174]
Stirred tank bioreactor using with two three-blade Elephant Ear.	Glycerol solutions	$C N^\alpha v_s^\beta \mu^\gamma$	0.12	0.99	0.32	-0.86	4.0L 600-1000 rpm 0.4-1.2 vvm	[175]
Stirred tank bioreactor using with two Rushton turbines.	Glycerol solutions	$C N^\alpha v_s^\beta \mu^\gamma$	0.14	0.84	0.27	-1.01	4.0L 600-1000 rpm 0.4-1.2 vvm	[175]
Stirred tank bioreactor using with a three-blade	Glycerol solutions	$C N^\alpha v_s^\beta \mu^\gamma$	0.19	0.92	0.24	-0.49	4.0L 600-1000 rpm	[175]

Device	Liquid media	Equation	$C \times 10^3$	α	β	χ	Range	Ref.
Elephant Ear and a Rushton turbine.							0.4-1.2 vvm	
1000L Xcellerex Single-use Bioreactor (XDR®) with 3-blade segment (40°) impeller.	PBS	$C \left(\frac{P}{V_L}\right)^\alpha v_s^\beta$	0.212	0.829	0.554	-	650-1000L Max. 108 rpm Max. 0.029	[168]
1000L Thermo Scientific Hyclone Single-use Bioreactor (S.U.B.) with 3-blade segment (45°) impeller.	PBS	$C \left(\frac{P}{V_L}\right)^\alpha v_s^\beta$	0.215	0.524	0.816	-	650-1000L Max. 95 rpm Max. 0.043	[168]
Four-baffled cylindrical vessel with two Pitched 4 blade turbines	Deionized water	$C \left(\frac{P}{V_L}\right)^\alpha v_s^\beta$	0.230	0.60	0.72	-	1.77L 0-1000 rpm 0.56-2.82 vvm	[174]
5L CelliGen® New Brunswick Disposable Bioreactor with a pitched blade impeller.	Water	$C \left(\frac{P}{V_L}\right)^\alpha$	0.24	0.29	-	-	Up to 5L 50-200 rpm	[163]

Device	Liquid media	Equation	$C \times 10^3$	α	β	χ	Range	Ref.
Stirred airlift biorreactor	Glycerol solutions	$C N^\alpha v_s^\beta \mu^\gamma$	0.263	0.50	0.66	-0.50	4.0L 400-800 rpm 0.5-1.5 vvm	[171]
3L Mobius CellReady® Millipore Disposable Bioreactor with a Marine type impeller.	Water	$C \left(\frac{P}{V_L}\right)^\alpha$	0.29	0.30	-	-	Up to 3L 50-200 rpm	[163]
Four-baffled cylindrical vessel with a Pitched 2 blade turbine	Deionized water	$C \left(\frac{P}{V_L}\right)^\alpha v_s^\beta$	0.320	0.46	0.75	-	1.77L 0-1000 rpm 0.56-2.82 vvm	[174]
Four-baffled cylindrical vessel with a Pitched 4 blade turbine	Deionized water	$C \left(\frac{P}{V_L}\right)^\alpha v_s^\beta$	0.340	0.55	0.77	-	1.77L 0-1000 rpm 0.56-2.82 vvm	[174]
2.5L UniVessel SU® Sartorius Disposable Bioreactor with two 3- blade segment (30°) impeller.	Water	$C \left(\frac{P}{V_L}\right)^\alpha$	0.36	0.24	-	-	Up to 2.5L 50-200 rpm	[163]

Device	Liquid media	Equation	$C \times 10^3$	α	β	χ	Range	Ref.
3L UniVessel® Sartorius Glass Bioreactor with 3-blade segment (45°) impeller.	Water	$C \left(\frac{P}{V_L} \right)^\alpha$	0.37	0.26	-	-	Up to 2L 50-200 rpm	[163]
Four-baffled cylindrical vessel with two Pitched 2 blade turbines	Deionized water	$C \left(\frac{P}{V_L} \right)^\alpha v_s^\beta$	0.455	0.55	0.81	-	1.77L 0-1000 rpm 0.56-2.82 vvm	[174]
Mechanically stirred bioreactor	Glycerol solutions	$C N^\alpha v_s^\beta \mu^\gamma$	1.84	0.25	0.70	-0.40	4.0L 400-800 rpm 0.5-1.5 vvm	[171]
250mL Spinner bioreactor	Deionized water	$C V_L^\alpha N^\beta$	4.1	-1.04	0.94	-	0.1-0.25 L 60-140 rpm	[94]
Unbaffled, cylindrical vessel mixed based on the application of a rotating magnetic field.	Distillated water	$C \left(\frac{P_{RMF}}{V_L} \right)^\alpha v_s^\beta$	5.2	0.49	0.29	-	4.0L 0.25-1.25 vvm 0-50 Hz	[170]
Unbaffled, cylindrical vessel mixed based on	Distillated water	$C \left(\frac{P_{RMF}}{V_L} \right)^\alpha v_s^\beta$	5.4	0.56	0.29	-	4.0L	[170]

Device	Liquid media	Equation	$C \times 10^3$	α	β	χ	Range	Ref.
the application of a rotating magnetic field.							0.25-1.25 vvm 0-50 Hz	
250mL Spinner bioreactor	Deionized water	$CV_L^\alpha N^\beta$	7.4	-0.97	0.94	-	0.1-0.25 L 60-140 rpm	[94]
1L Spinner bioreactor	Deionized water	$CV_L^\alpha N^\beta$	28	-0.68	0.94	-	0.1-0.25 L 60-140 rpm	[94]
550L Cylindrical, dished base stainless-steel vessel		$C \left(\frac{P}{V_L}\right)^\alpha v_s^\beta \mu^\gamma$	63	0.41	0.16	-0.39	228-475 rpm 0.25-1 vvm	[179]
Four-baffled, cylindrical vessel equipped with three identical A100 marine impellers	Chemical defined medium CHO Culture	$C \left(\frac{P}{V_L}\right)^\alpha v_s^\beta$	75	0.47	0.80	-	3000-4400 L P/V: 4.5- 125.4 W m ⁻³ v_s : 0.14-2.14 m s ⁻¹	[164]
5L Spinner bioreactor	Deionized water	$CV_L^\alpha N^\beta$	740	-3.19	1.15	-	0.1-0.25 L 60-140 rpm	[94]

E. Annex: Calibration curves for Flow Indicators (FI)

The rotameters were calibrated using a graduated cylinder and a container of water. First, the measuring cylinder was utterly immersed in the water. Then, the graduated cylinder was partially removed from the water since it had to be placed in a vertical position upside down with the mouth submerged in the water to prevent air from entering the cylinder. Subsequently, the flow and pressure conditions to be evaluated were set, and the air outlet hose was taken to the container so that the air began to displace the water stored in the cylinder. Since the flask had graduation marks, it was possible to record the time in which a given volume of water was displaced. The water temperature for these experiments was, on average, 17°C.

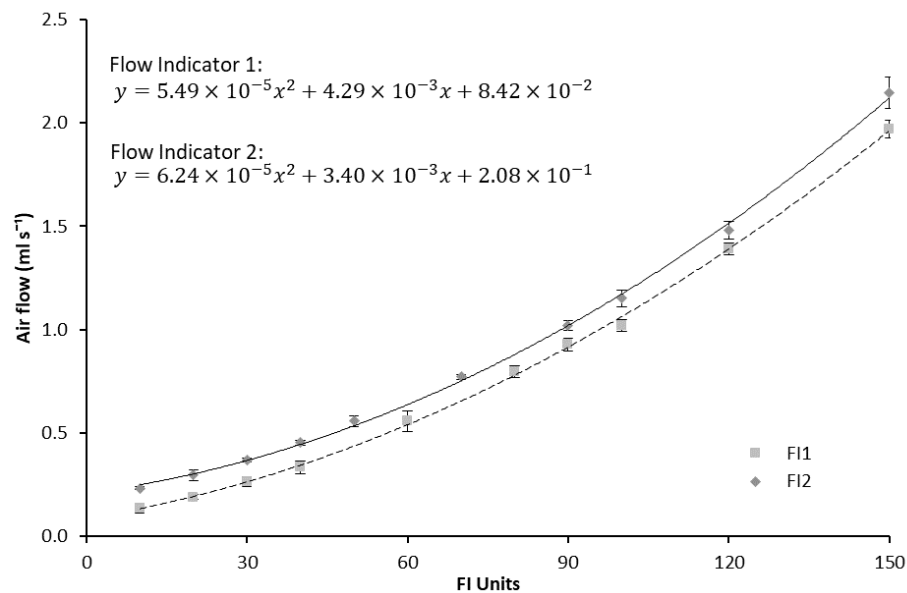
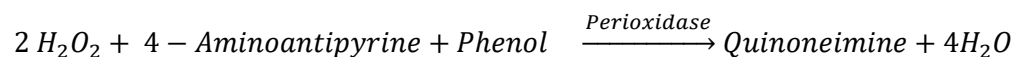
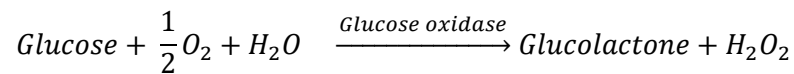


Figure 4-1: Calibration curve for the rotameters or Flow Indicators (FI). Air at 20°C and 15.83 psia was employed. N=4 and Error bars = σ .

F. Annex: Calibration Curve for the measurement of Glucose concentration

Glucose concentration was quantified by absorbance measurement employing the enzymatic kit 11538 (Biosystems®, Barcelona, Spain). The reactive is a mix of glucose oxidase and peroxidase. Following coupled reactions (equation), glucose present in the sample produces a colored complex that can be quantified by spectrophotometry. Glucose peroxidase oxidizes glucose into gluco lactone, converting oxygen to peroxide, which is in turn transformed by peroxidase in the presence of amino antipyrine and phenol. As a result, a red-violet complex is formed, using quinone imine as an indicator.



Due to the valid range of concentrations and the initial glucose concentration of the medium, every sample was centrifuged. The cell pellet was discarded, and the supernatant was stored at -20°C. A fraction of the supernatant was diluted with distilled water by a factor of seven, and 10µl of this solution was mixed with 100 µl of enzyme solution in a 96 well-plate. A Cytation 3 imaging reader (Biotek®, Winooski, USA) was used for reading absorbance after 20 min shaking at 37°C. Calibration was performed with the standard provided by the kit.

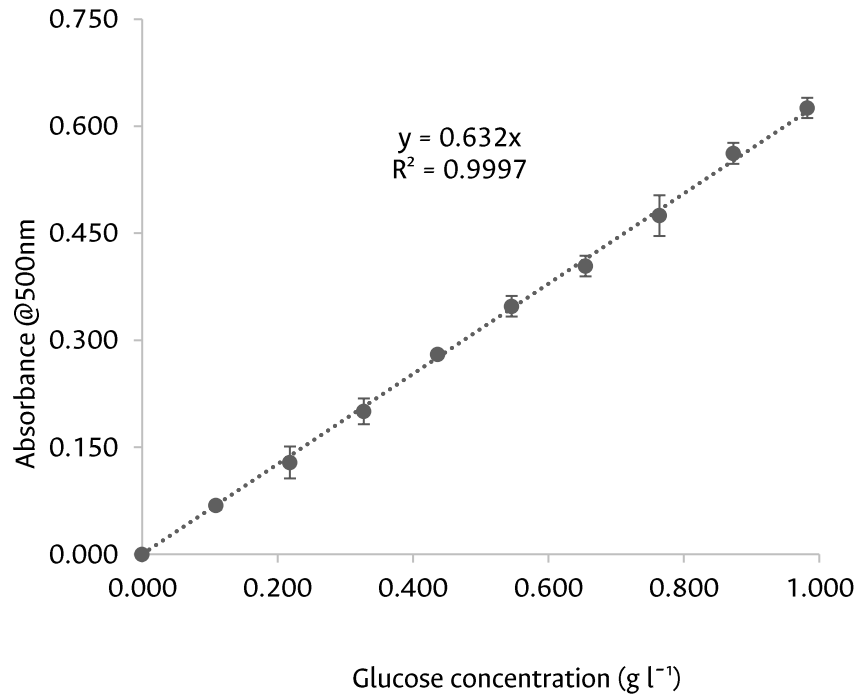


Figure 4-2: Calibration curve of the enzymatic method for glucose concentration determination after shaking the sample in a 96-well plate during 30 min at 37°C. Trendline equation: $y=0.632x$, $R^2 = 0.9989$; x =Glucose concentration, y =Absorbance.

G. Annex: Calibration Curve for the measurement of Lactic Acid concentration

The lactic acid concentration was quantified by High-Performance Liquid Chromatography (HPLC), with a column for the analysis of organic acids. The column employs ion and size exclusion modes plus reversed-phase mode RSpak KC-811, 8 x 300 mm (Shodex®, Tokyo, Japan) and guard column RSpak KC-G, 6 x 50 mm (Shodex®, Tokyo, Japan). The mobile phase used was a solution of H₃PO₄ at 0.1% w/v (obtained by diluting in deionized water an 88% w/v H₃PO₄ stock solution (ITW Reagents, Darmstadt, Germany)), the flow rate of 0.9 mL min⁻¹, 30°C, the volume of injection of 20 µL and running time of 20 minutes. Every sample was diluted 20 times in deionized water and was filtered through a GN-6 Metrical® (Pall, Mexico City, Mexico) cellulose acetate (CA) membrane with a pore size of 0.47µm. The retention time for the evaluated peaks was 10.3min.

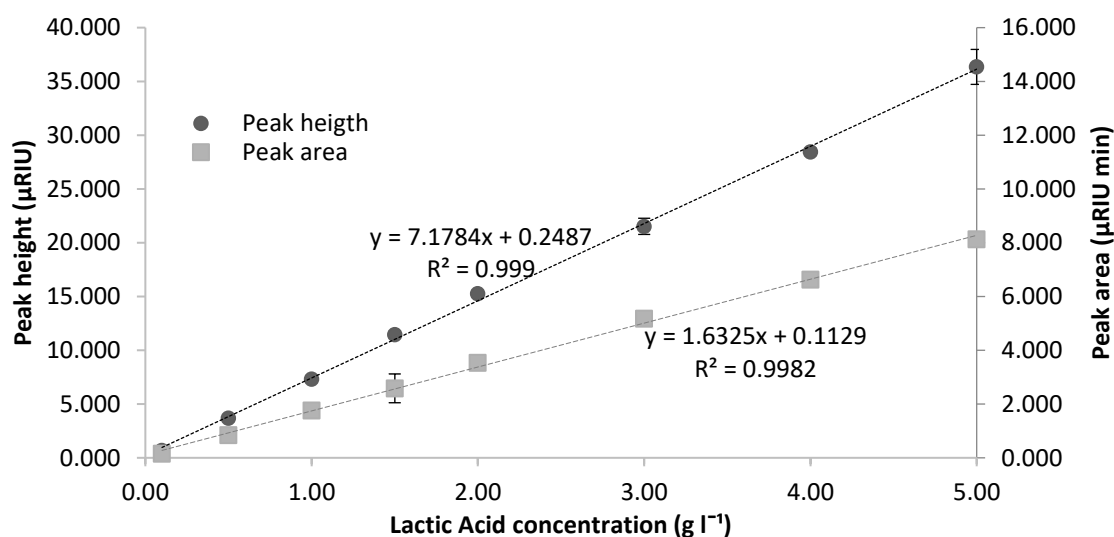


Figure 4-3: Calibration curve of the HPLC method for lactic acid concentration determination. $N=2$,

Error bars= σ .

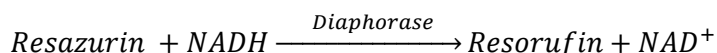
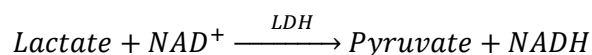
H. Annex: Calibration Curve for the measurement of Free lactate dehydrogenase (LDH) concentration

Measurement of the leakage of components from the cytoplasm into the culture medium is a method to estimate the culture health and the lethality of the bioreactor environment in terms of shear stress rates. Lactate dehydrogenase (LDH) is an intracellular enzyme associated with the conversion of pyruvate to lactate and back, whose presence in the culture medium implies cell membrane leakage due to necrosis. Contrary to the viability, which is a punctual measurement, the concentration of the LDH enzyme usually tends to increase with the culture time, and therefore it can be used as a memory of the culture performance.

Free LDH enzyme concentration was quantified by fluorescence measurement employing a Promega enzymatic kit CytoTox-ONE (Promega®, Madison, USA). For standardizing the method, a previous CHO cell culture was performed. It started from a 2ml thaw cryovial with approx. 1.0×10^7 cells that were inoculated in a Spinner flask with approx. 40ml of Dynamis® culture medium. After three days, the cell concentration was 1.80×10^9 cells l^{-1} and 99% viability. Cell concentration and viability were measured with 20 μ l of a 1:1 solution of culture sample and 0.4% w/v Trypan blue. This solution was placed in a Neubauer chamber, and the counting procedure was three times performed. With the healthy culture and fresh medium, 1ml of ten solutions with cell concentrations between 0 and 5.00×10^7 cells l^{-1} were prepared in 2ml Eppendorf tubes. These solutions were submitted into liquid nitrogen for 10min and thaw in a 37°C water bath until there was no evidence of ice. These freezing-thawing steps were performed four times more. With this procedure, it can be assumed that all cells had experienced necrosis and that the free LDH concentration corresponds to the death of the known quantity of cells.

Following the manufacturer's instructions, 25 μ l of sample and 25 μ l of the kit enzyme solution were placed in a black 96 well-plate and incubated for 20min at 22°C. Then, fluorescence is measured by Cytation 3 imaging reader (Biotek®, Winooski, USA) with an excitation wavelength of 560 nm and an emission wavelength of 590 nm.

The kit contains lactate, NAD⁺ and resazurin as substrates, and diaphorase enzyme. In the presence of LDH, lactate is converted to pyruvate, and NADH is formed. Then, the diaphorase employs the NADH to transform resazurin into resorufin, which is fluorescent. Resorufin production is proportional to LDH quantity, and it was measured as fluorescence (560 nm/590 nm) in a microplate reader (Cytation® 3, BioTek®).



The background value was defined as the fluorescence registered for fresh medium, and it was subtracted from every sample result.

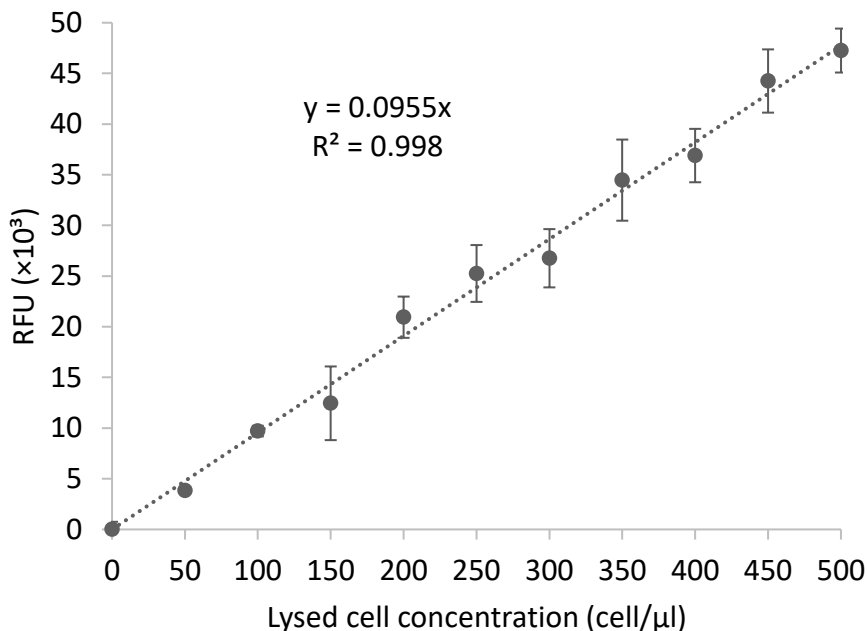


Figure 4-4: Calibration curve of the enzymatic method for free LDH concentration determination after shaking the sample in a 96-well plate for 20 min at 22°C. Trendline equation: $y=0.0955x$, $R^2 = 0.993$; x =equivalent lysed cell concentration, y =relative fluorescence units.

References

- [1] M. Al-rubeai, *Animal Cell Culture*, vol. 9. 2015.
- [2] R. Pörtner, "Characteristics of Mammalian Cells and Requirements for Cultivation," in *Cell and Tissue Reaction Engineering*, vol. 1, Berlin: Elsevier, 2009, pp. 13–53.
- [3] G. Lewis *et al.*, "Chemical Engineering Research and Design Scale-down studies for assessing the impact of different stress parameters on growth and product quality during animal cell culture," *Chem. Eng. Res. Des.*, vol. 91, no. 11, pp. 2265–2274, 2013, doi: 10.1016/j.cherd.2013.04.002.
- [4] R. A. Rader, "(Re) defining biopharmaceutical," *Nat. Biotechnol.*, vol. 26, no. 7, pp. 743–751, 2008.
- [5] G. Walsh, "Biopharmaceuticals and biotechnology medicines: An issue of nomenclature," *Eur. J. Pharm. Sci.*, vol. 15, no. 2, pp. 135–138, 2002, doi: 10.1016/S0928-0987(01)00222-6.
- [6] D. J. A. Crommelin, G. Storm, R. Verrijck, L. De Leede, W. Jiskoot, and W. E. Hennink, "Shifting paradigms: Biopharmaceuticals versus low molecular weight drugs," *Int. J. Pharm.*, vol. 266, no. 1–2, pp. 3–16, 2003, doi: 10.1016/S0378-5173(03)00376-4.
- [7] M. K. Parr, O. Montacir, and H. Montacir, "Physicochemical characterization of biopharmaceuticals," *J. Pharm. Biomed. Anal.*, vol. 130, pp. 366–389, 2016, doi: 10.1016/j.jpba.2016.05.028.
- [8] N. V. dos Santos, V. de Carvalho Santos-Ebinuma, A. Pessoa Junior, and J. F. B. Pereira, "Liquid–liquid extraction of biopharmaceuticals from fermented broth: trends and future prospects," *J. Chem. Technol. Biotechnol.*, vol. 93, no. 7, pp. 1845–1863, 2018, doi: 10.1002/jctb.5476.
- [9] RNCOS E-Services Private Limited, "Global protein therapeutics market outlook 2020,"

2015. <https://www.researchandmarkets.com/reports/3422491/global-protein-therapeutics-market-outlook-2020> (accessed Jul. 01, 2019).
- [10] EvaluatePharma, "World preview 2017, outlook to 2022," 2017. [Online]. Available: <http://info.evaluategroup.com/rs/607-YGS-364/images/WP17.pdf>.
- [11] M. Kesik-Brodacka, "Progress in biopharmaceutical development," *Biotechnol. Appl. Biochem.*, vol. 65, no. 3, pp. 306–322, 2018, doi: 10.1002/bab.1617.
- [12] PhRMA, "2016 Biopharmaceutical Research Industry Profile," *Pharm. Res. Manuf. Am.*, p. 86, 2016, [Online]. Available: <http://phrma-docs.phrma.org/sites/default/files/pdf/biopharmaceutical-industry-profile.pdf>.
- [13] G. Walsh, "Biopharmaceutical benchmarks 2018," *Nat. Biotechnol.*, vol. 36, no. 12, pp. 1136–1145, 2018, doi: 10.1038/nbt0706-769.
- [14] C. Morrison, "Fresh from the biotech pipeline—2018," *Nat. Biotechnol.*, vol. 37, no. 2, pp. 118–123, 2019, doi: 10.1038/s41587-019-0021-6.
- [15] C. Nick, "The US Biosimilars Act," *Pharmaceut. Med.*, vol. 26, no. 3, pp. 145–152, 2012, doi: 10.1007/bf03262388.
- [16] S. J. Shire, W. Gombotz, K. Bechtold-Peters, and J. Andya, *Current Trends in Monoclonal Antibody Development and Manufacturing*, vol. 17, no. 1. 2010.
- [17] A. M. Scott, J. P. Allison, and J. D. Wolchok, "Monoclonal antibodies in cancer therapy," *Dtsch Med Wochenschr*, vol. 12, pp. 14–21, 2012, [Online]. Available: <http://www.ncbi.nlm.nih.gov/pubmed/3886339>.
- [18] H. L. Levine and B. R. Cooney, "The Development of Therapeutic Monoclonal Antibody Products," 2016.
- [19] La Merie, "Blockbuster Biologics 2017: Sales of Recombinant Therapeutic Antibodies & Proteins," 2017. [Online]. Available: <https://lamerie.com/report/blockbuster-biologics-2017-sales-of-recombinant-therapeutic-antibodies-proteins/>.
- [20] L. Sompayrac, *How the Immune System works*, Wiley Desk. Wiley-Blackwell, 2012.
- [21] M. Reth, "Matching cellular dimensions with molecular sizes," *Nat. Publ. Gr.*, vol. 14, no. 8, pp. 765–767, 2013, doi: 10.1038/ni.2621.
- [22] K. H. Roux, "Immunoglobulin Structure and Function as Revealed by Electron Microscopy," *Int. Arch. Allergy Immunol.*, vol. 120, pp. 85–99, 1999.
- [23] J. M. Woof, D. R. Burton, and N. T. Pines, "Human antibody-Fc receptor interactions illuminated by crystal structures," *Nat. Rev. Immunol.*, vol. 4, no. February, pp. 1–11, 2004,

- doi: 10.1038/nri1266.
- [24] G. Vidarsson, G. Dekkers, and T. Rispens, "IgG subclasses and allotypes: From structure to effector functions," *Front. Immunol.*, vol. 5, no. OCT, pp. 1–17, 2014, doi: 10.3389/fimmu.2014.00520.
- [25] K. Imai and A. Takaoka, "Comparing antibody and small-molecule therapies for cancer," *Nat. Rev. Cancer*, vol. 6, no. 9, pp. 714–727, 2006, doi: 10.1038/nrc1913.
- [26] E. A. Padlan, "Anatomy of the antibody molecule," *Mol. Immunol.*, vol. 31, no. 3, pp. 169–217, 1994, doi: 10.1016/0161-5890(94)90001-9.
- [27] G. Köhler and C. Milstein, "Derivation of specific antibody-producing tissue culture and tumor lines by cell fusion," *Eur. J. Immunol.*, vol. 6, no. 7, pp. 511–519, 1976, doi: 10.1002/eji.1830060713.
- [28] J. K. H. Liu, "The history of monoclonal antibody development - Progress, remaining challenges and future innovations," *Ann. Med. Surg.*, vol. 3, no. 4, pp. 113–116, 2014, doi: 10.1016/j.amsu.2014.09.001.
- [29] N. S. Lipman, L. R. Jackson, L. J. Trudel, and F. Weis-garcia, "Monoclonal Versus Polyclonal Antibodies: Distinguishing Characteristics, Applications, and Information Resources," *ILAR J.*, vol. 46, no. 3, pp. 258–268, 2005.
- [30] T. T. Hansel, H. Kropshofer, T. Singer, J. A. Mitchell, and A. J. T. George, "The safety and side effects of monoclonal antibodies," *Nat. Rev. Drug Discov.*, vol. 9, no. 4, pp. 325–338, 2010, doi: 10.1038/nrd3003.
- [31] J. P. Van Wauwe, J. R. De Mey, and J. G. Goossens, "OKT3 : a monoclonal anti-human T lymphocyte antibody with potent mitogenic properties," *J. Immunol.*, vol. 124, no. 6, pp. 2708–2713, 1980.
- [32] T. S. Mattu *et al.*, "The Glycosylation and Structure of Human Serum IgA1, Fab, and Fc Regions and the Role of N -Glycosylation on Fc α Receptor Interactions," *J. Biol. Chem.*, vol. 4, no. 23, pp. 2260–2272, 1998, doi: 10.1074/jbc.273.4.2260.
- [33] E. Specht, S. Miyake-Stoner, and S. Mayfield, "Micro-algae come of age as a platform for recombinant protein production," *Biotechnol. Lett.*, vol. 32, no. 10, pp. 1373–1383, 2010, doi: 10.1007/s10529-010-0326-5.
- [34] R. Verma, E. Boleti, and A. J. T. George, "Antibody engineering : Comparison of bacterial , yeast , insect and mammalian expression systems," *J. Immunol. Methods*, vol. 216, pp.

- 165–181, 1998.
- [35] M. Betrer, C. P. Chang, R. R. Robinson, and A. H. Horwitz, "Escherichia coli Secretion of an Active Chimeric Antibody Fragment," *Int. Genertic Eng. Inc.*, vol. 522, no. May, pp. 41–43, 1988.
- [36] O. Spadiut, S. Capone, F. Krainer, A. Glieder, and C. Herwig, "Microbials for the production of monoclonal antibodies and antibody fragments," *Trends Biotechnol.*, vol. 32, no. 1, pp. 54–60, 2014, doi: 10.1016/j.tibtech.2013.10.002.
- [37] M. Berdichevsky, M. R. Mallem, S. S. Shaikh, and T. I. Potgieter, "Improved production of monoclonal antibodies through oxygen-limited cultivation of glycoengineered yeast," *J. Biotechnol.*, vol. 155, no. 2, pp. 217–224, 2011, doi: 10.1016/j.jbiotec.2011.06.021.
- [38] Y. J. Lee and K. J. Jeong, "Challenges to production of antibodies in bacteria and yeast," *J. Biosci. Bioeng.*, vol. 120, no. 5, pp. 483–490, 2015, doi: 10.1016/j.jbiosc.2015.03.009.
- [39] K. R. Love, N. C. Dalvie, and J. C. Love, "The yeast stands alone: the future of protein biologic production," *Curr. Opin. Biotechnol.*, vol. 53, pp. 50–58, 2018, doi: 10.1016/j.copbio.2017.12.010.
- [40] S. R. Karg and P. T. Kallio, "The production of biopharmaceuticals in plant systems," *Biotechnol. Adv.*, vol. 27, no. 6, pp. 879–894, 2009, doi: 10.1016/j.biotechadv.2009.07.002.
- [41] B. De Muynck, C. Navarre, and M. Boutry, "Production of antibodies in plants : status after twenty years," *Plant Biotechnol. J.*, vol. 8, pp. 529–563, 2010, doi: 10.1111/j.1467-7652.2009.00494.x.
- [42] R. Strasser *et al.*, "Generation of glyco-engineered *Nicotiana benthamiana* for the production of monoclonal antibodies with a homogeneous human-like N-glycan structure," *Plant Biotechnol. J.*, vol. 6, pp. 392–402, 2008, doi: 10.1111/j.1467-7652.2008.00330.x.
- [43] D. Palmberger, D. Rendic, P. Tauber, F. Krammer, I. B. H. Wilson, and R. Grabherr, "Insect cells for antibody production : Evaluation of an efficient alternative," *J. Biotechnol.*, vol. 153, pp. 160–166, 2011, doi: 10.1016/j.jbiotec.2011.02.009.
- [44] S. C. L. Ho, Y. W. Tong, and Y. Yang, "Generation of monoclonal antibody-producing mammalian cell lines," *Pharm. Bioprocess.*, no. May, pp. 71–87, 2014, doi: 10.4155/pbp.13.8.
- [45] F. Li, N. Vijayasankaran, A. Shen, R. Kiss, and A. Amanullah, "Cell culture processes for monoclonal antibody production," *MAbs*, vol. 2, no. 5, pp. 466–479, 2010, doi:

- 10.4161/mabs.2.5.12720.
- [46] J. Zhu, "Mammalian cell protein expression for biopharmaceutical production," *Biotechnol. Adv.*, vol. 30, no. 5, pp. 1158–1170, 2012, doi: 10.1016/j.biotechadv.2011.08.022.
- [47] L. A. Palomares and O. T. Ramírez, "The effect of dissolved oxygen tension and the utility of oxygen uptake rate in insect cell culture," *Cytotechnology*, vol. 22, no. 1–3, pp. 225–237, 1996, doi: 10.1007/BF00353943.
- [48] M. De Jesus and F. M. Wurm, "Manufacturing Recombinant Proteins in kg-ton Quantities Using Animal Cells in Bioreactors," *Compr. Biotechnol. Second Ed.*, vol. 3, no. 2, pp. 357–362, 2011, doi: 10.1016/B978-0-08-088504-9.00544-4.
- [49] J. Y. Kim, Y. G. Kim, and G. M. Lee, "CHO cells in biotechnology for production of recombinant proteins: Current state and further potential," *Appl. Microbiol. Biotechnol.*, vol. 93, no. 3, pp. 917–930, 2012, doi: 10.1007/s00253-011-3758-5.
- [50] S. Kumar *et al.*, "Proceedings of the 21st Annual Meeting of the European Society for Animal Cell Technology (ESACT), Dublin, Ireland, June 7-10, 2009," 2009. doi: 10.1007/978-94-007-0884-6.
- [51] S. Sommerfeld and J. Strube, "Challenges in biotechnology production - Generic processes and process optimization for monoclonal antibodies," *Chem. Eng. Process. Process Intensif.*, vol. 44, no. 10, pp. 1123–1137, 2005, doi: 10.1016/j.cep.2005.03.006.
- [52] S. Hammond, M. Kaplarevic, N. Borth, M. J. Betenbaugh, and K. H. Lee, "Chinese hamster genome database: An online resource for the CHO community at," *Biotechnol. Bioeng.*, vol. 109, no. 6, pp. 1353–1356, 2012, doi: 10.1002/bit.24374.
- [53] J. R. Birch and A. J. Racher, "Antibody production," *Adv. Drug Deliv. Rev.*, vol. 58, no. 5–6, pp. 671–685, 2006, doi: 10.1016/j.addr.2005.12.006.
- [54] J. Dumont, D. Ewart, B. Mei, S. Estes, and R. Kshirsagar, "Human cell lines for biopharmaceutical manufacturing: history, status, and future perspectives," *Crit. Rev. Biotechnol.*, vol. 36, no. 6, pp. 1110–1122, 2016, doi: 10.3109/07388551.2015.1084266.
- [55] A. S. Rathore, R. Bhambure, and V. Ghare, "Process analytical technology (PAT) for biopharmaceutical products," *Anal. Bioanal. Chem.*, vol. 398, no. 1, pp. 137–154, 2010, doi: 10.1007/s00216-010-3781-x.
- [56] H. Eagle, "Buffer Combinations for Mammalian Cell Culture," *Science (80-)*, vol. 174, pp. 500–503, 1971.

- [57] D. Gospodarowicz and J. S. Moran, "Growth Factors in Mammalian Cell Culture," *Annu. Rev. Biochem.*, vol. 45, no. 1, pp. 531–558, 2003, doi: 10.1146/annurev.bi.45.070176.002531.
- [58] X. Pan, M. Streefland, C. Dalm, R. H. Wijffels, and D. E. Martens, "Selection of chemically defined media for CHO cell fed-batch culture processes," *Cytotechnology*, vol. 69, no. 1, pp. 39–56, 2017, doi: 10.1007/s10616-016-0036-5.
- [59] L. E. Quek, S. Dietmair, J. O. Krömer, and L. K. Nielsen, "Metabolic flux analysis in mammalian cell culture," *Metab. Eng.*, vol. 12, no. 2, pp. 161–171, 2010, doi: 10.1016/j.ymben.2009.09.002.
- [60] M. Schneider, I. W. Marison, and U. Von Stockar, "The importance of ammonia in mammalian cell culture," *J. Biotechnol.*, vol. 46, no. 3, pp. 161–185, 1996, doi: 10.1016/0168-1656(95)00196-4.
- [61] M. W. Glacken, R. J. Fleischaker, and A. J. Sinskey, "Large-scale Production of Mammalian Cells and Their Products: Engineering Principles and Barriers to Scale-up," *Ann. N. Y. Acad. Sci.*, vol. 413, no. 1, pp. 355–372, 1983, doi: 10.1111/j.1749-6632.1983.tb47912.x.
- [62] R. Eibl, C. Loffelholz, and D. Eibl, *Single Use Technology In Biopharmaceutical Manufacture*, 2011th ed. Hoboken, New Jersey, 2011.
- [63] S. Junne and P. Neubauer, "How scalable and suitable are single-use bioreactors?," *Curr. Opin. Biotechnol.*, vol. 53, pp. 240–247, 2018, doi: 10.1016/j.copbio.2018.04.003.
- [64] S. Werner, "Development of method for reliable power input measurements in conventional and single use stirred bioreactors at laboratory scale," pp. 8–10, 2016, doi: 10.1002/elsc.201600096.This.
- [65] X. Zou, H. feng Hang, J. Chu, Y. ping Zhuang, and S. liang Zhang, "Oxygen uptake rate optimization with nitrogen regulation for erythromycin production and scale-up from 50 L to 372 m³scale," *Bioresour. Technol.*, vol. 100, no. 3, pp. 1406–1412, 2009, doi: 10.1016/j.biortech.2008.09.017.
- [66] J. P. Clark, *Process and equipment selection*. Elsevier, 2008.
- [67] J. S. Crater and J. C. Lievens, "Scale-up of industrial microbial processes," *FEMS Microbiol. Lett.*, vol. 365, no. 13, pp. 1–5, 2018, doi: 10.1093/femsle/fny138.
- [68] A. Das, "Impact of Continuous Processing Techniques on Biologics Supply Chains," in *Continuous Processing in Pharmaceutical Manufacturin*, First., G. Subramanian, Ed. Wiley-VCH Verlag GmbH & Co., 2015, pp. 53–70.

- [69] J. N. Warnock and M. Al-Rubeai, "Bioreactor systems for the production of biopharmaceuticals from animal cells," *Biotechnol. Appl. Biochem.*, vol. 45, no. 1, p. 1, 2006, doi: 10.1042/BA20050233.
- [70] J. Büchs, "Introduction to advantages and problems of shaken cultures," *Biochem. Eng. J.*, vol. 7, no. 2, pp. 91–98, 2001, doi: 10.1016/S1369-703X(00)00106-6.
- [71] X. Zhang *et al.*, "Shaken helical track bioreactors: Providing oxygen to high-density cultures of mammalian cells at volumes up to 1000 L by surface aeration with air," *N. Biotechnol.*, vol. 25, no. 1, pp. 68–75, 2008, doi: 10.1016/j.nbt.2008.03.001.
- [72] P. M. Doran, *Bioprocess Engineering Principles*, Second. 2013.
- [73] H. J. Noorman and J. J. Heijnen, "Biochemical engineering's grand adventure," *Chem. Eng. Sci.*, vol. 170, pp. 677–693, 2017, doi: 10.1016/j.ces.2016.12.065.
- [74] G. Amaral *et al.*, *Practical design, construction and operation of food facilities*, vol. 369, no. 1. 2013.
- [75] Q. Ye, J. Bao, and Z. Jian-Jiang, *Bioreactor Engineering Research and Industrial Applications I*, vol. 155. 2016.
- [76] C. Lattermann and J. Büchs, "Microscale and miniscale fermentation and screening," *Curr. Opin. Biotechnol.*, vol. 35, pp. 1–6, 2015, doi: 10.1016/j.copbio.2014.12.005.
- [77] F. Garcia-Ochoa, E. Gomez, V. E. Santos, and J. C. Merchuk, "Oxygen uptake rate in microbial processes: An overview," *Biochem. Eng. J.*, vol. 49, no. 3, pp. 289–307, 2010, doi: 10.1016/j.bej.2010.01.011.
- [78] T. Yao, "cell culture media : History , characteristics , and current issues," no. January, pp. 99–117, 2017, doi: 10.1002/rmb2.12024.
- [79] W.-S. Hu and J. G. Aunins, "Large-scale mammalian cell culture," *Curr. Opin. Biotechnol.*, vol. 8, no. 2, pp. 148–153, 1997, doi: 10.1016/S0958-1669(97)80093-6.
- [80] M. Buchsteiner, L. E. Quek, P. Gray, and L. K. Nielsen, "Improving culture performance and antibody production in CHO cell culture processes by reducing the Warburg effect," *Biotechnol. Bioeng.*, vol. 115, no. 9, pp. 2315–2327, 2018, doi: 10.1002/bit.26724.
- [81] T. M. Duarte, N. Carinhas, L. C. Barreiro, M. J. T. Carrondo, P. M. Alves, and A. P. Teixeira, "Metabolic responses of CHO cells to limitation of key amino acids," *Biotechnol. Bioeng.*, vol. 111, no. 10, pp. 2095–2106, 2014, doi: 10.1002/bit.25266.
- [82] D. R. Gray, S. Chen, W. Howart, D. Inlow, and B. L. Maiorella, "CO₂ in large-scale and high

- density CHO cell perfusion culture," *Cytotechnology*, vol. 22, pp. 65–78, 1996.
- [83] M. Brunner, P. Doppler, T. Klein, C. Herwig, and J. Fricke, "Elevated pCO₂ affects the lactate metabolic shift in CHO cell culture processes," *Eng. Life Sci.*, vol. 18, no. 3, pp. 204–214, 2018, doi: 10.1002/elsc.201700131.
- [84] A. Rita Costa, M. Elisa Rodrigues, M. Henriques, J. Azeredo, and R. Oliveira, "Guidelines to cell engineering for monoclonal antibody production," *Eur. J. Pharm. Biopharm.*, vol. 74, no. 2, pp. 127–138, 2010, doi: 10.1016/j.ejpb.2009.10.002.
- [85] J. Varley and J. Birch, "Reactor design for large scale suspension animal cell culture," *Cytotechnology*, vol. 29, no. 3, pp. 177–205, 1999, doi: 10.1023/A:1008008021481.
- [86] N. Barbouche, "Réponse biologique de cellules animales à des contraintes hydrodynamiques : simulation numérique , expérimentation et modélisation en bioréacteurs de laboratoire," 2018.
- [87] S. K. W. Oh, A. W. Nienow, M. Al-Rubeai, and A. N. Emery, "The effects of agitation intensity with and without continuous sparging on the growth and antibody production of hybridoma cells," *J. Biotechnol.*, vol. 12, no. 1, pp. 45–61, 1989, doi: 10.1016/0168-1656(89)90128-4.
- [88] J. J. Chalmers, "Mixing, aeration and cell damage, 30 + years later : what we learned, how it affected the cell culture industry and what we would like to know more about," pp. 94–102, 2015.
- [89] R. V. Venkat, L. R. Stock, and J. J. Chalmers, "Study of hydrodynamics in microcarrier culture spinner vessels: A particle tracking velocimetry approach," *Biotechnol. Bioeng.*, vol. 49, no. 4, pp. 456–466, 1996, doi: 10.1002/(SICI)1097-0290(19960220)49:4<456::AID-BIT13>3.3.CO;2-I.
- [90] S. Xu *et al.*, "A practical approach in bioreactor scale-up and process transfer using a combination of constant P/V and vvm as the criterion," *Biotechnol. Prog.*, vol. 33, no. 4, pp. 1146–1159, 2017, doi: 10.1002/btpr.2489.
- [91] F. Scargiali, A. Busciglio, F. Grisafi, and A. Brucato, "Mass transfer and hydrodynamic characteristics of unbaffled stirred bio-reactors : Influence of impeller design," *Biochem. Eng. J.*, vol. 82, pp. 41–47, 2014, doi: 10.1016/j.bej.2013.11.009.
- [92] S. Xu and H. Chen, "High-density mammalian cell cultures in stirred-tank bioreactor without external pH control," *J. Biotechnol.*, vol. 231, pp. 149–159, 2016, doi: 10.1016/j.jbiotec.2016.06.019.

- [93] T. Dreher, U. Husemann, S. Ruhl, and G. Greller, "Design space definition for a stirred single-use bioreactor family from 50 to 2000 L scale," *BMC Proc.*, vol. 7, no. Suppl 6, pp. 6–8, 2013.
- [94] J. R. Vallejos, K. A. Brorson, A. R. Moreira, and G. Rao, "Integrating a 250 mL-spinner flask with other stirred bench-scale cell culture devices: A mass transfer perspective," *Biotechnol. Prog.*, vol. 27, no. 3, pp. 803–810, 2011, doi: 10.1002/btpr.578.
- [95] F. Buttgereit, M. D. Brandt, T. C. Road, and C. Cb, "A hierarchy of ATP-consuming," vol. 167, pp. 163–167, 1995.
- [96] J. M. Willey, L. M. Sherwood, and C. J. Woolverton, *Prescott, Harley, and Klein's Microbiology*, McGraw-Hil. New York: Colin Whealey/Janice Roering-Blang, 2008.
- [97] B. C. Mulukutla, S. Khan, A. Lange, and W. Hu, "Glucose metabolism in mammalian cell culture : new insights for tweaking vintage pathways," *Trends Biotechnol.*, vol. 28, no. 9, pp. 476–484, 2010, doi: 10.1016/j.tibtech.2010.06.005.
- [98] W. G. Hopkins, *Photosynthesis and Respiration*. New York: Chelsea House, 2006.
- [99] J. Van der Valk *et al.*, "Optimization of chemically defined cell culture media - Replacing fetal bovine serum in mammalian in vitro methods," *Toxicol. Vitro.*, vol. 24, pp. 1053–1063, 2010, doi: 10.1016/j.tiv.2010.03.016.
- [100] P. W. Hochachka, "Defense Strategies Against Hypoxia and Hypothermia," *Science (80-)*, vol. 231, pp. 234–241, 1986.
- [101] M. Bonora *et al.*, "ATP synthesis and storage," pp. 343–357, 2012, doi: 10.1007/s11302-012-9305-8.
- [102] A. Vazquez, J. Liu, Y. Zhou, and Z. N. Oltvai, "Catabolic efficiency of aerobic glycolysis : The Warburg effect revisited," 2010.
- [103] A. R. Fernie, F. Carrari, and L. J. Sweetlove, "Respiratory metabolism : glycolysis , the TCA cycle and mitochondrial electron transport," *Curr. Opin. Plant Biol.*, vol. 7, pp. 254–261, 2004, doi: 10.1016/j.pbi.2004.03.007.
- [104] M. Akram, "Citric Acid Cycle and Role of its Intermediates in Metabolism," *Cell Biochem Biophys*, vol. 68, pp. 475–478, 2014, doi: 10.1007/s12013-013-9750-1.
- [105] C. Nazaret, M. Heiske, K. Thurley, and J. Mazat, "Mitochondrial energetic metabolism : A simplified model of TCA cycle with ATP production," vol. 258, pp. 455–464, 2009, doi: 10.1016/j.jtbi.2008.09.037.

- [106] E. Racker, *A New Look at Mechanisms in Bioenergetics*, First. New York: Academic Press, 1976.
- [107] S. Dietmair, N. E. Timmins, P. P. Gray, L. K. Nielsen, and J. O. Krömer, "Towards quantitative metabolomics of mammalian cells : Development of a metabolite extraction protocol," *Anal. Biochem.*, vol. 404, no. 2, pp. 155–164, 2010, doi: 10.1016/j.ab.2010.04.031.
- [108] V. Chevallier, M. R. Andersen, and L. Malphettes, "Oxidative stress - alleviating strategies to improve recombinant protein production in CHO cells," no. November 2019, pp. 1172–1186, 2020, doi: 10.1002/bit.27247.
- [109] M. Vergara *et al.*, "High glucose and low specific cell growth but not mild hypothermia improve specific r-protein productivity in chemostat culture of CHO cells," *PLoS One*, vol. 13, no. 8, pp. 1–22, 2018, doi: 10.1371/journal.pone.0202098.
- [110] C. T. Goudar, J. M. Piret, and K. B. Konstantinov, "Estimating cell specific oxygen uptake and carbon dioxide production rates for mammalian cells in perfusion culture," *Biotechnol. Prog.*, vol. 27, no. 5, pp. 1347–1357, 2011, doi: 10.1002/btpr.646.
- [111] L. V. Berkner and L. C. Marshall, "On the Origin and Rise of Oxygen Concentration in the Earth's Atmosphere," *J. Atmos. Sci.*, vol. 22, no. 3, pp. 255–261, 1965.
- [112] J. M. Prausnitz, R. N. Lichtenthaler, and E. Gomez de Azevedo, *Molecular Thermodynamics of Fluid-Phase Equilibria-PH PTR (1999).pdf*, Third. Upper Saddle River, New Jersey, 1999.
- [113] C. E. Boyd, *Water Quality*, Third Edit. Springer Nature Switzerland, 2019.
- [114] J. D. Seader, E. J. Henley, and D. K. Roper, *Separation Process Principles with Applications Using Process Simulators*, Fourth. 2011.
- [115] D. D. McClure, J. M. Kavanagh, D. F. Fletcher, and G. W. Barton, "Oxygen transfer in bubble columns at industrially relevant superficial velocities: Experimental work and CFD modelling," *Chem. Eng. J.*, vol. 280, pp. 138–146, 2015, doi: 10.1016/j.cej.2015.06.003.
- [116] P. Sucusky, D. F. Osorio, J. B. Brown, and G. P. Neitzel, "Fluid Mechanics of a Spinner-Flask Bioreactor," *Biotechnol. Bioeng.*, vol. 85, no. 1, pp. 34–46, 2004, doi: 10.1002/bit.10788.
- [117] T. Anderlei, W. Zang, M. Papaspyrou, and J. Büchs, "Online respiration activity measurement (OTR, CTR, RQ) in shake flasks," *Biochem. Eng. J.*, vol. 17, no. 3, pp. 187–194, 2004, doi: 10.1016/S1369-703X(03)00181-5.
- [118] Z. Zheng, D. Sun, J. Li, X. Zhan, and M. Gao, "Improving oxygen transfer efficiency by developing a novel energy-saving impeller," *Chem. Eng. Res. Des.*, vol. 130, pp. 199–207,

- 2018, doi: 10.1016/j.cherd.2017.12.021.
- [119] P. A. Ruffieux, U. Von Stockar, and I. W. Marison, "Measurement of volumetric (OUR) and determination of specific (qO₂) oxygen uptake rates in animal cell cultures," *J. Biotechnol.*, vol. 63, no. 2, pp. 85–95, 1998, doi: 10.1016/S0168-1656(98)00046-7.
- [120] T. E. Riedel, W. M. Berelson, K. H. Neelson, and S. E. Finkel, "Oxygen consumption rates of bacteria under nutrient-limited conditions," *Appl. Environ. Microbiol.*, vol. 79, no. 16, pp. 4921–4931, 2013, doi: 10.1128/AEM.00756-13.
- [121] F. Garcia-Ochoa, S. Escobar, and E. Gomez, "Specific oxygen uptake rate as indicator of cell response of *Rhodococcus erythropolis* cultures to shear effects," *Chem. Eng. Sci.*, vol. 122, pp. 491–499, 2015, doi: 10.1016/j.ces.2014.10.016.
- [122] F. Garcia-Ochoa and E. Gomez, "Bioreactor scale-up and oxygen transfer rate in microbial processes: An overview," *Biotechnol. Adv.*, vol. 27, no. 2, pp. 153–176, 2009, doi: 10.1016/j.biotechadv.2008.10.006.
- [123] C. M. Cooper, G. A. Fernstrom, and S. A. Miller, "Performance of Agitated Gas-Liquid Contactors—Correction," *Ind. Eng. Chem.*, vol. 36, no. 9, p. 857, 1944, doi: 10.1021/ie50417a601.
- [124] P. V. Danckwerts, "Significance of Liquids in Gas Absorption," *Eng. Process Dev.*, vol. 43, no. 6, pp. 1460–1467, 1951.
- [125] K. Ortiz-Ochoa, S. D. Doig, J. M. Ward, and F. Baganz, "A novel method for the measurement of oxygen mass transfer rates in small-scale vessels," *Biochem. Eng. J.*, vol. 25, no. 1, pp. 63–68, 2005, doi: 10.1016/j.bej.2005.04.003.
- [126] G. A. Hill, "Measurement of overall volumetric mass transfer coefficients for carbon dioxide in a well-mixed reactor using a pH probe," *Ind. Eng. Chem. Res.*, vol. 45, no. 16, pp. 5796–5800, 2006, doi: 10.1021/ie060242t.
- [127] L. A. Tribe, C. L. Briens, and A. Margaritis, "Communication to the Editor Determination of the Volumetric Mass Transfer Coefficient (k_a) Using the Dynamic 'Gas Out-Gas In' Method: Analysis of Errors Caused by Dissolved Oxygen Probes," *Biotechnol. Bioeng.*, vol. 46, no. 4, pp. 388–392, 1995, doi: 10.1002/bit.260460412.
- [128] U. Maier, M. Losen, and J. Büchs, "Advances in understanding and modeling the gas-liquid mass transfer in shake flasks," *Biochem. Eng. J.*, vol. 17, no. 3, pp. 155–167, 2004, doi: 10.1016/S1369-703X(03)00174-8.

- [129] A. A. Lin and W. M. Miller, "CHO cell responses to low oxygen: Regulation of oxygen consumption and sensitization to oxidative stress," *Biotechnol. Bioeng.*, vol. 40, no. 4, pp. 505–516, 1992.
- [130] A. A. Lin, R. Kimura, and W. M. Millert, "Cells Under Oxygen-Limited Conditions," vol. 42, pp. 339–350, 1993.
- [131] R. S. Senger *et al.*, "Oxygen transfer characteristics of miniaturized bioreactor systems," *Biotechnol. Bioeng.*, vol. 110, no. 1, pp. 339–350, 2014, doi: 10.1016/j.apm.2013.05.032.
- [132] D. Flitsch *et al.*, "Respiration activity monitoring system for any individual well of a 48-well microtiter plate," *J. Biol. Eng.*, vol. 10, no. 1, 2016, doi: 10.1186/s13036-016-0034-3.
- [133] P. A. Apostolidis, A. Tseng, M. E. Koziol, M. J. Betenbaugh, and B. Chiang, "Investigation of low viability in sparged bioreactor CHO cell cultures points to variability in the Pluronic F-68 shear protecting component of cell culture media," *Biochem. Eng. J.*, vol. 98, pp. 10–17, 2015, doi: 10.1016/j.bej.2015.01.013.
- [134] J. P. Clark, *Practical Design, Construction and Operation of Food Facilities*. 2009.
- [135] G. Jagschies, E. Lindskog, K. Lacki, and P. Galliher, Eds., *Biopharmaceutical Processing: Development, design and implementation of manufacturing processes*. 2018.
- [136] K. G. Clarke, *Bioprocess engineering. An Introductory Engineering and Life Science Approach*. Cambridge: Woodhead Publishing, 2013.
- [137] V. I. Sikavitsas, G. N. Bancroft, and A. G. Mikos, "Formation of three-dimensional cell/polymer constructs for bone tissue engineering in a spinner flask and a rotating wall vessel bioreactor," *J. Biomed. Mater. Res.*, vol. 62, no. 1, pp. 136–148, 2002, doi: 10.1002/jbm.10150.
- [138] M. Singh, F. K. Kasper, and A. G. Mikos, *Tissue Engineering Scaffolds*, Third Edit. Elsevier, 2013.
- [139] N. K. Gill, M. Appleton, F. Baganz, and G. J. Lye, "Design and characterisation of a miniature stirred bioreactor system for parallel microbial fermentations," *Biochem. Eng. J.*, vol. 39, no. 1, pp. 164–176, 2008, doi: 10.1016/j.bej.2007.09.001.
- [140] D. T. Monteil *et al.*, "Disposable 600-mL orbitally shaken bioreactor for mammalian cell cultivation in suspension," *Biochem. Eng. J.*, vol. 76, pp. 6–12, 2013, doi: 10.1016/j.bej.2013.04.008.
- [141] L. Zhu *et al.*, "Fluid dynamics of flow fields in a disposable 600-mL orbitally shaken bioreactor," *Biochem. Eng. J.*, vol. 129, pp. 84–95, 2018, doi: 10.1016/j.bej.2017.10.019.

- [142] T. A. Barrett, A. Wu, H. Zhang, M. S. Levy, and G. J. Lye, "Microwell engineering characterization for mammalian cell culture process development," *Biotechnol. Bioeng.*, vol. 105, no. 2, pp. 260–275, 2010, doi: 10.1002/bit.22531.
- [143] S. Suresh, V. C. Srivastava, and I. M. Mishra, "Critical analysis of engineering aspects of shaken flask bioreactors," *Crit. Rev. Biotechnol.*, vol. 29, no. 4, pp. 255–278, 2009, doi: 10.3109/07388550903062314.
- [144] R. J. Fleischaker Jr and A. J. Sinskey, "Oxygen demand and supply in cell culture," *Eur. J. Appl. Microbiol. Biotechnol.*, vol. 12, no. 4, pp. 193–197, 1981, doi: 10.1007/BF00499486.
- [145] P. Jorjani and S. Ozturk, "Effects of Cell Density and Temperature on Oxygen Consumption Rate for Different Mammalian Cell Lines," *Biotechnol. Bioeng.*, vol. 64, no. 3, pp. 349–356, 1999.
- [146] B. Bienz-Tadmor, P. A. Dicerbo, G. Tadmor, and L. Lasagna, "Biopharmaceuticals and conventional drugs: Clinical Success Rates," *Nat. Biotechnol.*, vol. 10, pp. 667–674, 1992, doi: doi:10.1038/nbt0692-667.
- [147] H. Schellekens, "Biosimilar therapeutics — what do we need to consider?," 2009, doi: 10.1093/ndtplus/sfn177.
- [148] R. M. Alldread *et al.*, "Large Scale Suspension Culture of Mammalian Cells," 2014. doi: 10.1002/9783527683321.ch12.
- [149] R. P. Evens and K. I. Kaitin, "The biotechnology innovation machine: A source of intelligent biopharmaceuticals for the pharma industry - Mapping biotechnology's success," *Clin. Pharmacol. Ther.*, vol. 95, no. 5, pp. 528–532, 2014, doi: 10.1038/clpt.2014.14.
- [150] K. Jayapal, K. Wlaschin, W. Hu, and G. Yap, "Recombinant protein therapeutics from CHO cells-20 years and counting," *Chem. Eng. Prog.*, vol. 103, no. 10, pp. 40–47, 2007, [Online]. Available: <http://www.aiche.org/sites/default/files/docs/pages/CHO.pdf>.
- [151] L. Xie, W. Zhou, and D. Robinson, "Protein production by large-scale mammalian cell culture," *New Compr. Biochem.*, vol. 38, pp. 605–623, 2003, doi: 10.1016/S0167-7306(03)38035-4.
- [152] S. Reuveny, D. Velez, J. D. Macmillan, and L. Miller, "Factors affecting cell growth and monoclonal antibody production in stirred reactors," *J. Immunol. Methods*, vol. 86, no. 1, pp. 53–59, 1986, doi: 10.1016/0022-1759(86)90264-4.
- [153] N. Kurano, C. Leist, F. Messi, S. Kurano, and A. Fiechter, "Growth behavior of Chinese

- hamster ovary cells in a compact loop bioreactor: 1. Effects of physical and chemical environments," *J. Biotechnol.*, vol. 15, no. 1–2, pp. 101–112, 1990, doi: 10.1016/0168-1656(90)90054-F.
- [154] T. Link *et al.*, "Bioprocess development for the production of a recombinant MUC1 fusion protein expressed by CHO-K1 cells in protein-free medium &," vol. 110, pp. 51–62, 2004, doi: 10.1016/j.jbiotec.2003.12.008.
- [155] E. Trummer *et al.*, "Process parameter shifting: Part I. Effect of DOT, pH, and temperature on the performance of Epo-Fc expressing CHO cells cultivated in controlled batch bioreactors," *Biotechnol. Bioeng.*, vol. 94, no. 6, pp. 1033–1044, Aug. 2006, doi: 10.1002/bit.21013.
- [156] L. Zhiming, W. Kang, J. Gaofeng, H. Kang, and H. Jingfeng, "CFD studies on hydrodynamic characteristics of shaking bioreactors with wide conical bottom," *J. Chem. Technol. Biotechnol.*, 2017, doi: 10.1002/jctb.5431.
- [157] D. T. Monteil *et al.*, "A comparison of orbitally-shaken and stirred-tank bioreactors: pH modulation and bioreactor type affect CHO cell growth and protein glycosylation," *Biotechnol. Prog.*, vol. 32, no. 5, pp. 1174–1180, 2016, doi: 10.1002/btpr.2328.
- [158] S. Tissot, P. O. Michel, D. L. Hacker, L. Baldi, M. De Jesus, and F. M. Wurm, "KLa as a predictor for successful probe-independent mammalian cell bioprocesses in orbitally shaken bioreactors," *N. Biotechnol.*, vol. 29, no. 3, pp. 387–394, 2012, doi: 10.1016/j.nbt.2011.10.010.
- [159] C. Li, J. Xia, J. Chu, Y. Wang, Y. Zhuang, and S. Zhang, "Regular article CFD analysis of the turbulent flow in baffled shake flasks," *Biochem. Eng. J.*, vol. 70, pp. 140–150, 2013, doi: 10.1016/j.bej.2012.10.012.
- [160] W. Klöckner *et al.*, "Correlation between mass transfer coefficient $k_L a$ and relevant operating parameters in cylindrical disposable shaken bioreactors on a bench-to-pilot scale," *J. Biol. Eng.*, vol. 7, no. 1, pp. 1–14, 2013, doi: 10.1186/1754-1611-7-28.
- [161] L. K. Zhu *et al.*, "Studies on fluid dynamics of the flow field and gas transfer in orbitally shaken tubes," *Biotechnol. Prog.*, vol. 33, no. 1, pp. 192–200, 2017, doi: 10.1002/btpr.2375.
- [162] Y. Rigual-González *et al.*, "Application of a new model based on oxygen balance to determine the oxygen uptake rate in mammalian cell chemostat cultures," *Chem. Eng. Sci.*, vol. 152, pp. 586–590, 2016, doi: 10.1016/j.ces.2016.06.051.

- [163] G. van Eikenhorst, Y. E. Thomassen, L. A. van der Pol, and W. A. M. Bakker, "Assessment of mass transfer and mixing in rigid lab-scale disposable bioreactors at low power input levels," *Biotechnol. Prog.*, vol. 30, no. 6, pp. 1269–1276, 2014, doi: 10.1002/btpr.1981.
- [164] Z. Xing, A. M. Lewis, M. C. Borys, and Z. J. Li, "A carbon dioxide stripping model for mammalian cell culture in manufacturing scale bioreactors," *Biotechnol. Bioeng.*, vol. 114, no. 6, pp. 1184–1194, 2017, doi: 10.1002/bit.26232.
- [165] J. Wutz *et al.*, "Predictability of k_La in stirred tank reactors under multiple operating conditions using an Euler–Lagrange approach," *Eng. Life Sci.*, vol. 16, no. 7, pp. 633–642, 2016, doi: 10.1002/elsc.201500135.
- [166] L. Gimenez, C. Simonet, and L. Malphettes, "Scale-up considerations for monoclonal antibody production process: an oxygen transfer flux approach," *BMC Proc.*, vol. 7, no. Suppl 6, p. P49, 2013, doi: 10.1186/1753-6561-7-S6-P49.
- [167] T. Dreher, U. Husemann, T. Adams, D. de Wilde, and G. Greller, "Design space definition for a stirred single-use bioreactor family from 50 to 2000 L scale," *Eng. Life Sci.*, vol. 14, no. 3, pp. 304–310, 2014, doi: 10.1002/elsc.201300067.
- [168] B. Minow *et al.*, "Biological performance of two different 1000 L single-use bioreactors applying a simple transfer approach," *Eng. Life Sci.*, vol. 14, no. 3, pp. 283–291, 2014, doi: 10.1002/elsc.201300147.
- [169] A. L. Damiani, M. H. Kim, and J. Wang, "An improved dynamic method to measure k_La in bioreactors," *Biotechnol. Bioeng.*, vol. 111, no. 10, pp. 2120–2125, 2014, doi: 10.1002/bit.25258.
- [170] R. Rakoczy, J. Lechowska, M. Kordas, M. Konopacki, K. Fijałkowski, and R. Drozd, "Effects of a rotating magnetic field on gas-liquid mass transfer coefficient," *Chem. Eng. J.*, vol. 327, no. 3, pp. 608–617, 2017, doi: 10.1016/j.cej.2017.06.132.
- [171] S. S. de Jesus, J. Moreira Neto, and R. Maciel Filho, "Hydrodynamics and mass transfer in bubble column, conventional airlift, stirred airlift and stirred tank bioreactors, using viscous fluid: A comparative study," *Biochem. Eng. J.*, vol. 118, pp. 70–81, 2017, doi: 10.1016/j.bej.2016.11.019.
- [172] J. R. Mounsef, D. Salameh, N. Louka, C. Brandam, and R. Lteif, "The effect of aeration conditions, characterized by the volumetric mass transfer coefficient $K_L a$, on the fermentation kinetics of *Bacillus thuringiensis kurstaki*," *J. Biotechnol.*, vol. 210, pp.

- 100–106, 2015, doi: 10.1016/j.jbiotec.2015.06.387.
- [173] F. Scargiali, A. Busciglio, F. Grisafi, and A. Brucato, “Mass transfer and hydrodynamic characteristics of unbaffled stirred bioreactors influence of impeller design.pdf,” vol. 82, pp. 41–47, 2013.
- [174] A. Karimi *et al.*, “Oxygen mass transfer in a stirred tank bioreactor using different impeller configurations for environmental purposes,” *Iranian J. Environ. Health Sci. Eng.*, vol. 10, no. 1, p. 6, 2013, doi: 10.1186/1735-2746-10-6.
- [175] M. M. Buffo, L. J. Corrêa, M. N. Esperança, A. J. G. Cruz, C. S. Farinas, and A. C. Badino, “Influence of dual-impeller type and configuration on oxygen transfer, power consumption, and shear rate in a stirred tank bioreactor,” *Biochem. Eng. J.*, vol. 114, pp. 130–139, 2016, doi: 10.1016/j.bej.2016.07.003.
- [176] M. Xie, J. Xia, Z. Zhou, J. Chu, Y. Zhuang, and S. Zhang, “Flow Pattern , Mixing , Gas Hold-Up and Mass Transfer Coe ffi cient of Triple-Impeller Con fi gurations in Stirred Tank Bioreactors,” *Ind. Eng. Chem. Res.*, p. 140320091633005, 2014, doi: 10.1021/ie400831s.
- [177] J. C. Gabelle *et al.*, “Impact of rheology on the mass transfer coefficient during the growth phase of *Trichoderma reesei* in stirred bioreactors,” *Chem. Eng. Sci.*, vol. 75, pp. 408–417, 2012, doi: 10.1016/j.ces.2012.03.053.
- [178] C. Bach *et al.*, “Evaluation of mixing and mass transfer in a stirred pilot scale bioreactor utilizing CFD,” *Chem. Eng. Sci.*, vol. 171, no. 1, pp. 19–26, 2017, doi: 10.1016/j.ces.2017.05.001.
- [179] M. O. Albaek, K. V. Gernaey, M. S. Hansen, and S. M. Stocks, “Modeling enzyme production with *Aspergillus oryzae* in pilot scale vessels with different agitation, aeration, and agitator types,” *Biotechnol. Bioeng.*, vol. 108, no. 8, pp. 1828–1840, 2011, doi: 10.1002/bit.23121.